ENGINEERING BIOACTIVE MATERIALS FROM RECOMBINANT OLEOSIN TOWARDS DRUG

DELIVERY APPLICATIONS

Chen Gao

A DISSERTATION

in

Chemical and Biomolecular Engineering

Presented to the Faculties of the University of Pennsylvania

in

Partial Fulfillment of the Requirements for the

Degree of Doctor of Philosophy

2018

Supervisor of Dissertation

_____

Professor Daniel A. Hammer

Alfred G. and Meta A. Ennis Professor Bioengineering and Chemical and Biomolecular Engineering

Graduate Group Chairperson

_____

Professor John C. Crocker, Professor of Chemical and Biomolecular Engineering

Dissertation Committee

Jason A. Burdick, Professor of Bioengineering
Daeyeon Lee, Professor of Chemical and Biomolecular Engineering
Kathleen J. Stebe, Richer & Elizabeth Goodwin Professor of Chemical and Biomolecular Engineering

ENGINEERING BIOACTIVE MATERIALS FROM RECOMBINANT OLEOSIN

TOWARDS DRUG DELIVERY APPLICATIONS

This thesis is dedicated to my parents:

Maoxia Wang and Song Gao

and

my friends and family

ACKNOWLEDGMENTS

I would first like to thank my advisor, Daniel A. Hammer. Dan has been a wonderful

mentor who taught me how to become an independent researcher, have confidence in my

work, and be creative in solving problems. He motivated me to explore outside my scope

of work and steered me back on track at critical moments. Dan has an inspirational

vision, a thoughtful approach, and most importantly an enthusiastic spirit towards

science. Dan has taught me lessons on and far beyond research, and has made my time at

Penn more interesting and rewarding than I could have hoped for.

I would like to thank my thesis committee, Jason Burdick, Daeyeon Lee, and Kate

Stebe for their interest in my project, insightful discussions, and helping me to think

about my research with a fresh perspective.

I am thankful to Kevin Vargo, who started the oleosin project and taught me

everything about molecular biology. My project would not have existed without him, and

his work continued to be a source of inspiration for me throughout the last five years.

Laurel Hind, Aaron Dominguz, Nimil Sood, Steven Henry, Amy Bendell, Nick Anderson, Eric Wang, Joanna MacKay, Woo-Sik Jang, and Seung Chul Park welcomed me into the lab and taught me techniques that helped to kickstart my project, and all the other little things about working in a lab. Laurel encouraged me to take my oleosin experiments to mammalian cells and trained me on cell culture. Joanna taught me confocal microscopy, which turned out to be a core component of my research. Nick kept the lab running smoothly from day to day, and has always been patient and helpful with my beginner questions. Without you it would have taken me a lot longer to finish my projects. Everyone who has joined since I arrived including Ellen Reed, Sarah Kim, Adam Suppes, Ben Schuster, Alex Buffone, Yeongseon Jang and Katie Pulsipher, you have continued teaching me new things both in and out of lab, and offered much helpful discussions over the years. I had the pleasure to work with a wonderful undergraduate student, Vera Lee, who asked questions that I rarely considered before and helped me to grow as a mentor.

To my peers at Penn CBE who have been amazing friends since we met during recruitment weekend in 2013, thank you for all the time well spent together. Especially Jyolyn, Brad, Sang, and Ming. Whether it was spending hours on a transport homework, starting out in lab, writing the very first paper, going thorough proposal, looking for jobs, and eventually getting ready to defend, I feel fortunate to have you around every step of the way. You have all made the graduate school journey a lot more fun and a lot less stressful, and I am sure we will be lifelong friends.

To friends I have made after I moved to Philly, who are like family to me on the east coast. Summer is one of the first few people I came to know in Philly and my best friend at Penn. We spent countless hours exploring the city together and I hope you could have stayed here longer. Fanny, Guan, Seki and Zipei – thank you for keeping me updated with the world, and for always being positive and encouraging. You have over and over again made my bad days not so bad and good days even better.

Lastly, I would like to thank my family. I am extremely grateful for my parents, who have always been loving and supportive. My mother has been and still is my role model, who gave me invaluable lessons on work and life, and cheered me on when I needed it most. My father inspired me to work as an engineer from a young age by explaining science in an interesting and relevant way. Without you I would not be who I am today. And finally, to my grandparents, who taught me to explore the world with kindness in heart.

ABSTRACT

ENGINEERING BIOACTIVE MATERIALS FROM RECOMBINANT OLEOSIN

TOWARDS DRUG DELIVERY APPLICATIONS

Chen Gao

Daniel A. Hammer

Drug carrier plays a critical role in achieving therapeutic effect in human or animals.

Existing commercial drug carriers are mostly chemically synthesized, making the

materials polydisperse in size, carry heavy residuals and extremely difficult to

functionalize for bioactivity. Recombinant protein expressed through molecular biology

presents a promising alternative to chemically synthesized materials due to several

advantages. Molecular biology techniques allow for precise design of the genetic

sequence, thus giving the recombinant protein the ability to incorporate specific motifs

that mediates cell recognition. Protein expressed through molecular biology would have

the exact amino acid sequence as designed and monodisperse in weight, which makes

recombinant protein superior than synthesized materials for quality control purposes. For

this thesis, we have chosen a naturally occurring plant protein oleosin, which has been

previously demonstrated in our lab to self-assemble into a variety of nanostructures upon

gene modification, as the starting template. We have designed many variants of oleosin to self-assemble into spherical micelles and carry bioactive motifs. First, we created a variant of oleosin that possesses dual control by protecting the bioactive ligand RGDS with a thrombin cleavable domain. Cellular uptake studies showed that this model is effective in protecting 74% of the RGDS bioactivity in 15 hours when interacted with breast cancer cells. We further enhanced the cellular uptake performance of oleosin by inserting a synergy PHSRN and cell penetrating peptide HIV-1 Tat, where the Tat peptide and the RGDS motif combination increased cell uptake by sixfold in 15 hours. We proved the ability of oleosin micelles to carry a cargo by successfully encapsulating an anti-cancer drug paclitaxel into oleosin micelles through brief sonication, and achieved integrin mediated cell killing on breast cancer cells over 15 hours. We then applied our oleosin variants to other cell lines by functionalizing with AFA and BPT ligands, and observed significantly improved cell killing on non-small cell lung cancer cells. All protein variants were confirmed for molecular weight and purity by gel electrophoresis and mass spectroscopy, and the second structures analyzed through circular dichroism. Protein self-assembly sizes were analyzed by dynamic light scattering. Oleosin micelles were stable in aqueous solutions for at least one month under refrigerated conditions, and has been found to be stable after drug encapsulation and variant blending. Oleosin has been shown to be a versatile and powerful tool for drug applications, and these results opened a new horizon for oleosin to be further engineered and utilized for therapeutic applications.

TABLE OF CONTENTS

CHAPTER 3. ENHANCED CELL KILLING BY PACLITAXEL-LOADED OLEOSIN 43

CHAPTER 4. OLEOSIN DRUG CARRIERS SPECIFICALLY TARGETING ERBB RECEPTORS 73

LIST OF TABLES

LIST OF FIGURES

Chapter 1. Introduction

1.1 An Overview of Drug Delivery

Cancer remains to be one of the leading causes of death in the world. Over the past few decades, significant advances in fundamental cancer biology have led to better diagnostic tools and treatment methods. Despite these changes, mortality of cancer remains high. In 2016, there is an estimated 1,685,210 diagnoses and 595,690 deaths from cancer in the United States alone.[1] Current therapeutics for most cancers involve surgical resection, radiation therapy, and chemotherapy. These treatments are associated with significant mortality due to their non-specific effects on surrounding tissues. The efficacy of a therapeutic can be greatly improved if the carrier can selectively target diseased tissue, respond to the disease environment, and overcome biological barriers.[2] Nanotechnology coupled with effective therapeutic agents is a promising strategy to address these challenges.[2,3]

The basic properties required for drug and imaging agent carriers are that they are biodegradable, biocompatible, and able to carry both hydrophilic and hydrophobic cargos.[4–6] Nano-scale carriers can be of different constructs, each with their strengths and weaknesses. Vesicles are hollow spherical structures with an aqueous interior and the shell composed of amphiphilic molecules, and presents as promising carriers due to their ability to carry a large payload of aqueous drug, and their ability to also carry hydrophobic drugs.[7] However, lipid vesicles have some drawbacks, including poor colloidal stability, short shelf life, restricted and expensive conditions of preparation/fabrication complexity, and they only work best for works well for soluble drugs.[8] On the other hand, spherical micelles are formed by amphiphilic materials in aqueous solutions where the hydrophobic blocks come together to form the hydrophobic core, protected by the solvated hydrophilic corona. The hydrophobic block region can serve as a reservoir for poorly soluble drugs. Micelles are of particular interest due to their small size, biocompatibility, and are ideal candidates for applications such as intravenous administration or for crossing the blood-brain barrier.[9–12] Micelles of elongated morphology, often referred to as wormlike micelles or filomicelles, have shown to have double the drug loading capacity, sustainably shrink tumors, as well as prolonged circulation times, when compared to spherical micelles of the same composition.[13–16]

Over the past few decades, there has been increasing interest in constructing delivery nanomaterials that are robust, stable, and can be engineered to both incorporate

targeting moieties and promote sustained release. Targeting, in particular, has the potential to reduce harmful systemic side effects such as systemic toxicity; the challenge is to find suitable materials that are both robust and can be easily functionalized.

Phospholipid molecules are extensively studied for their potential to construct delivery vesicles.[17,18] Phospholipid and lipid blends readily form biocompatible vesicles. However, phospholipid vesicles have limited potential due to their lack of mechanical and chemical stability. Phospholipid vesicles are mechanically weak and does not survive against the shear stress in blood circulation.[19] Chemically, phospholipids oxidize quickly and are hard to modify to incorporate bioactive sites. In order to improve upon the deficiencies of phospholipid vesicles, studies have been done on numerous synthetic materials to construct vesicles that are both physically and chemically stable. Materials such as block copolymers and amphiphilic dendrimers can be made with a variety of different chemistries and molecular weights to achieve widely tunable mechanical properties.[20–22] Polymersomes and dendrimersomes can be covalently linked to ligands for targeting. However, the addition of ligands on the vesicle surfaces can lead to changes in the phase behavior of polymers and dendrimers, and can even perturb the assembled structure away from the vesicular phase.[23] Furthermore, synthetic materials, such as polymers, cannot be made monodisperse,[24] and using synthetic materials in vivo also raises the concern of toxicity as heavy metals and organic solvents are common residuals from the synthesis process.[25,26]

Expressing recombinant protein through molecular biology presents a powerful alternative. Molecular biology is able to achieve precise gene modification, and therefore able to insert functionalization anywhere in a protein molecule. The precise gene modification also results in monodisperse molecular weights and gives product materials uniform quality, which chemically synthesized polymers cannot achieve perfectly. Within this thesis, we use the naturally occurring oleosin as the starting template, which is discussed in detail in the following section.

1.2 Oleosin

To address issues of biocompatibility, monodispersity, and functionalization, our laboratory has been assembling materials from recombinant oleosin and its variants. Oleosin is a group of naturally occurring structural proteins found across a wide range of oil-rich plants (maize, sesame, soybean, sunflower and etc.).[27,28] Oleosin molecules from various plant sources all share a similar triblock structure with a central hydrophobic domain, and two hydrophilic arms at the N- and C-termini.[27] The amphiphilicity of oleosin makes it a natural surfactant that functions to stabilize oil bodies in plant seeds.[29] Our laboratory demonstrated that recombinant oleosin and truncation variants thereof can self-assemble into different structures including micelles, fibers, sheets, and vesicles, depending on the architecture of the oleosin and ionic strength of the buffer.[30] Because

4

oleosin is made recombinantly, it is possible to precisely control the amino acid sequence, and to insert bioactive sites anywhere in the oleosin molecule. Previously, the Hammer Lab has demonstrated that a bioactive motif RGDS added to the C-terminus of oleosin can increases the uptake by Ovcar-5 cells by 3-fold.[31] Additionally, Her2/neu affibody fused to the N-terminus of the oleosin 30G variant can stabilize and target superparamagnetic iron oxide nanoparticle (SPIO)-loaded micelles to a Her2/neu+ cell line (T6-17 cells).[32] Oleosin is a promising biomaterial that has plenty of potential yet to be studied.

1.3 Description of Thesis

This work addresses the potential of building smart drug carriers from recombinant oleosin. Oleosin has a unique triblock structure which is rarely found in natural surfactant proteins, and offers itself as a versatile platform where numerous motifs can be engineered towards a wide range of applications.[27,29,33] In this work, we attempt to merge the existing knowledge of oleosin self-assembly structures and integrin mediated cell behavior, and create variants of oleosin that self-assemble into nanoscale carriers that can be targeted towards specific cell lines. The specific aims of this work are as follows:

1. Create a recombinant oleosin that is bioactive and answers to an environmental cue in physiological conditions

2. Encapsulate an anti-cancer drug in self-assembled oleosin nanostructure, and achieve enhanced cell killing

3. Create oleosin drug carriers that specifically target a family of receptors

This work is composed of five chapters. This chapter provides an overview of current drug carriers, previously established knowledge of oleosin, and briefly describe the techniques used to complete this work.

Chapter 2 of this work presents the construction of a oleosin variants that was engineered to have dual control over cellular uptake. This variant was built to have the bioactive motif RGDS protected by 20 amino acid that could be cleaved off by thrombin, and achieved RGDS 74% bioactivity shield in 15 hours on breast cancer cells. This work demonstrated that a single recombinant oleosin molecule can be engineered to be both bioactive and protease sensitive, and gave rise to multiple directions where this research can be carried further.

Chapter 3 of this work took the previous results further by exploring the effects of synergy ligand PHSRN and a cell-penetrating peptide HIV-1 Tat with different local

ligand concentrations via oleosin blending. The oleosin variants has been shown to successfully encapsulate an anti-cancer drug, paclitaxel, and achieve enhanced breast cancer cell killing in a short as 3 hours. This work expanded our knowledge in the capability of using oleosin as drug carriers.

Chapter 4 of this work explored outside the RGDS motif and breast cancer cell lines, and proved oleosin as an effective carrier on delivering paclitaxel into non-small cell lung cancer cells.

Finally, **Chapter 5** details the major conclusions and future directions of this work. Here, we discuss the next steps of engineering oleosin towards drug delivery and other therapeutic applications. There exists extensive knowledge on bioactive motifs ready to be merged with the oleosin model, and make oleosin an outstanding and universal platform of a wide range of applications.

1.4 Background

To facilitate the reader's understanding, this section offers background of frequently mentioned terms and concepts throughout this thesis.

1.4.1 Paclitaxel and Nanoparticles

Paclitaxel (PX) is a chemical isolated from the bark of Pacific Yew, and is one of the most effective chemotherapeutic so far and is mainly used to treat lung, ovarian and breast cancer. [16,34–36] Paclitaxel is a mitotic inhibitor that stabilizes microtubules. It inhibits the G2 and M phases of cell cycle and disrupt cell division, thereby causing cell death. [35,36]

Despite the effectiveness of paclitaxel as an anti-cancer drug, it also has several drawbacks. First, PX is an irritant that causes inflammation of veins that it's administered through, and low blood count is a common side effect from PX that can lead to infection/anemia in patients. Second, PX has a low water solubility (~ 0.4 µg/mL) and need to be formulated in organic solvents such as a mixture of polyexyethylated castor oil and dehydrated ethanol, and those organic solvents is known to cause serious side effects such as hypersensitivity, as well as altering the pharmacokinetics of PX.[36] Last but not least, PX is a substrate of P-glycoprotein (P-gp), which pumps PX out of cells and induce drug resistance.[36,37]

Extensive efforts has been made in hope to enhance the solubility of PX and decrease systematic side effects, and over the years nanoparticles have emerged as a promising strategy. Nanoparticles as drug carriers of paclitaxel can be polymeric nanoparticles, albumin nanoparticles, lipid-based nanoparticles, emulsions, drug-polymer conjugates, metal nanoparticles, carbon nanotubes, and several other constructs.[37] Some important nanoparticle-based paclitaxel delivery systems are discussed here.

Poly (lactic-co-glycolic acid) (PLGA) Nanoparticles: PLGA is one of the most widely used biodegradable co-polymers investigated for nano-delivery systems, with a minimal systemic toxicity.[37] PX-loaded PLGA demonstrated enhanced cytotoxicity in various cancer cell lines such as glioma C6, human non-small cell lung cancer (NCI-H69), HeLa cells, and transplantable liver tumors.[14,37,38] The release of PX from PLGA nanoparticles can be slowed down by coating nanoparticles with chitosan.[37]

Poly (Ethylene Glycol)-Phophatidyl Ethanolamine (PEG-PE) Nanoparticles: PEG-PE polymeric micelles developed by the Torchilin group presents two hydrocarbon chains in PE and achieved better stability of the micelles.[2,37] PX-loaded PEG-PE micelles shoed better antitumor activity both *in vitro* and *in vivo* in a Lewis lung carcinoma mouse model.[11]

Liposomes: Yoshizawa and colleagues formulated PX into liposomes composed of cholesterol, PEG-DSPE$_{2000}$, and hydrogenated soybean phophatidylcholine (HSPC), which showed significantly improved antitumor efficiency in colon-26 solid tumor-bearing mice.[37] EndoTAG-1 is a PX-loaded cationic liposome developed by MediGene, and binds to negatively charged endothelial cells in tumor blood vessels. EndoTAG-1 significantly decreased tumor size in a prostate cancer mouse model, and a combination of EndoTAG-1 and gemcitabine inhibited pancreatic metastasis in an orthotopic pancreatic cancer model.[37]

Gold Nanoparticles: Gibson *et al.* demonstrated that PX can be coated to phenol-terminated gold nanoparticles with a hexaethylene glycol linker.[39] A gold/chitosan nanoparticle dispersed with PX, as described by Oh *et al*., can achieve sustainable release over a 12-day period with minimal initial burst release.[40] Heo and co-workers presented a complex PX-functionalized gold nanoparticle system where PEG served as an anti-fouling shell, biotin as a targeting ligand, and rhodamine B as a fluorescence probe.[41] This PX system demonstrated enhanced cytotoxicity in cancer cell lines including HeLa, A549, and MG63.[41]

Nanoparticles have several other advantages as drug carriers, depending on the specific material and construct. The aqueous solubility of PX can be significantly

increased when it is conjugated with water-soluble polymers or encapsulated by

lipids.[14,38,42] The size of nanoparticles, usually several hundred nanometers in diameter,

enables the preferential delivery of PX into tumor site due to the enhanced permeability

and retention (EPR) effect.[37,43,44] However, the targeting effect of nanoparticles is limited

due to the challenge of conjugating bioactive peptide ligands on polymers, lipids, or

metal nanoparticles, while conjugating or encapsulating the drug.

1.4.2 Bioactivity from Fibronectin

Fibronectin (FN) is a glycoprotein of the extracellular matrix that binds to integrins.[45] FN

have multiple forms as a result of alternative splicing of a single pre-mRNA, and usually

exists as a dimer composed of two identical subunits ~250 kDa covalently linked by a

disulfide bonds.[46] It plays critical roles in a variety of cell activities such as cell adhesion,

migration, growth and differentiation, and is therefore widely studied in the past two

decades.

Previously, researchers have narrowed down the regions involved in cell adhesion

to several short integrin-recognition sequences. The most studied short sequence is RGD

located in the 10th domain of FN. The RGD (Arg-Gly-Asp) sequence is the cell

attachment site of a large number of adhesive extracellular matrix, blood, and cell surface

proteins.[47] It is recognized by nearly half of the over 20 known integrins in human body,

especially the αβ family integrins.[48] Due to its short nature, RGD is often incorporated

into drug and drug carrier design, and has shown enhanced cell uptake in systems such as polymers, lipids, and metal nanoparticles.[48–53]

A second sequence PHSRN, found in the 9th domain of FN, acts in synergy with RGD by binding to a non-overlapping site on the α_5 integrin and strengthen RGD binding.[45,48] The synergy effect is heavily dependent on the spatial orientation and distance between RGD and PHSRN sequences, and previous research have suggested that the synergy effect is usually maximized by mimicking the natural distance of 30-40Å between RGD and PHSRN.[49,53–56]

Chapter 2. Protease-Triggered, Integrin-Targeted Cellular Uptake of Recombinant Protein Micelles

Abstract

Targeting nano-particles for drug delivery has great potential for improving efficacy and reducing side effects from systemic toxicity. New developments in the assembly of materials afford the opportunity to expose cryptic targeting domains in tissue-specific microenvironments in which certain proteases are expressed. Here, recombinant proteins are designed to combine the responsiveness to environmental proteases with specific targeting. Materials made recombinantly allow complete control over amino acid sequence, in which each molecule is identically functionalized. Previously, oleosin, a naturally occurring plant protein that acts as a surfactant, has been engineered to self-assemble into spherical micelles - a useful structure for drug delivery. To make oleosins that are locally activated to bind receptors, oleosin is genetically modified to incorporate the integrin-binding motif RGDS just behind a domain cleavable by thrombin. The

resulting modified oleosin self-assembles into spherical micelles in aqueous environments, with the RGDS motif protected by the thrombin-cleavable domain. Upon the addition of thrombin, the RGDS is exposed and the binding of the spherical micelles to breast cancer cells is increased 4-fold.

2.1 Introduction

Targeting has the potential to reduce harmful systemic side effects of drug delivery. Additionally, positive results have been found where materials such as polymers, peptides, and nanoparticles are designed to become bioactive only in the presence of environmental cues, such as ligand/receptor concentration, the activity of enzymes, pH, temperature, magnetic field, and ultrasound.[57–61] However, the development of synthetic materials that incorporate specific targeting is limited by stability of the carrier, reproducibility, and particle size control.[24] Recombinant proteins present an attractive strategy for addressing many of the issues in biocarrier design. Recombinant proteins are monodisperse, can self-assemble into a variety of nanostructures, and be equipped with sensitivity to environment through sequence design.[9,61,62] The manipulation of the amino acid sequence is made possible through molecular biology, where DNA sequence is designed to precisely alter the sequence of amino acids.

Our laboratory has been assembling materials from recombinant oleosin and its variants.[31,32] Oleosin is a group of naturally occurring structural proteins found across a

wide range of oil-rich plants (maize, sesame, soybean, sunflower and etc.).[27,28] Oleosin

molecules from various plant sources all share a similar triblock structure with a

hydrophobic domain at the center, and two hydrophilic arms at the N- and C-termini.[27]

The amphiphilicity of oleosin makes it a natural surfactant that functions to stabilize oil

bodies in plant seeds.[29] Our laboratory demonstrated that recombinant oleosin and

truncation variants thereof can self-assemble into different structures including micelles,

fibers, sheets, and vesicles, depending on the architecture of the oleosin and ionic

strength of the buffer.[30] In this paper, we focus on a subset of oleosins in which the

internal hydrophobic core has been trimmed to 30 amino acids, and several large bulky

hydrophobic residues have been replaced by glycines. We call variants that contain this

sequence the -30G- family. These molecules have been shown to self-assemble into

spherical micelles with CMCs in the micromolar range.[31] Micellar structures are

attractive drug carriers – they can encapsulate insoluble drugs, have long circulation

times in body, and protect the hydrophobic drugs from biological surroundings.[11]

A common approach for targeting a cell line with a nanocarrier is to functionalize

the carrier with a ligand that binds a cell-surface receptor. The RGDS motif is widely

used for biomedical applications; it is present in fibronectin and other extracellular matrix

proteins, and is recognized by many known integrins.[63–65] RGDS has been studied for its

effects on cell adhesion and internalization when incorporated with polymers and

peptides, and promising results have been seen in studies where RGD is used to target

nanocarriers to cancer cells.[12,31,48,51,66–70] Most previous studies have focused on

covalently linking the RGD tag to synthetic polymers and nanoparticles. However, using

synthetic materials *in vivo* raises the concern of toxicity as heavy metals and organic solvents are common residuals from their synthesis.[25,26]

Another approach in targeted drug delivery is to use enzyme-sensitive carriers. It has been found that specific enzymes have abnormal expression profiles near pathological sites, such as cancer and inflammation.[71] This abnormality can be exploited to achieve enzyme-triggered release from liposomes and nanoparticles.[57,72–74] For example, thrombin (also known as coagulation factor II) is a serine protease that has important roles in hemostasis and blood coagulation. Aside from its functions in hemostasis, thrombin is known to induce invasion and metastasis in various cancers.[75–77] Therefore, using a thrombin-sensitive material as a drug carrier may be a promising way to enhance targeted cancer therapy. The thrombin cleavage site has been identified to be a short peptide sequence (LVPR|GS) that can be easily incorporated into the chain of an oleosin molecule, make the molecule sensitive towards thrombin proteolytic reaction.

To improve from previous research, here we present an approach to design and engineer a recombinant version of oleosin, which self-assembles into micelles and exhibits integrin-binding activity only under the specific cue of thrombin reaction, and therefore giving us greater control over targeting and drug delivery. The naturally occurring protein surfactant oleosin was mutated to incorporate both the bioactive motif RGDS and thrombin cleavable sites, where the RGDS motif was placed behind the thrombin cleavable domain and protected from interacting with cell surface unless activated by thrombin. This multifunctional recombinant protein assembles into spherical

16

micelles, and targets cells overexpressing $\alpha_v\beta_3$ most avidly in the presence of thrombin. This multiple specificity enables both dynamic and regional control of cell binding, and may be of potential in developing a highly specific targeted cancer therapy.

2.2 Materials and Methods

2.2.1 Protein Design and Expression

Genetic modification on the previous oleosin-30G(-) was done through PCR and the genes were inserted into the expression vector pBamUK and later transformed into the BL21 (DE3) strain of *E. coli* for expression. DNA sequencing was performed before protein expression by the *E. coli* strain BL21 DE3 (Stratagene) controlled by the *lac* promotor on the pBamUK. Cultures are grown at 37°C in Luria Broth (LB) with 50 µg/ml kanamycin until OD_{600} reaches 0.6. Isopropyl β-D-thiogalactoside (IPTG) was added to the culture to a final concentration of 1.0 mM to induce the expression of oleosin. Cells were collected by spinning down the culture at 15,000g for 15min and were kept frozen at -20°C until purification. pBamUK adds a 6-histidine tag to the C-terminus of oleosin molecule which facilitates purification through immobilized metal affinity chromatography (IMAC). All variants of proteins in this study express solubly. Yields for all variants in this study were ~80-100 mg of purified protein per liter of culture. All four oleosin variants were highly soluble and stable in buffered solutions (pH~7.4).

All oleosin strands in this project have 6-Histidine tag to the C-terminus and were purified with Ni-NTA columns (Pierce). All protein strands in this study are soluble and can be purified with the protocol suggested by Vargo et al.[31] In brief, frozen protein pellet was re-suspended in B-PER Bacterial Protein Extraction Reagent (Fisher). After spinning down at 15,000g for 15min, the supernatant was left to bind with the Ni-NTA resin for at least 1 hour. Then the column was repeatedly washed and protein sample was eluted out.

2.2.2 Protein Characterization

SDS-PAGE: To determine the purity of protein samples, purified oleosin samples were loaded on NuPAGE Novex 4-12% Bis-Tris mini gels (Invitrogen) in 2-(N-morpholino)-ethanesulfonic acid (MES) buffer. SimplyBlue SafeStain (Invitrogen) was used to stain the gel following electrophoresis. The gel was imaged with a Kodak Gel Logic 100 imaging system.

Mass Spectroscopy: To prepare matrix solution, sinapinic acid was added to 50:50 (v/v) ACN: [0.1 vol.% TFA in water] to a final concentration of 10mg/ml. 0.5 μL of matrix solution was added to Bruker AnchorChip, immediately followed by 0.5 μL of oleosin solution. Solutions were mixed on the AnchorChip using a pipet tip and air-dried.

Samples were analyzed with matrix-assisted laser desorption ionization (MALDI) mass spectroscopy (Bruker, PennChemistry Mass Spectrometry Facility).

Circular Dichroism (CD) : An AVIV 410 spectrometer (AVIV Biomedical, Inc.) was used to collect UV CD spectra at 25°C in a 1 mm quartz cell. The protein sample concentration was 10 µM in 50 mM phosphate and 140 mM NaF. The CD data was analyzed with the CDSSTR algorithm using Dichroweb.

Critical Micelle Concentration (CMC) - Pyrene Assay : The critical micelle concentration (CMC) was determined by pyrene assay, where pyrene was used as a fluorescence probe that prefers non-polar environments.[78] The ratio of the first and third peaks of the emission spectrum (I_1/I_3) decreases as a function of polarity of the protein sample solution (**Figure 2.10**), and this ratio is considered as an index of polarity in the environment.[78–80] The pyrene assay data were fit with a sigmoidal Boltzmann equation (SBE) suggested by Aguiar et al, and the CMC value is determined to be the inflection point.[81]

$$\frac{I_1}{I_3} = \frac{(a_i - a_f)}{1 + \exp[(x - x_0)/\Delta x]} + a_f \tag{1}$$

where x is the concentration of protein, a_i and a_f are initial and final asymptotes of the sigmoid respectively, x_0 is the center of the sigmoid and Δx is the interval of x.[82] It has

been suggested that the for curves with the ratio $x_0/\Delta x < 10$, the CMC will be the concentration at the inflection point.

7 µL of 12 mM pyrene (Sigma-Aldrich, St. Louis, MO) in ethanol (200 Proof) was added to 20ml of PBS. Protein samples were prepared by serial dilution from the high-concentration protein stock to as low as 0.001 µM. In each low-volume cuvette, 600 µL of protein sample and 100 µL of pyrene in PBS solution were added. Samples were excited at 334 nm and the emission spectrums were collected at 360-400 nm (excitation slit, 8nm; emission slit, 2nm) using a Fluoromax-4 spectrophotometer (Horiba Jobin Yvon). The ratio of intensities of the first and third peaks (I_1/I_3) was plotted as a function of protein concentration. The inflection point of the best-fit sigmoidal curve was determined to be the CMC.

Dynamic Light Scattering (DLS): 700 µL of protein sample was added to a small-volume cuvette cleaned with compressed air. DLS was performed with a Malvern Zetasizer Nano ZS (Westborough, MA).

Thrombin Reaction: Thrombin cleaving reaction was performed with Human Thrombin (Haematologic Technologies Inc., HCT-0020, Essex Junctions, VT) using the protocol provided by the manufacturer. Reaction results were checked with SDS-PAGE and mass spectroscopy.

Oleosin Labeling: Oleosin was labeled with 10 molar-fold excess of amine-reactive fluorophore Dylight 488 NHS-ester (Thermo Scientific) according to manufacturer's protocol. Excess dye was removed by repeated dialysis against PBS until background fluorescence was undetectable.

2.2.3 Mammalian Cell Culture and Cellular Uptake Study

Cell Culture: The human breast cancer cell line MDA-MB-231 (ATCC HTB-26) was acquired from the University of Pennsylvania Cell Center. MDA-MB-231 cells were cultured in RPMI 1640 (Life Technologies 22400, Carlsbad, Ca) supplemented with 10% heat-inactivated fetal bovine serum (Sigma Aldrich F2442, St. Louis, MO) and 100 units/ml penicillin and 100 µg/ml streptomycin (Life Technologies 15140) on tissue-culture treated plastic in a 37°C humidified incubator with 5% CO_2.

Targeted Cellular Uptake: When MDA-MB-231 cells reach 60-70% confluency, the growth media was aspirated and the cell culture was triple washed and left in RPMI 1640 without phenol red (Life Technologies 11835). Labeled oleosin micelle solution was added to the cell culture to a final concentration of 10 µM. After the internalization period (3-15hrs), the cell culture was triple washed with RPMI 1640 media (no phenol red). When testing the cellular uptake levels of the thrombin-cleaved versions of oleosin-Throm-RGDS-30G(-) and oleosin-Throm-RADS-30G(-), the variants were fully cleaved with thrombin before being introduced to cell media.

Cell Fixing and Membrane Staining: Following internalization, the cell culture was fixed with fixed with 4% PFA and cell membrane was labeled with Wheat Germ Agglutinin - Alexa Fluor 633 Conjugate (Invitrogen W21404), using the protocol provided by the manufacturer.

2.2.4 Cellular Uptake Visualized by Confocal Microscopy

Confocal Microscopy: Cell cultures were imaged with a Leica TCS SP5 confocal microscope (Bioengineering Confocal and Multiphoton Imaging Core Facility, UPenn). Fixed cell cultures on a tissue-culture treated surface were directly imaged with a HCX IRAPD L 25x/0.95 W dipping lens. Dylight 488 and Alexa Fluor 633 were excited using 10% strength Argon laser and HeNe laser, respectively. Images were acquired at 400 Hz scanning frequency at slice thickness of 296.40 nm. Gain was set to be 749.9 V and 777.1 V for the 633 and 488 channels, respectively. Offset was kept at 0.0% for all acquisitions.

Quantification of Oleosin Uptake: From the z-stack images taken for each sample, 5 images were chosen at 5 μm apart in vertical depth. Total number of cells was counted, as well as cells with fluorescence from labeled oleosin inside the cell membrane. If a cell

has only oleosin micelle adhering to the cell surface, it was not included for the purpose of quantifying cellular uptake.

2.3 Results and Discussions

2.3.1 Oleosin Design, Self-Assembly and Secondary Structure

It has been demonstrated that the naturally occurring 20 kDa wild-type sunflower seed oleosin can be widely modified.[30–32] Previously, oleosin-30G(-) was designed from the wild-type sunflower seed oleosin by: (i) truncating 57 amino acid out of the hydrophobic block to remove hydrogen bridges; (ii) adding five glycines into the hydrophobic block to increase flexibility; and (iii) mutating the hydrophilic arms to contain only negatively charged amino acids to improve protein expression.[31]

In this current study, four further variants were created from oleosin-30G(-). Previously, we demonstrated that the addition of the RGDS tag to the C-terminus of oleosin can increase the uptake by Ovcar-5 cells by 3-fold.[31] Two of these are controls. A positive control oleosin-RGDS-30G(-), contains an integrin-binding motif RGDS to the N-terminus of oleosin-30G(-). A second molecule, oleosin-RADS-30G(-), contains a

non-active peptide sequence RADS (Arg-Ala-Asp-Ser) at the same location to serve as a

negative control (**Figure 2.1 A**).
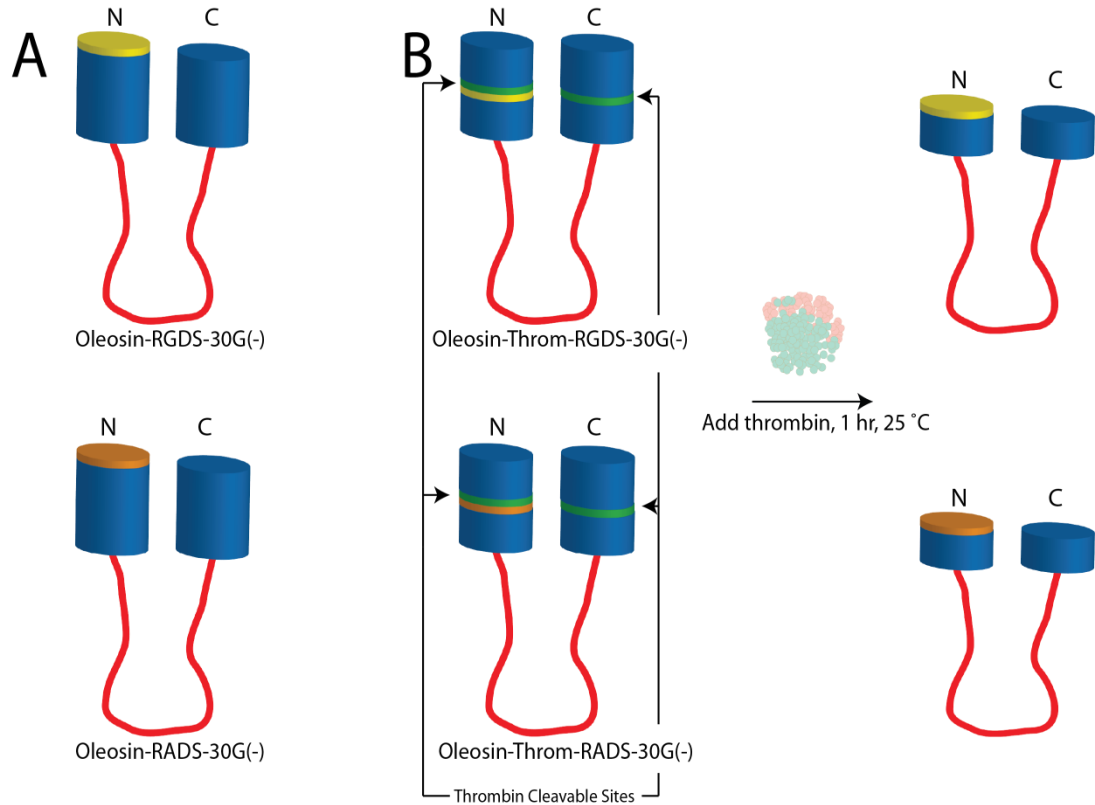
Figure 2.1. Molecular view of Oleosin-30G(-) variants. (A) Illustrations depicting addition of motifs RGDS (yellow) and RADS (orange) to the variants Oleosin-RGDS-30G(-) and Oleosin-RADS-30G(-), respectively. (B) Oleosin-Throm-RGDS-30G(-) is mutated from Oleosin-RGDS-30G(-) where the RGDS motif is moved to the center of the N-terminus hydrophilic arm and protected by a thrombin cleavable domain (green). Another thrombin cleavable domain is added to the C-terminus hydrophilic arm so that the remaining protein molecule have two hydrophilic arms similar in length after the thrombin cleaving reaction. Oleosin-Throm-RADS-30G(-) is constructed in a similar way from Oleosin-RADS-30G(-).

Since it would be beneficial to have greater dynamic control over targeting, we designed two additional oleosins that can target cells in a protease-triggered manner. To achieve this, oleosin-Throm-RGDS-30G(-) was designed to incorporate a thrombin cleavable domain (LVPR|GS) on the N-terminus hydrophilic arm, followed by a RGDS motif which is only exposed when the oleosin molecule is cleaved by thrombin (**Figure 2.1B and Figure 2.2**). Another thrombin cleavable domain is added in the C-terminus hydrophilic arm such that the N- and C-terminus hydrophilic arms remain at approximately equal lengths after the thrombin cleavage reaction. Similarly, oleosin-Throm-RADS-30G(-) was designed as a negative control that contains the non-targetable motif RADS (**Figure 2.1 B**). We show that these molecules self-assemble into micelles and can be used to target a cancer cell line in a highly controllable manner.
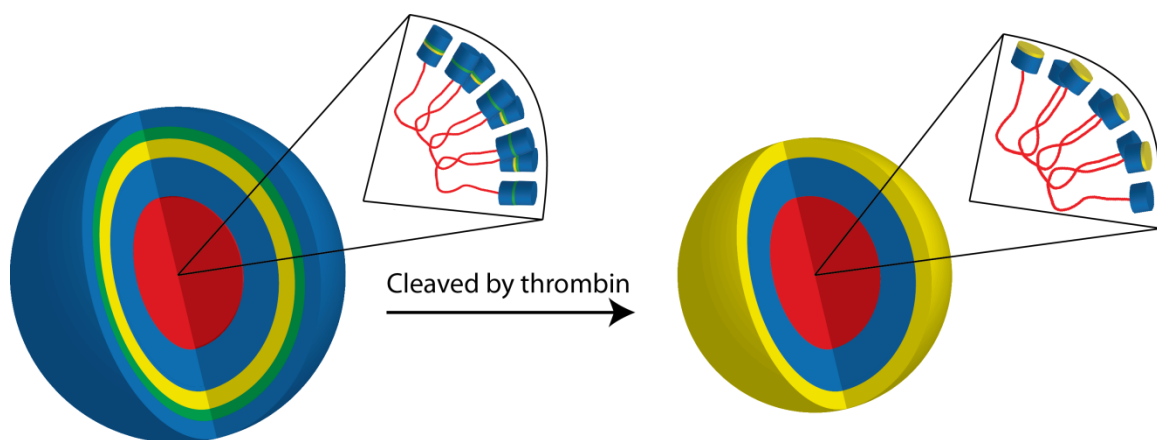
Figure 2.2. Micellar view of Oleosin-Throm-RGDS-30G(-). When in aqueous solution above its critical micelle concentration, the molecules self-assembly to micelles by collapsing hydrophobic blocks (red) together surrounded by the hydrophilic arms (blue). After thrombin cleaves the hydrophilic arms at the thrombin cleavable sites (green), the RGDS motif will be exposed at the N-terminus end of the hydrophilic arm. Oleosin-Throm-RADS-30G(-) share the same thrombin cleaving mechanism.

To monitor the purity of the recombinant protein samples and ensure that the

protein has the exact peptide sequence as designed, SDS-PAGE and MALDI-TOF tests

were carried out for each sample after purification (see Supporting Information). Both

assessments show that recombinant proteins are highly purified and are monodisperse.

Since self-assembly into a micellar structure is critical for carrying a drug, the critical

micelle concentration (CMC) for each construct was determined using a pyrene assay.

Dynamic light scattering (DLS) was used to verify that the oleosin molecules self-

assemble into micelles above the CMC (**Figure 2.3**). Measurements were taken at 10 μM,

above the CMC value for all variants. Oleosin-Throm-RGDS-30G(-) is designed to be

protease-sensitive, where the presence of thrombin results in the cleaving of both

hydrophilic arms and the exposure of the bioactive RGDS motif. MALDI-TOF-MS was

used to check the effect of thrombin cleaving reaction, and the resulting molecular weight

was as expected. DLS confirmed that the cleaved product still self-assembles to micelles

at 10 μM (**Figure 2.3**), and the thrombin cleaving reaction results in a 4 nm decrease in

the hydrodynamic diameter of the spherical micelle. Molecular weight, CMC, and

micelle size for all variants are listed in **Table 2.1**.

Table 2.1. Protein Characterization Results

Oleosin-	Expected Molecular Weight [Da]	Measured Molecular Weight [Da]	CMC [μM]	Hydrodynamic diameter [nm]	PDI
RADS-30G(-)	15376	15372	3.6	21.23	0.196
RGDS-30G(-)	15362	5358	3.6	20.96	0.189
Throm-RADS-30G(-)	16587 9101 cleaved	16574 9006 cleaved	3.1	19.57 16.03 cleaved	0.168 0.124 cleaved
Throm-RGDS-30G(-)	16573 9087 cleaved	16566 9083 cleaved	3.8	19.96 15.79 cleaved	0.165 0.117 cleaved
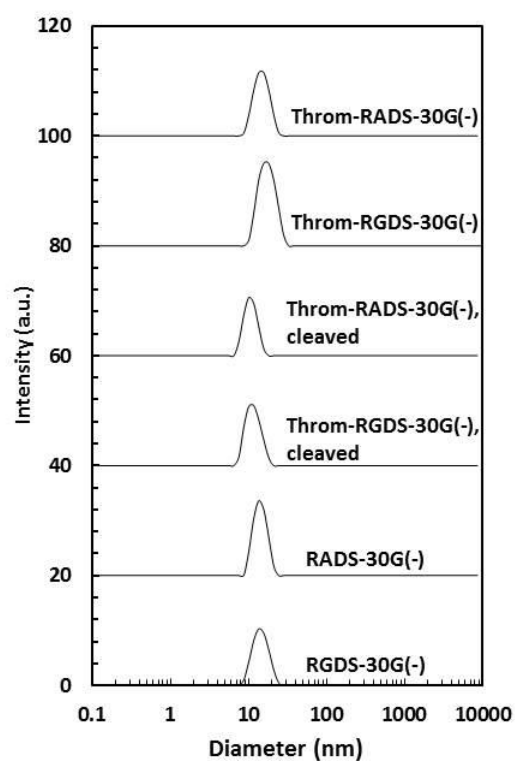
Figure 2.3. Micellar structures for all variants above their CMC were confirmed with DLS. All protein variant not cleaved by thrombin show a similar hydrodynamic diameter ~20 nm. Cleaved variants have hydrodynamic diameters ~16 nm.
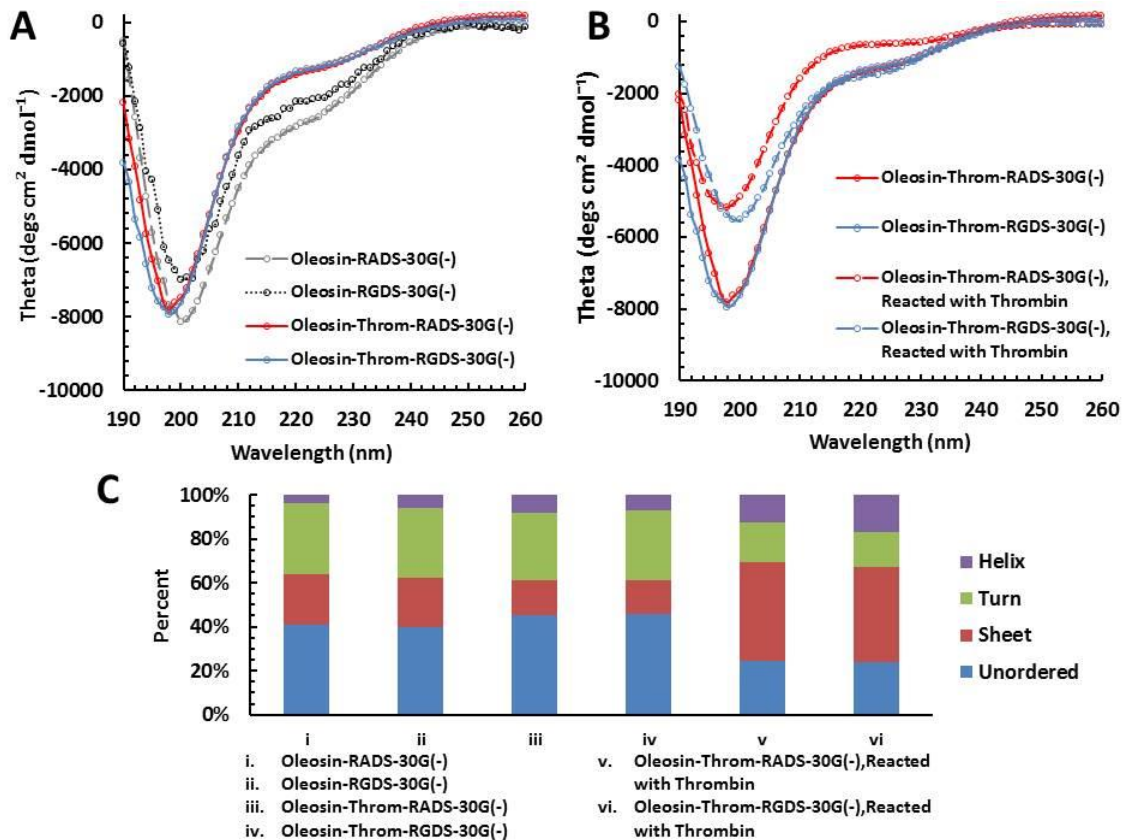
Figure 2.4. (A) CD spectra of all oleosin variants at 10 µM. (B) Comparison of CD spectra on Oleosin-Throm-RADS-30G(-) and Oleosin-Throm-RGDS-30G(-) before and after cleaved by thrombin. (C) CDSSTR analysis of the CD spectrum data that shows 40-50% of the secondary structure for all oleosin variants is unordered. The remaining oleosin molecules after thrombin cleaving reaction show relatively higher contents of helix and sheet structure.

The goal of this study is to explore the effect of integrin-binding motifs and protease cleavable sites on cell binding and uptake, and thus it is desirable for all protein variants to have similar secondary structures to minimize variation due to secondary structure. The secondary structure of proteins was elucidated with circular dichroism (CD) (**Figure 2.4A**). The spectrum data were analyzed with the CDSSTR algorithm on Dichroweb (**Figure 2.4C**).[83,84] When inserted at the same location, the motifs RADS and RGDS do not alter the overall secondary structure of the oleosin molecules. Both oleosin-RADS-30G(-) and oleosin-RGDS-30G(-) have a similar construct of ~40% unordered structure, ~20% β-sheet, ~30% turn, and <10% α-helix structure. The addition of thrombin cleavable domains only caused slight changes in the percentages of unordered and β-sheet structures: unordered structure increased by 5% and β-sheet structure decreased by 3%, whereas the percentages of turn and α-helix are roughly unchanged. The secondary structures of all protein variants in this study are very similar, suggesting differences in cellular uptake of protein variants is not due to structural differences.

2.3.2 Integrin Mediated Oleosin Micelle Uptake by Breast Cancer Cells

The MDA-MB-231 cell line, a human breast cancer cell line that has been shown to upregulate the RGDS binding integrin $\alpha_v\beta_3$ [63,85,86], was chosen to test the *in vitro* cell uptake of recombinant oleosin variants. After the breast cancer cell culture reached 60-70% confluency, DyLight-488 labeled protein micelles were introduced to the cell culture media at 10 μM. Protein micelles were allowed to interact with cells at 37 °C for 3, 6, 9 and 15 hours before unbound material was washed away. Cells were immediately fixed and labeled with fluorescently-tagged wheat germ agglutinin to visualize the cell membrane. Due to the unique advantage of producing images from a single focal plane, confocal microscopy was chosen over wide-field to visualize the uptake of oleosin micelles by breast cancer cells (**Figure 2.5**). For drug delivery, it is desirable to have the protein micelles being internalized by breast cancer cells, as opposed to attaching to the cell surface. To investigate the location of the protein micelles, a z-stack analysis was done by taking images at a z-step size of 0.5 μm for a total thickness of 30 μm for all samples. Each image reflects fluorescence signals coming from one focal plane. An example z-stack imaging series after a 15hr uptake of oleosin-RGDS-30G(-)is shown in **Figure 2.6** where image from a horizontal focal plane is shown at every 5 μm. The results indicate that the majority of the fluorescence comes from inside the breast cancer cells, while in some rare instances the protein micelles stayed adhered to the cell surface

after repeated washing and were crosslinked to the cell surface during the cell fixing step. This observation could mean that cellular uptake is rapid once protein micelles adhere to the cell surface, or that the adhered protein micelles were washed off prior to the fixation step.

The level of cellular uptake was quantified by comparing the percentage of cells with fluorescence signal from labeled oleosin (**Figure 2.7**). For the purpose of quantifying the oleosin micelles being internalized as opposed to adhering to the cell surface, only cells with fluorescence signals inside the cell were included for analysis.

First, the addition of the bioactive RGDS motif showed significantly increased uptake, when compared to the non-active RADS motif. After 3 hours of incubation, internalization levels of all oleosin variants were similar, with an average percentage of fluorescent cells at 9.1%. Following longer incubation periods, the internalization of the negative control oleosin-RADS-30G(-) slowly increased, until 16% fluorescent cells were labeled after 15 hours of incubation. However, the structurally similar, but the positive control which contained RGDS, oleosin-RGDS-30G(-), showed a significantly faster increase in cell internalization as a function of incubation time. Compared to the negative control, oleosin-RGDS-30G(-) increased cell internalization by factors of 1.8, 3.3 and 4.6 at 6, 9, and 15 hours of incubation time, respectively. Similar trends were observed when comparing the uptake of versions of oleosin-Throm-RGDS-30G(-) after thrombin

32

cleavage and the corresponding negative control containing RADS. The increased uptake

facilitated by the RGDS motif, compared to the RADS motif, indicates that the specific

sequence of recombinant oleosin is essential in this study. We show that the RGDS motif

can be successfully engineered into oleosin molecules and exhibits significant bioactivity

in the self-assembled spherical micelle form. A single RGDS motif added on each oleosin

molecule is able to effectively increase the cellular uptake of protein micelles. Oleosin-

RGDS-30G(-) is demonstrated to be a recombinant protein material that can self-

assemble, target breast cancer cells by increasing the cellular uptake.

To improve on previous research, here we illustrate the effect of protease-

triggered cell uptake by comparing the performances of oleosin-Throm-RGDS-30G(-)

and its cleaved form. Compared to the RGDS motif being protected, cleavage by

thrombin demonstrated a clear advantage in cell uptake starting at 6 hours of incubation.

After 15 hours of incubation, the exposure of the RGDS after thrombin cleavage led to a

4.2x increase in cell internalization compared to the non-active RADS control.

When comparing the uptake levels between oleosin-Throm-RGDS-30G(-) and its

RADS control, it appears that the 24 amino acid peptide on the hydrophilic arm did not

completely shield the RGDS motif from making contact with the cell surface. The

protected RGDS motif led to similar cellular uptake levels compared to the negative

control at 3 hours of incubation, but showed a two-fold increase in uptake at both 9 hours

and 15 hours of incubation. This observation suggests that when in a micelle, the hydrophilic arms of oleosin are flexible and highly solvated into the surrounding aqueous environment, thus allowing the embedded bioactive RGDS to come in contact with cell surface integrin receptors. However, 72% of the activity attributed to the RGDS motif is still shielded by the protection of 27 amino acids, and can only be released after thrombin activity, thereby offering greater control over the integrin-binding activities.

These results demonstrate that the oleosin-Throm-RGDS-30G(-) is a successful construct whose integrin-binding activity is triggered by a specific protease thrombin, and that oleosin is a valuable model for engineering responsive materials for targeted drug delivery applications. Aside from the ability of recombinant proteins to incorporate bioactive motifs, recombinant protein can also be conjugated with clinically proven drugs to increase tumor-specific uptake[38,56,70]. Recently, Bhattacharyya et al. demonstrated that the hydrophobic drug paclitaxel can be conjugated with recombinant chimeric polypeptides that self-assemble into nanoparticles, and resulted in increased systemic exposure of paclitaxel[38]. Nanoscale micelles can be readily made with multiple variants of recombinant protein surfactants each presenting its own bioactive moieties (e.g. cell targeting, imaging, therapeutics)[70,87], and are thus able to achieve both high specificity and direct applications. We believe the recombinant oleosin model offers much future potential for drug delivery purposes to be explored.

Oleosin-RADS-30G(-)
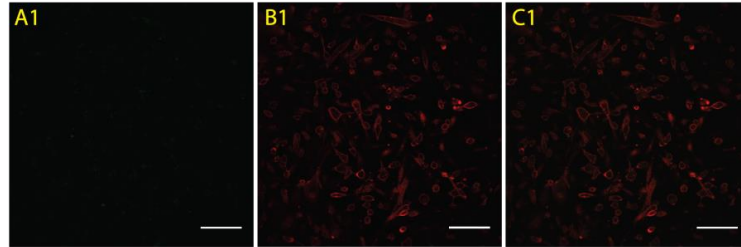
Oleosin-RGDS-30G(-)
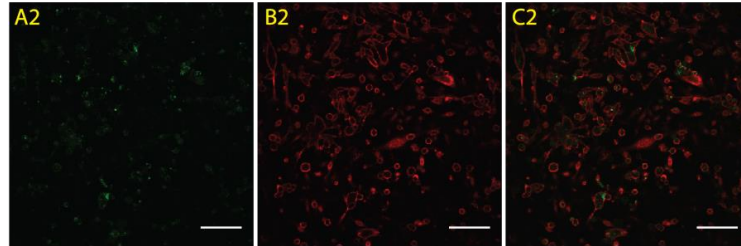
Oleosin-Throm-RADS-30G(-)
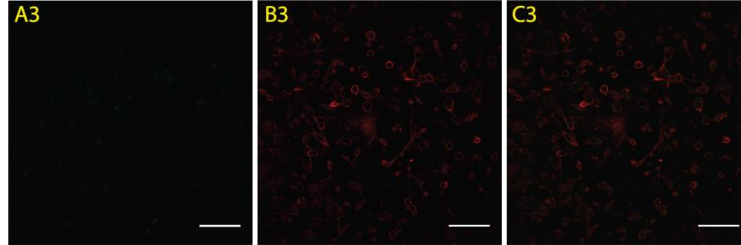
Oleosin-Throm-RGDS-30G(-)
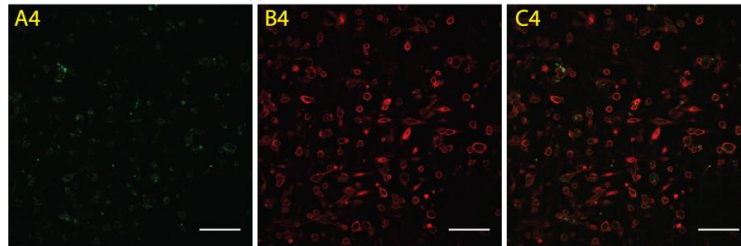
Oleosin-Throm-RADS-30G(-), Cleaved
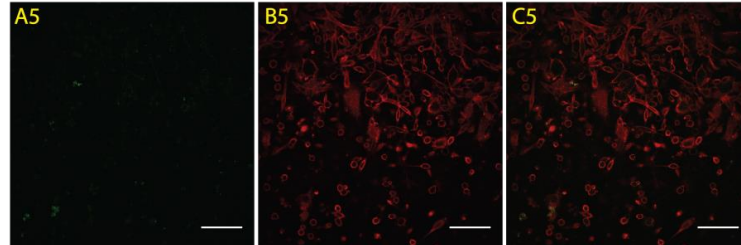
Oleosin-Throm-RGDS-30G(-), Cleaved
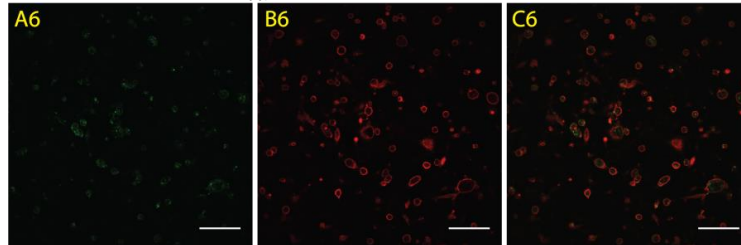
Figure 2.5. *In vitro* confocal microscopy images of DyLight 488 labeled oleosin micelle solutions uptake in MDA-MB-231 cells incubated at 37°C for 15 hours. Scale bars are 100 μm for all images. Cells were fixed with 4% PFA and labeled with Alexa Fluor 633. Images from the 488 nm channel, 633 nm channel, and merged channels were shown in panels A, B, and C, respectively. Cell membrane is shown as red and oleosin micelles are shown as green.
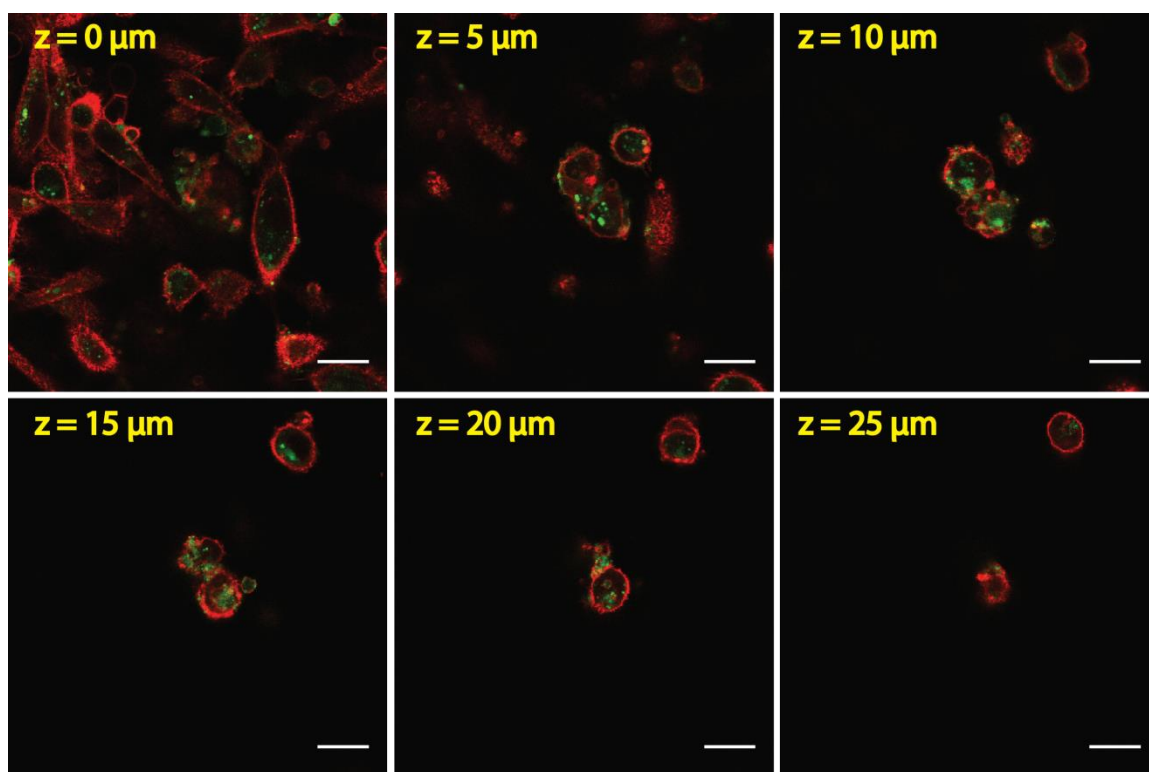
Figure 2.6. Confocal microscopy images for z-stack analysis same sample: Oleosin-RGDS-30G(-) on MDA-MB-231 cells, incubated for 15 hours under 37 °C. All scale bars represent 20 μm. Each image reflects fluorescent signals coming from one specific focal plane. Most protein micelles are internalized in breast cancer cell, while in some instances oleosin micelles adheres to the cell surface after repeated washing after the incubation period.
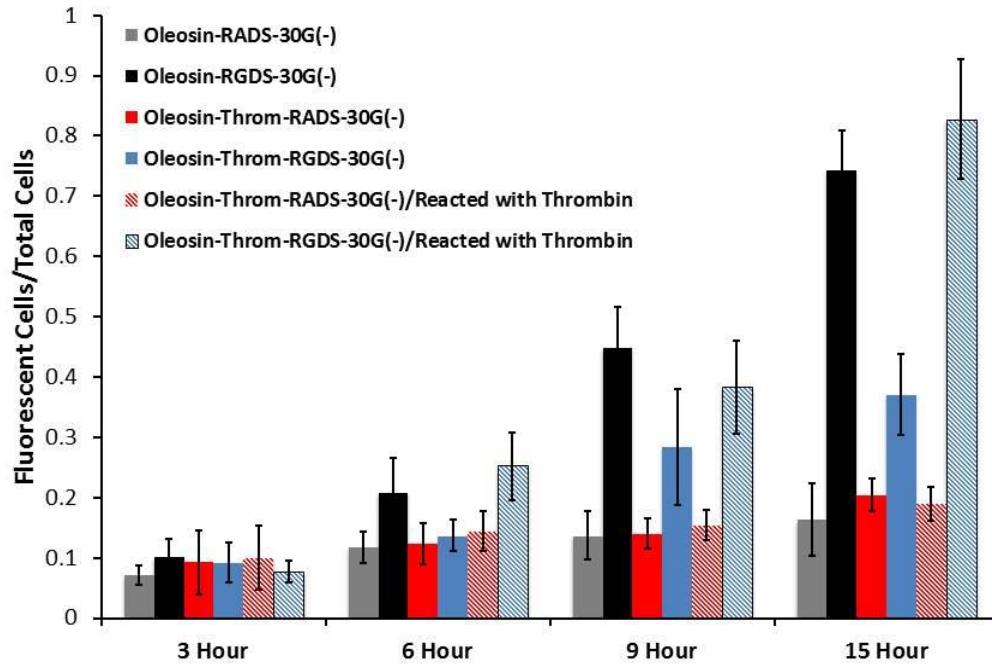
Figure 2.7. The addition of exposed RGDS led to a 4.6 times increase in cellular uptake over 15 hours, compared to the scrambled sequence of RADS. When RGDS motif was protected by 24 amino acids on the hydrophilic arm, increased uptake is observable starting from 9 hours of incubation where it showed 2.0 and 1.8 times increase at 9 hours and 15 hours, respectively. Oleosin-Throm-RGDS-30G(-), when fully reacted with thrombin, resembled very closely to Oleosin-RGDS-30(-) smaller in micellar size, and showed a similar 4.4 times increase in cellular uptake compared to Oleosin-Throm-RADS-30G(-) over 15 hours.
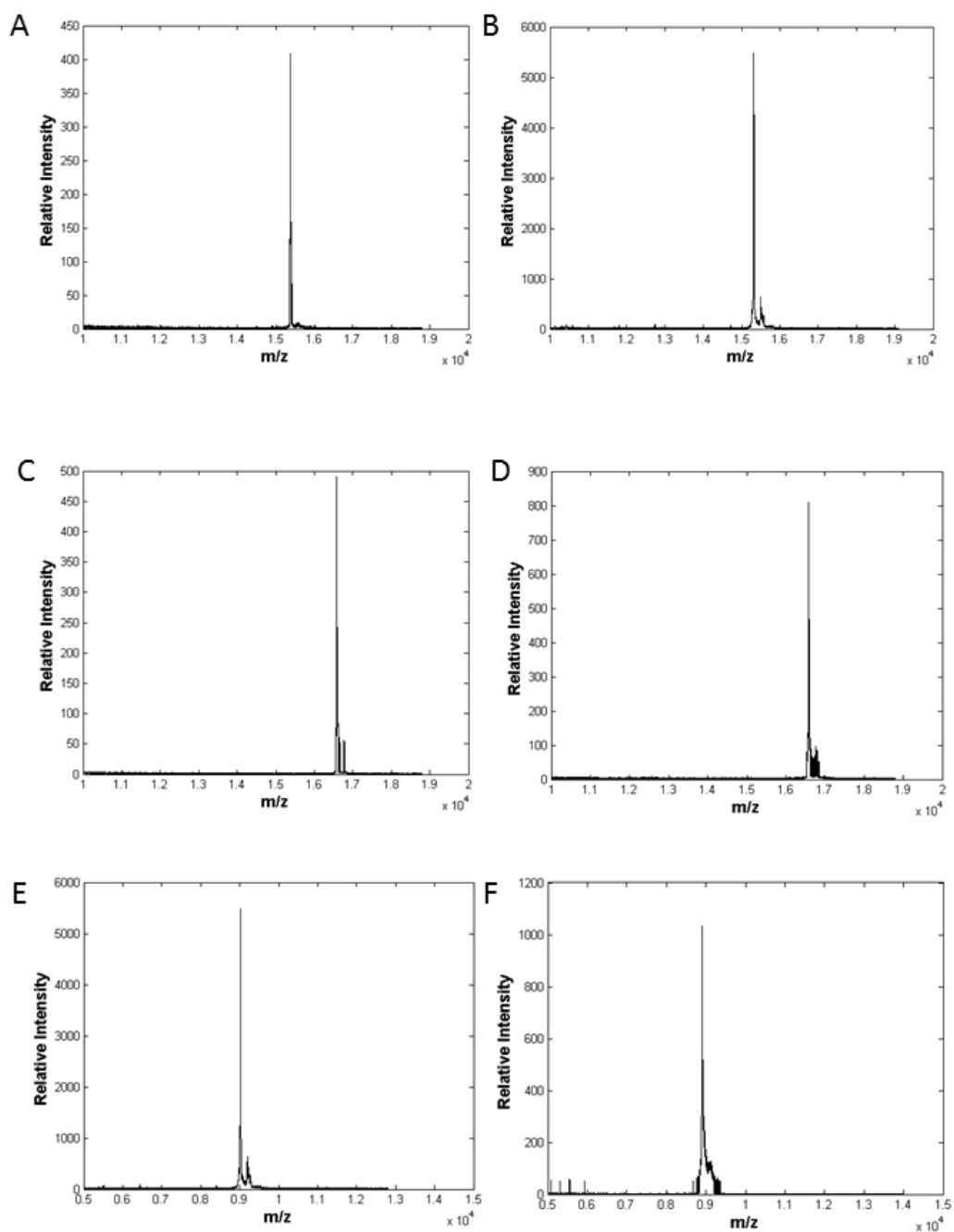
Figure 2.8. Mass spectra of (A) Oleosin-RADS-30G(-), (B) Oleosin-RGDS-30G(-), (C) Oleosin-Throm-RADS-30G(-), (D) Oleosin-Throm-RGDS-30G(-),(E) Oleosin-Throm-RADS-30G(-), cleaved with thrombin, and (F) Oleosin-Throm-RGDS-30G(-), cleaved with thrombin.
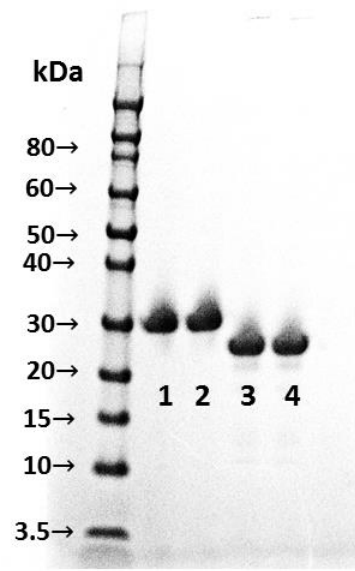
Figure 2.9. SDS-PAGE gel image demonstrates that the protein products were highly purified after IMAC purification. Lane 1: Oleosin-RADS-30G(-); Lane 2: Oleosin-RGDS-30G(-); Lane 3: Oleosin-Throm-RADS-30G(-); Lane 4: Oleosin-Throm-RGDS-30G(-). All protein variants are highly charged and therefore the bands did not match the expected molecular weight. Molecular weights were verified with mass spectrometry.
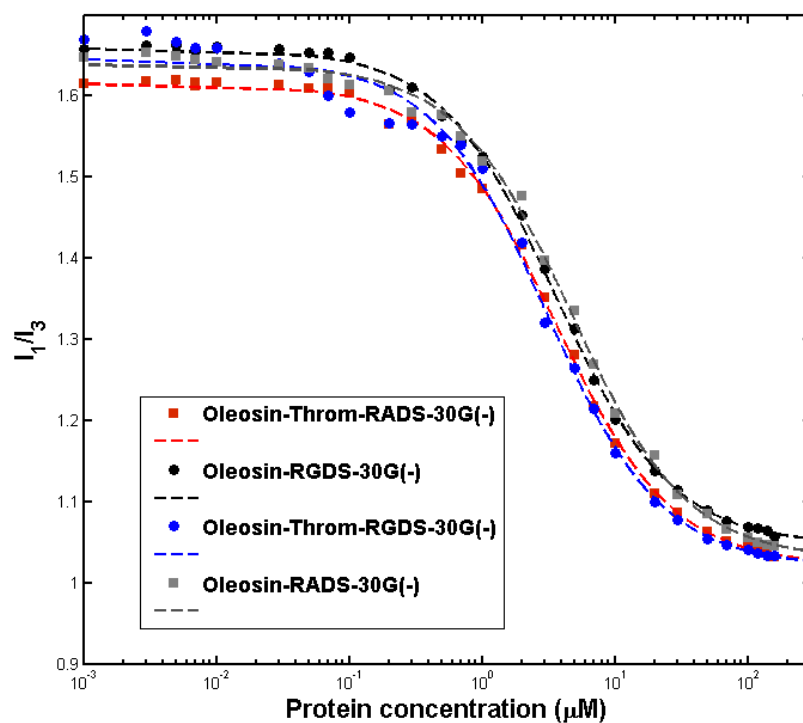
Figure 2.10. Pyrene assay results for all oleosin variants. The ratio of the first and third peaks of the emission spectrum (I_1/I_3) is plotted as a function of polarity of the protein solution. Data is fit with the SBE equation (Equation 1) and the inflection point is determined to be the critical micelle concentration (CMC).

2.4 Conclusions

In this study, we functionalized oleosin molecules to incorporate both integrin-binding motifs that could be activated by proteases. We have shown that adding the integrin-binding motif RGDS to the end of the oleosin molecule significantly increases its internalization by a breast cancer cell line MDA-MB-231. In addition, we created a protease-sensitive oleosin, oleosin-Throm-RGDS-30G(-), in which the bioactive motif RGDS is only fully exposed by the specific protease thrombin. This construct of oleosin serves as a flexible template in which multiple functionalizations can be engineered into the same molecule to achieve highly specific, regulated cell targeting and dynamic control over localized binding. Apart from self-assembled micelles, as shown in this study, oleosin can also be engineered to self-assemble into other structures including sheets, worm-like micelles, and vesicles, giving a wide range of possible structural biomaterials, all of which can be modulated with different dynamic switches. Genetically-engineered oleosin offers an exciting platform in which combinations of multiple bioactive sites can be precisely engineered and integrated as a part of the self-assembled structure.

2.5 Acknowledgements

Chapter 3. Enhanced Cell Killing by Paclitaxel-Loaded Oleosin

Abstract

Bioactive peptide ligands are effective and specific vectors that targets cell receptors, and have shown great potential as strategies for drug delivery. Conventional materials used as drug delivery matrices are chemically synthesized and difficult to functionalize, which compromises their capability in becoming smart drug carriers. Here, we present recombinant protein as a novel appoach to overcome these limitations. Previously, oleosin, a natural surfactant protein, has been engineered to self-assemble into spherical micelles and increase cellular uptake with a built-in RGDS motif. To enhance the cellular uptake performance and investigate the practicality of transforming oleosin from a surfactant to a drug carrier, oleosin is further genetically modified to incorporate a synergy peptide PHSRN and a cell-penetrating peptide HIV-1 Tat. The resulting modified oleosin variants retain the spherical micellar structure in aqueous environments, and can increase uptake by breast cancer cells by as much as sixfold compared to the

negative control. Upon encapsulation of an anti-cancer drug paclitaxel, oleosin drug carriers can achieve a twofold cell killing than free form paclitaxel in 15 hours.

3.1 Introduction

In order for pharmaceutical agents to be safe and effective, the properties desired for drug carriers are that they are biodegradable, can target specific disease cells, and carry a therapeutic cargo.[4–6] A variety of chemically synthesized materials including polymersomes, phospholipids, and dendrimers have been explored for their potential to construct smart drug carriers. Despite the promising results seen for conjugating cell targeting peptide sequences to these materials, the size and location of the bioactive inserts remained limited, and the uniform quality of synthesized product continued to be difficult to solve in practice.[11,24,88,89]

Here we present an alternative strategy of designing recombinant protein towards smart drug carriers. Molecular biology provides the precise control over the amino acids in the end protein product, which gives full freedom in functionalizing a protein molecule, while simultaneously ensuring that all protein molecules are of the same size. Previously, our lab has established a library of recombinant protein variants from the

naturally occurring protein oleosin. Oleosin is a group of natural surfactants and has an unique triblock structure, where the hydrophobic domain is centered between two hydrophilic arms at the N- and C- termini.[27] Our laboratory demonstrated that recombinant oleosin variants and self-assemble into different nanoscale structures including spherical micelles, worm-like micelles, sheets, and vesicles.[30] A particular subset of oleosin (the -30G family) where the hydrophobic part was trimmed to 30 amino acids, self-assemble into nanoscale spherical micelles and was explored for its ability to target breast cancer cells. Previously, we have demonstrated that oleosin can be mutated towards drug delivery applications by creating a variant where the integrin-binding motif RGDS was only active when triggered by thrombin, and successfully increased cellular uptake in breast cancer cells.[90] This work explores strategies to enhance the performance of oleosin internalization, and subsequent cell killing with an encapsulated anti-cancer drug paclitaxel.

PHSRN (Pro-His-Ser-Arg-Asn) is a ligand found in the 9th type III domain of fibronectin, adjacent to the 10th domain that contains the RGD motif, and has been found to act synergistically with RGD to enhance cell adhesion and spreading.[55,91,92] Previously, studies have been done to mimic the natural distance of 30-40Å between RGD and PHSRN by inserting various numbers of glycine as spacers.[55,93,94] In a 2007 study done by Schmidt and Kao, it is found that the synergy is most noticeable when 13 glycines are added as interposition spacers.[93] Most previous studies on PHSRN were done on PEG

and lipids, , and were limited by the purity of PEG/lipid-peptide ligand conjugates from peptide synthesizers. [49,54,94]

Besides targeting the disease cells to reducing systematic side effects, intracellular delivery of therapeutic molecules is another key problem in drug delivery. Many pharmaceutic agents require intracellular delivery to exert their therapeutic actions. For example, mitochondria, nuclei and lysosomes are intracellular targets for pro-apoptotic anticancer drugs.[7,24,95] However, cell membranes prevent protein and nanoparticulate drug carriers from entering cells, as well as causing lysosomal degradation, unless an active transport mechanism is present. A promising approach to overcome cellular barrier was the discovery of cell-penetrating peptides (CPPs), where certain peptides can be tethered to drugs of interest and translocate across the plasma membrane. Tat peptide, a short sequence derived from the transcriptional activator protein encoded by human immunodeficiency virus type I (HIV-1), is a frequently used CPP that's been shown to carry cargoes of various molecular weights.[23,50,96–99] The limitations of current research on using Tat-peptide to enhance intracellular delivery are challenges in conjugating Tat-peptide to drugs and drug carriers.

To improve previous research, here we present several variants of oleosin enhanced by PHSRN bioactivity and a cell-penetrating peptide HIV-1 Tat, that self-assemble into spherical micelles and are capable of carrying a drug payload. The naturally occurring protein surfactant oleosin was mutated to incorporate the bioactive

46

RGDS on one hydrophilic arm, with PHSRN or Tat-peptide on the other hydrophilic arm. This family of recombinant proteins can be blended at different ratios and are able to encapsulate an anti-cancer drug paclitaxel and achieve effective cell killing on breast cancer cells. This study demonstrates the potential for oleosin variants to have a major impact in the design of smart drug carriers.

3.2 Materials and Methods

3.2.1 Protein Design and Expression

Oleosin Gene Construction and Expression: Genetic modification were purchased through Integrated DNA Technologies and the genes were inserted into the expression vector pBamUK and later transformed into the BL21 (DE3) strain of *E. coli* for expression. DNA sequencing was performed before protein expression by the *E. coli* strain BL21 DE3 (Stratagene) controlled by the *lac* promotor on the pBamUK. Cultures are grown at 37°C in Luria Broth (LB) with 50 µg/ml kanamycin until OD_{600} reaches 0.6. Isopropyl β-D-thiogalactoside (IPTG) was added to the culture to a final concentration of 1.0 mM to induce the expression of oleosin. Cells were collected by spinning down the culture at 15,000g for 15min and were kept frozen at -20°C until purification. All oleosin variants presented in this study adds a 6-histidine tag to the C-terminus of oleosin molecule which facilitates purification through immobilized metal affinity chromatography (IMAC). All variants of proteins in this study express solubly. Yields for

all variants in this study were within the range of 40-100 mg of purified protein per liter of culture. All oleosin variants were stable in buffered solutions (pH~7.4) for 4 weeks in 4°C, and for at least 48 hours in 37°C.

Protein Purification: All oleosin strands in this study have 6-Histidine tag to the C-terminus and were purified with Ni-NTA columns (Pierce). All protein strands in this study are soluble and can be purified with the protocol suggested by Vargo et al.[31] In brief, frozen protein pellet was re-suspended in B-PER Bacterial Protein Extraction Reagent (Fisher). After spinning down at 15,000g for 15min, the supernatant was left to bind with the Ni-NTA resin for at least 1 hour. Then the column was repeatedly washed and protein sample was eluted out.

3.2.2 Protein Characterization

SDS-PAGE: To determine the purity of protein samples, purified oleosin samples were loaded on NuPAGE Novex 4-12% Bis-Tris mini gels (Invitrogen) in 2-(N-morpholino)-ethanesulfonic acid (MES) buffer. SimplyBlue SafeStain (Invitrogen) was used to stain the gel following electrophoresis. The gel was imaged with a Kodak Gel Logic 100 imaging system.

Mass Spectroscopy: To prepare matrix solution, sinapinic acid was added to 50:50 (v/v) ACN: [0.1 vol.% TFA in water] to a final concentration of 10mg/ml. 0.5 µL of matrix solution was added to Bruker AnchorChip, immediately followed by 0.5 µL of oleosin solution. Solutions were mixed on the AnchorChip using a pipet tip and air-dried. Samples were analyzed with matrix-assisted laser desorption ionization (MALDI) mass spectroscopy (Bruker, PennChemistry Mass Spectrometry Facility).

Circular Dichroism (CD): An AVIV 410 spectrometer (AVIV Biomedical, Inc.) was used to collect UV CD spectra at 25°C in a 1 mm quartz cell. The protein sample concentration was 10 µM in 50 mM phosphate and 140 mM NaF. The CD data was analyzed with the CDSSTR algorithm using Dichroweb.

Critical Micelle Concentration (CMC) - Pyrene Assay : The critical micelle concentration (CMC) was determined by pyrene assay, where pyrene was used as a fluorescence probe that prefers non-polar environments.[78] The ratio of the first and third peaks of the emission spectrum (I_1/I_3) decreases as a function of polarity of the protein sample solution, and this ratio is considered as an index of polarity in the environment.[78–80] The pyrene assay data were fit with a sigmoidal Boltzmann equation (SBE) suggested by Aguiar et al, and the CMC value is determined to be the inflection point.[81]

Dynamic Light Scattering (DLS): 700 µL of protein sample was added to a small-volume cuvette cleaned with compressed air. DLS was performed with a Malvern Zetasizer Nano ZS (Westborough, MA).

Oleosin Labeling: Oleosin was labeled with 10 molar-fold excess of amine-reactive fluorophore Dylight 488 NHS-ester (Thermo Scientific) according to manufacturer's protocol. Excess dye was removed by repeated dialysis against PBS until background fluorescence was undetectable.

Oleosin Blending: Oleosin were blended at 20 µM by gently mixing the micellar solutions, sonicating for 20 seconds, and let recover at room temperature for at least 10 minutes. Blended samples were checked under DLS to verify self-assembly structure.

3.2.3 Mammalian Cell Culture

The human breast cancer cell line MDA-MB-231 (ATCC HTB-26) was acquired from the University of Pennsylvania Cell Center. MDA-MB-231 cells were cultured in RPMI 1640 (Life Technologies 22400, Carlsbad, Ca) supplemented with 10% heat-inactivated fetal bovine serum (Sigma Aldrich F2442, St. Louis, MO) and 100 units/ml penicillin and

100 µg/ml streptomycin (Life Technologies 15140) on tissue-culture treated plastic in a 37°C humidified incubator with 5% CO_2.

When MDA-MB-231 cells reach 60-70% confluency, the growth media was aspirated and the cell culture was triple washed and left in RPMI 1640 without phenol red (Life Technologies 11835). Labeled oleosin micelle solution was added to the cell culture to a final concentration of 10 µM. After the internalization period (3-15hrs), the cell culture was triple washed with RPMI 1640 media (no phenol red).

Following internalization, the cell culture was fixed with fixed with 4% PFA and cell membrane was labeled with Wheat Germ Agglutinin - Alexa Fluor 633 Conjugate (Invitrogen W21404), using the protocol provided by the manufacturer.

3.2.4 Cellular Uptake Study

Confocal Microscopy: Cell cultures were imaged with a Leica TCS SP5 confocal microscope (Bioengineering Confocal and Multiphoton Imaging Core Facility, UPenn). Fixed cell cultures on a tissue-culture treated surface were directly imaged with a HCX IRAPD L 25x/0.95 W dipping lens. Dylight 488 and Alexa Fluor 633 were excited using 10% strength Argon laser and HeNe laser, respectively. Images were acquired at 400 Hz

scanning frequency at slice thickness of 296.40 nm. Gain was set to be 749.9 V and 777.1

V for the 633 and 488 channels, respectively. Offset was kept at 0.0% for all acquisitions.

Flow Cytometry: Flow cytometry was performed on live cells with BD LSRII (Upenn

FCCSRL) immediately following incubation time. Sample population of each run was

kept at 10,000 cells. For every flow cytometry experiment, blank data was collected by

running cell culture treated with PBS for all four time durations (3, 6, 9, and 15 hours).

Then cell culture treated with RADS-30G(-) for the same four time durations were tested

as negative controls. Negative control results were compared to historical data and

experiment only proceeded when negative control error fell within 5%. Flow cytometry

histogram was collected from each run and analyzed by FlowJo. Cellular uptake was

quantified by first eliminating background signal measured by PBS blank, then taking the

weighted average of fluorescence per cell.

3.2.5 Paclitaxel Encapsulation

Paclitaxel (ThermoFisher P3456) was resuspended in 200 proof ethanol and carefully

injected into oleosin micellar solution at concentration of 20 μM. The mixture was then

briefly sonicated for 20 seconds and let sit for 10 minutes in room temperature. The

mixture was then dialyzed against PBS. Protein concentration was measured by

Nanodrop and adjusted to 10 μM. Each sample was verified to be in micellar solution form with Dynamic Light Scattering (DLS) before dosed onto cells. The encapsulation efficiency of paclitaxel by oleosin was measured with a labeled version of paclitaxel (ThermoFisher P22310). A calibration of paclitaxel fluorescence signal vs. concentration was established with a Fluoromax-4 spectrophotometer (Horiba Jobin Yvon), and the procedure described here resulted in a 3.21±1.2% encapsulating efficiency of paclitaxel.

3.2.6 Cell Viability Assay

After the MDA-MB-231 cells reached 60% confluency, the cell culture media was aspirated away, triple washed and replaced by RPMI 1640 without phenol red. PX-loaded protein micelle solution was added to the cell culture at working PX concentrations of 35, 105, and 350 nM. Following an incubation time of 3-15 hours, cell culture was trypsinized and resuspended in RPMI 1640 without phenol red, mixed with equal volume of 0.4% trypan blue solution that only stained dead cells. The mixture solution was injected into a hemacytometer (Reichert Bright-Line) and incubated at room temperature for 90 seconds. The total number of cells and number of stained cells were counted under an optical microscope within 1 minute after incubation. The cell viability was recorded as (total number of cells – number of stained cells)/(total number of cells).

3.3 Results and Discussions

3.3.1 Oleosin Design, Self-Assembly and Secondary Structure

Previously, we have created two variants from oleosin-30G(-) that serve as controls. The positive control RGDS-30G(-) contains an integrin-binding motif RGDS to the N-terminus and has been observed to increase uptake by breast cancer cells by a factor of 4.6. The negative control RADS-30G(-) contains an nonactive peptide sequence RADS (Arg-Ala-Asp-Ser) at the same location and does not increase protein uptake significantly over 15 hours (**Figure 3.1**).

In this current study, initially three further variants were created from oleosin 30G(-) to incorporate PHSRN and Tat-peptide and study their effects on enhancing cellular uptake. PHSRN-30G(-) was designed to have PHSRN (Pro-His-Ser-Arg-Asn) attached to the end of the N-terminus hydrophilic arm. To study the colocaliztion effect of PHSRN and RGDS ligands, PHSRN-30G(-)-RGDS was engineered to have PHSRN and RGDS on the same oleosin molecule, with PHSRN at the N-terminus and RGDS (Arg-Gly-Asp-Ser) at the C-terminus. RGDS-30G(-)-Tat incorporated RGDS and Tat (Gly-Arg-Lys-Lys-Arg-Arg-Gln-Arg-Arg-Arg-Pro-Gln) at the ends of the N- and C-terminus hydrophilic arms, respectively (**Figure 3.1**)

To monitor the purity of the recombinant oleosin products and confirm that the mutated oleosin has the exact peptide sequence as designed, SDS-PAGE and MALDI-TOF (Matrix-Assisted Laser Desorption/Ionization – Time of Flight) were performed on each sample after purification. Both tests confirmed that the recombinant oleosin products are highly purified and monodisperse in molecular weight (**Figure 3.2**). CMC (critical micelle concentration) was determined using a pyrene assay (**Table 3.1**). Dynamic light scattering (DLS) was used to verify that the protein self-assembles into micellar structures above CMC (**Figure 3.3**). The secondary structures were analyzed by CDSSTR and shown in **Figure 3.4**.

Table 3.1. Protein Characterization Results

Oleosin-	Expected Molecular Weight [Da]	Measured Molecular Weight [Da]	CMC [μM]	Hydrodynamic diameter [nm]	PDI
RADS-30G(-)	15376	15372	3.6	21.23	0.196
RGDS-30G(-)	15362	5358	3.6	20.96	0.189
PHSRN-30G(-)	15538	15531	3.4	19.97	0.192
PHSRN-30G(-)-RGDS	15954	15950	3.6	20.22	0.190
Tat-30G(-)	16644	16638	3.3	22.01	0.197
RGDS-30G(-)-Tat	17069	17062	3.4	21.98	0.196
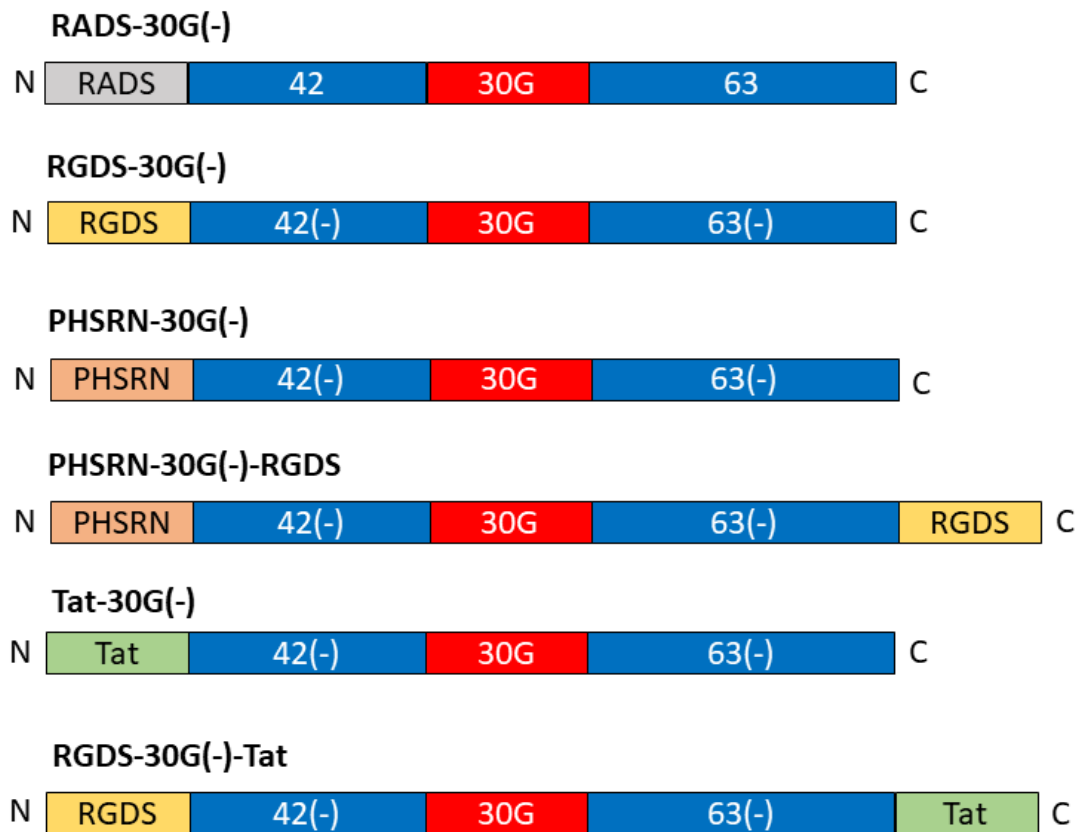
Figure 3.1. Molecular view of 30G(-) variants functionalized with PHSRN and Tat.
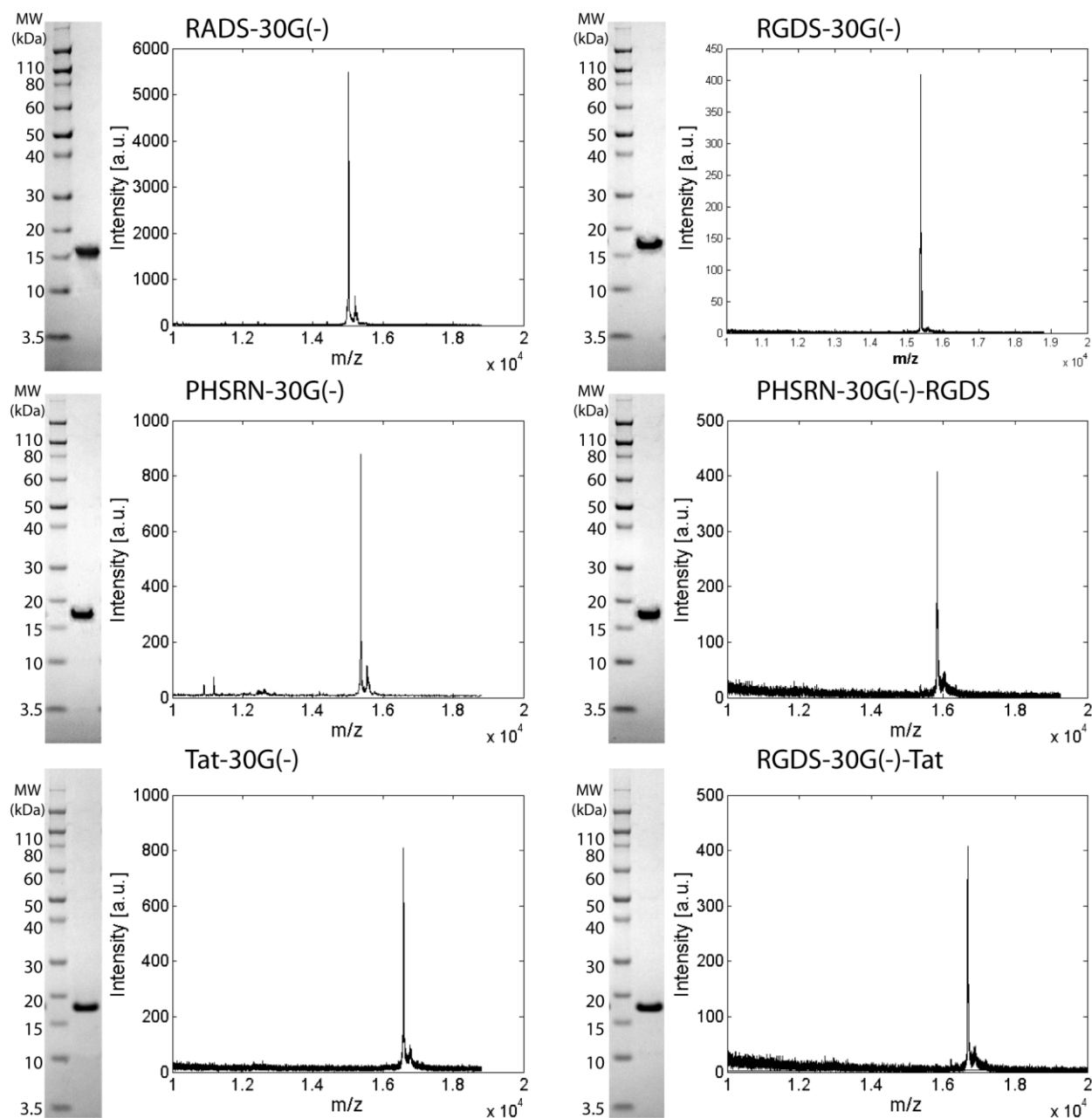
Figure 3.2. Protein characterization and MALDI-TOF spectrum. Protein purity was measured after IMAC purification to be >95% with SDS-PAGE. Protein molecular weight was confirmed by MALDI-TOF and closely match expected weights of protein variants in Table 3.1
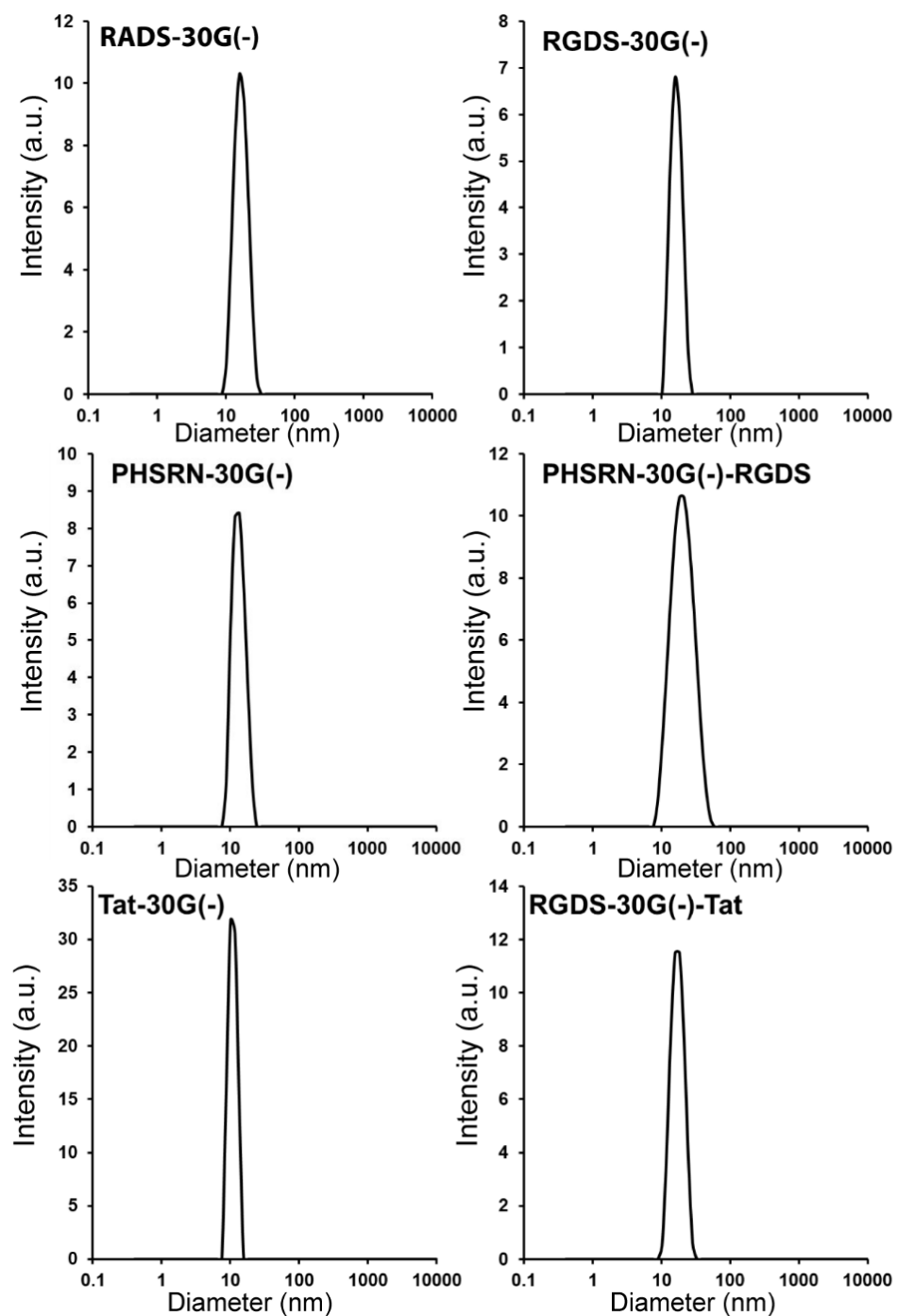
Figure 3.3. Dynamic Light Scattering of all recombinant oleosin variants. Measurement taken at 10 μM and DLS spectrum suggests spherical micellar formation. Hydrodynamic diameters and PDI are listed in Table 3.1.
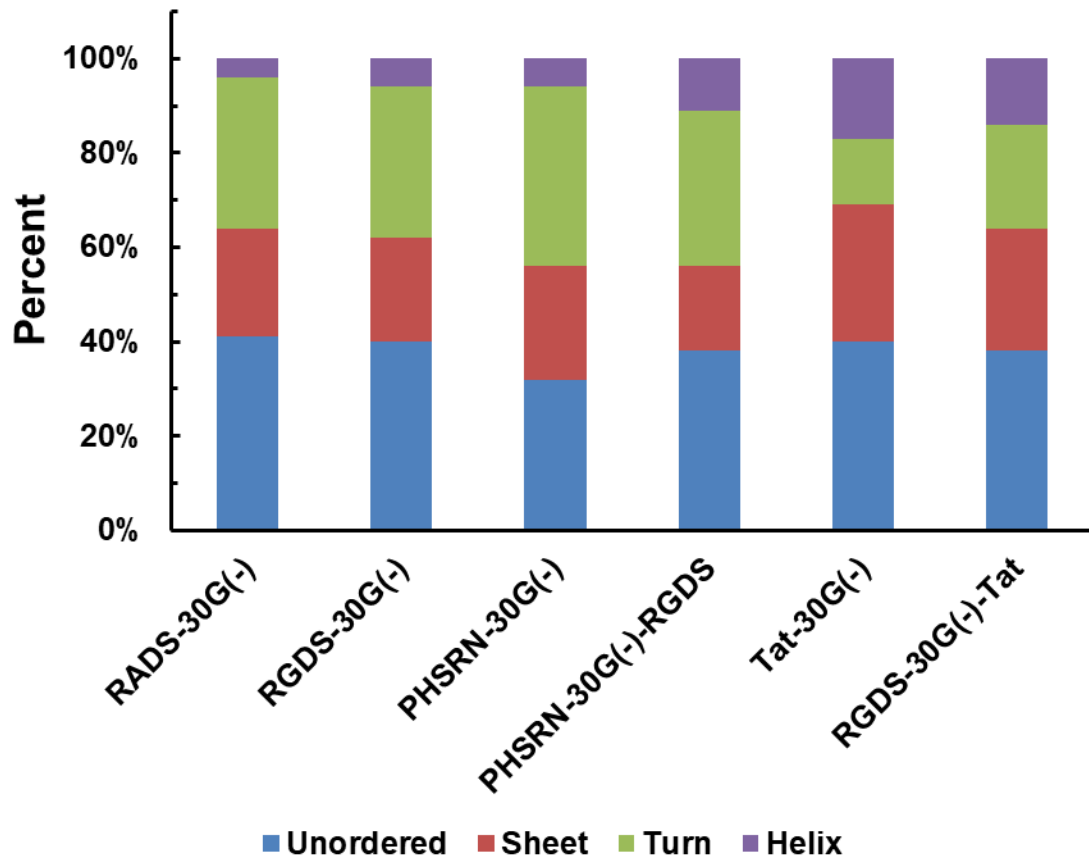
Figure 3.4. Secondary structure of protein variants. CDSSTR analysis shows 30%-40% of the secondary structure for all oleosin variants are unordered, while the Tat-30G(-) has a slightly higher sheet structure.

3.3.2 Oleosin Micelle Uptake by Breast Cancer Cells Measured with Flow Cytometry

The cellular uptake study was carried out on MDA-MB-231 cell line, a human breast cancer cell line that has been shown to upregulate the RGDS binding domain $\alpha v \beta 3$ [63,85,86]. After the breast cancer cell culture reached 60-70% confluency, DyLight-488 labeled protein micelles were introduced to the cell culture media at 10 μM. The cell culture was

59

then put back to 37 °C incubation to mimic physiological conditions. Time points were taken at 3, 6, 9 and 15 hours before unbound material was washed away. Cells were then immediately resuspended and analyzed with flow cytometry, or immediately labeled to visualized the cell membrane and fixed for confocal microscopy.

First, the flow cytometry quantification methods was validated by comparing to the previously published the cellular uptake of the positive and negative controls by the MDA-MB-231 cell line, where cellular uptake was quantified via cell counting.[90] The flow cytometry results on cellular uptakes of previously published variants resemble the trends observed through cell counting, indicating that an additional RGDS motif increased the cellular uptake by 2.5x in 15 hours. A representative flow cytometry spectrum is shown in **Figure 3.5** and the uptake of each variant shown in **Figure 3.6**.

The additional Tat-peptide on the C-terminus showed significantly enhanced cellular uptake at all time points. Compared to the RGDS alone, the Tat-peptide increases cellular uptake by factors of 1.32, 1.43, 1.86, and 1.93 at 3 hours, 6 hours, 9 hours, and 15 hours respectively. The Tat-peptide acted as a effective cell penetration peptide that enhanced the performance of the bioactive ligand RGDS.

On the other hand, the additional PHSRN on the N-terminus did not lead to significant different cellular uptake when compared to the negative control RADS-30G(-). PHSRN-30G(-)-RGDS variant possessed co-localized PHSRN and RGDS motifs and performed similarly to the RGDS-30G(-), where only the RGDS motif and present. These

results suggest that PHSRN alone does not stimulate cellular uptake. To further

investigate the effect of co-localized RGDS and PHSRN, PHSRN-30G(-) and RGDS-

30G(-) were blended at various ratios for the cellular uptake study, which is discussed at

the following section.
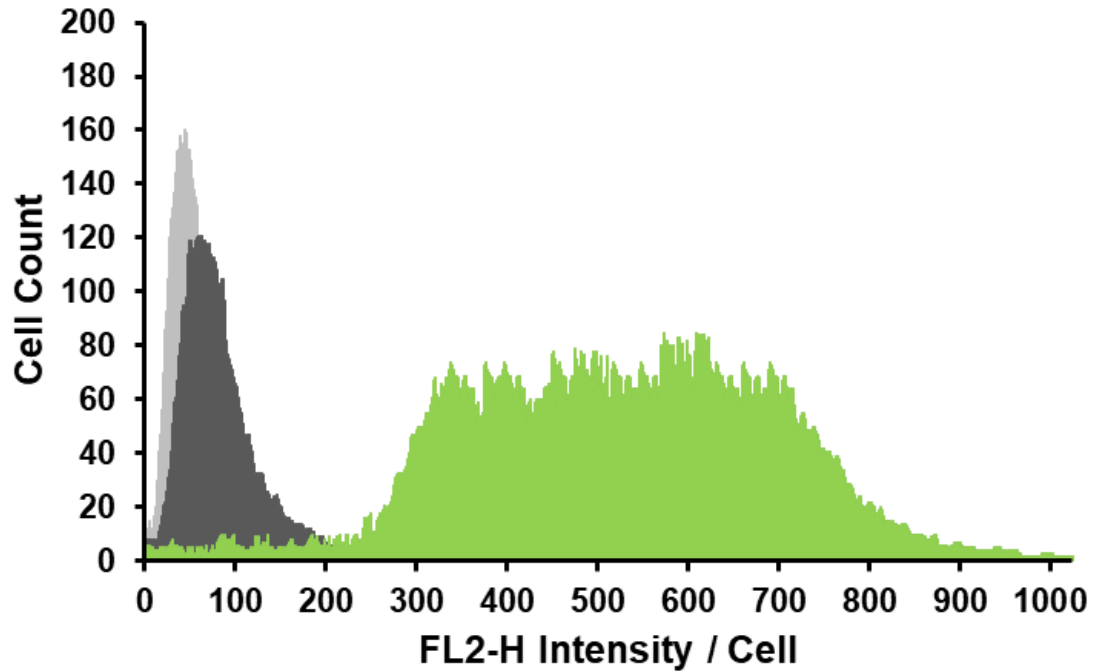
Figure 3.5. Flow cytometry histogram showing fluorescence of MDA-MB-231 cells under treatments for 15 hours. Grey histogram corresponds to PBS as blank, black histogram corresponds to the negative control 10 μM RADS-30G(-), and green histogram corresponds to 10 μM RGDS-30G(-)-Tat.
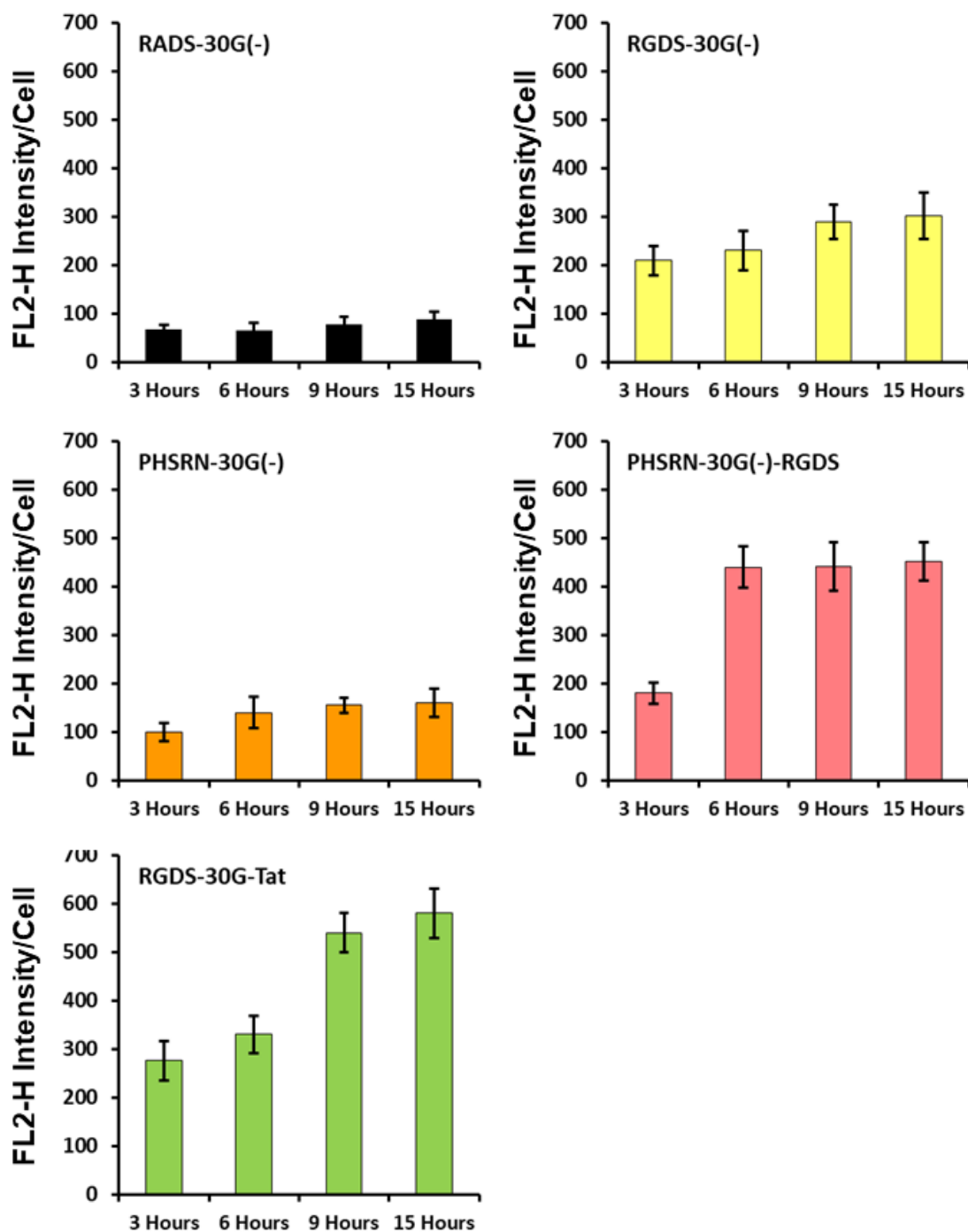
Figure 3.6. Cellular uptake of oleosin micelles quantified with flow cytometry.

3.3.3 Effect of RGDS vs. PHSRN Ligand Concentration on Cellular Uptake

To investigate the effect of the ligand ratio between RGDS and PHSRN on cellular uptake, RGDS-30G(-) and PHSRN-30G(-) were blended at ratios of 7:3, 5:5, and 3:7, adjusted to a final concentration of 10 μM and tested for cellular uptake by MDA-MA-231 cells at 37 °C for 15 hours. The flow cytometry results are shown in **Figure 3.7**, where the uptake of RGDS-30G(-), PHSRN-30G(-) and PHSRN-30G(-)-RGDS were included as comparison.

While the peptide ligand concentration was kept at 10 μM, an interesting observation was the comparison of cell uptake levels of 5:5 RGDS-30G(-):PHSRN-30G(-), PHSRN-30G(-) and RGDS-30G(-). The 5:5 blend construct is able to reach the same uptake level as the positive control RGDS-30G(-), and suggests that the PHSRN act synergistically with RGDS on integrin mediated cell uptake. The blend of 7:3 RGDS-30G(-):PHSRN-30G(-) resulted in significantly higher cellular uptake than other blend ratios. The cellular uptake of this particular blend at the end of 15 hours led to a 1.5x increase than the positive control RGDS-30G(-), and was statistically parallel to the PHSRN-30G(-)-RGDS, where the ligand concentration is doubled. The behavior of cell uptake based on ligand ratios may be explained by the spatial distance between ligands.

63

Altering the ratios between RGDS and PHSRN effective changes the mean spatial distance between the two ligands, and in this work the 7:3 blend may resemble the natural distance between PHSRN and RGD in fibronectin. The comparison between the 7:3 and 3:7 blends suggest that RGDS is essential in achieving integrin mediated cell uptake, which agrees with previous work.
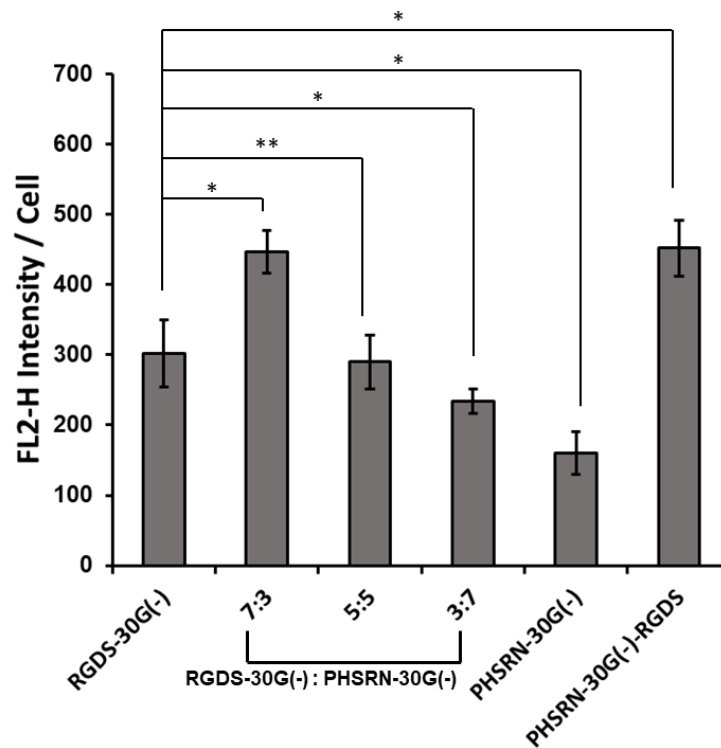
Figure 3.7. Cellular uptake of blended RGDS-30G(-) and PHSRN-30G(-) variants at a final concentration of 10 μM, by MDA-MB-231 cells at 37°C for 15 hours. * indicates p<0.001 and ** indicates p = 0.41

3.3.4 Paclitaxel Encapsulation

Paclitaxel encapsulation were carried out to investigate the cargo ability of oleosin micelles. To test the encapsulation efficiency of oleosin micelles, paclitaxel was fluorescently labeled, mixed with oleosin micellar solution by brief sonication, then let recover at room temperature for at least 10 minutes. A fluorescent level vs. paclitaxel concentration was established with a Fluoromax-4 spectrophotometer (Horiba Jobin Yvon) and used to obtain paclitaxel concentration after encapsulation. The encapsulation efficiency of oleosin micelles were found to be around 3.2%, and samples were adjusted for paclitaxel concentration before used for cell viability tests.
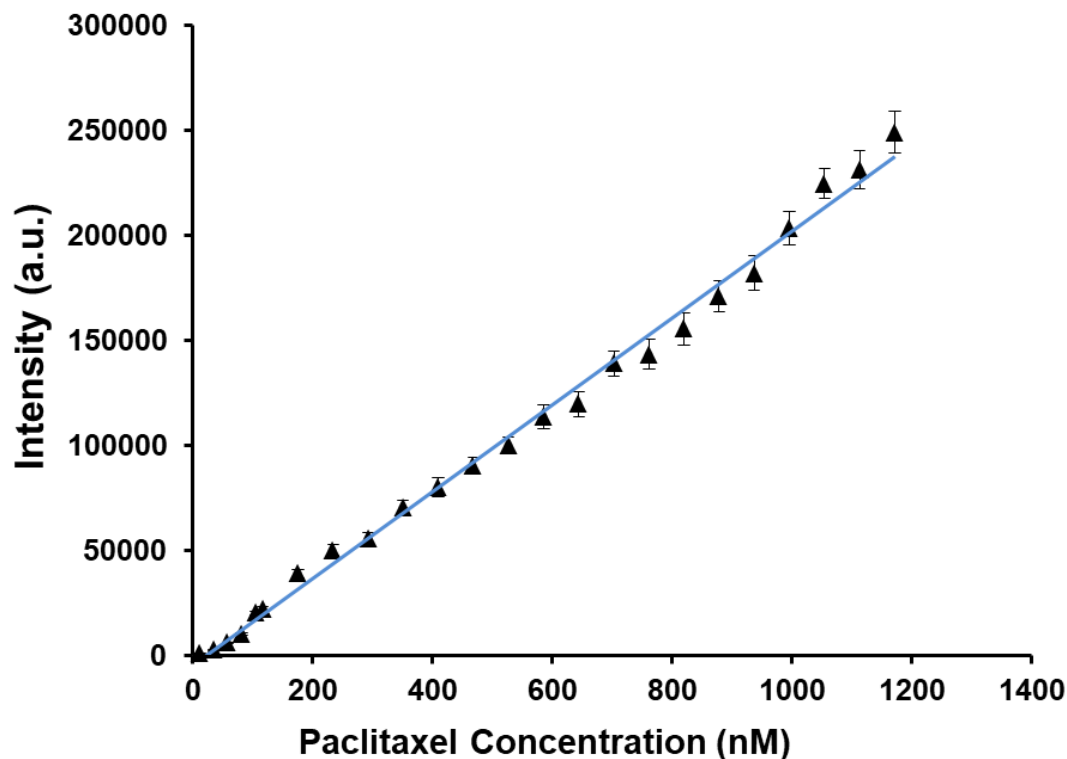
Figure 3.8. Paclitaxel emission intensity (excitation 496 nm, emission 524) vs. concentration. Data was linear fitted and the calibration equation is y= 206.7x – 4686, R^2 = 0.99.

3.3.5 Integrin Mediated Cell Killing

Oleosin micelles with a paclitaxel cargo were dosed on MDA-MB-231 cells at paclitaxel concentrations of 35 nM, 105 nM, and 350 nM, and cell viability were collected at 3 hour, 6 hour, 9 hour, and 15 hour time points, shown in **Figure 3.9**. Drug delivery was visualized by encapsulating paclitaxel with fluorescently labeled oleosin and imaged with confocal microscopy, shown in **Figure 3.10**. The z-stack series images indicate effective cell internalization of oleosin micelles, and some degree of localization within the cell.

The cell killing rate from the viability study follows the trend observed with flow cytometry. Variants that have high cellular uptake levels observed in flow cytometry also have high cell killing rates. PBS and RADS-30(-) without paclitaxel solutions were tested as negative controls, and indicated that oleosin itself does not exhibit cell killing abilities in the absence of paclitaxel.

Effect of functionalized oleosin micelles as drug carriers can be observed by comparing cell viability of breast cancer cell treated with paclitaxel encapsulated in oleosin micelles to the cells treated with paclitaxel solution at the same concentration. At 15 hours, the positive control RGDS-30G(-) improves the cell killing rate by 1.3x with 35 nM and 105 nM paclitaxel, and by 1.6x with 350 nM paclitaxel. Variant PHSRN-30G(-) where only PHSRN is present does not significantly facilitate cell killing, where the synergy between PHSRN and RGDS as demonstrated by variant PHSRN-30G(-)-RGDS increased cell killing by 1.18x with 350 nM paclitaxel at 15 hours.

To better understand the effect of Tat-peptide on increasing cellular penetration and achieving cell killing, a new variant Tat-30G(-) with the Tat peptide attached to the N-terminus was created for the cell viability study (**Figure 3.1**). The characterizations of this new variant is similar to other variants presented in this study, and are listed in **Table 3.1** and **Figure 3.2**, **Figure 3.3**, and **Figure 3.4**. The Tat-peptide alone does not

significantly improve cell killing at 35 nM paclitaxel, but increases cell killing by around

1.2x at 105 nM and 350 nM paclitaxel.

The RGDS-30G(-)-Tat peptide achieved a 88% cell killing with 350 nM

paclitaxel in 15 hours, an 1.95x increase than the same concentration of paclitaxel

solution not encapsulated by protein micelles, and an 1.2x increase than RGDS-30G(-)

where only RGDS is present, and 1.6x increase than the Tat peptide alone. These results

indicated that oleosin micelles can successfully deliver a hydrophobic cargo into breast

cancer cells and achieve cell killing, and Tat peptide is an effective CCP that assisted cell

penetration and drug delivery.
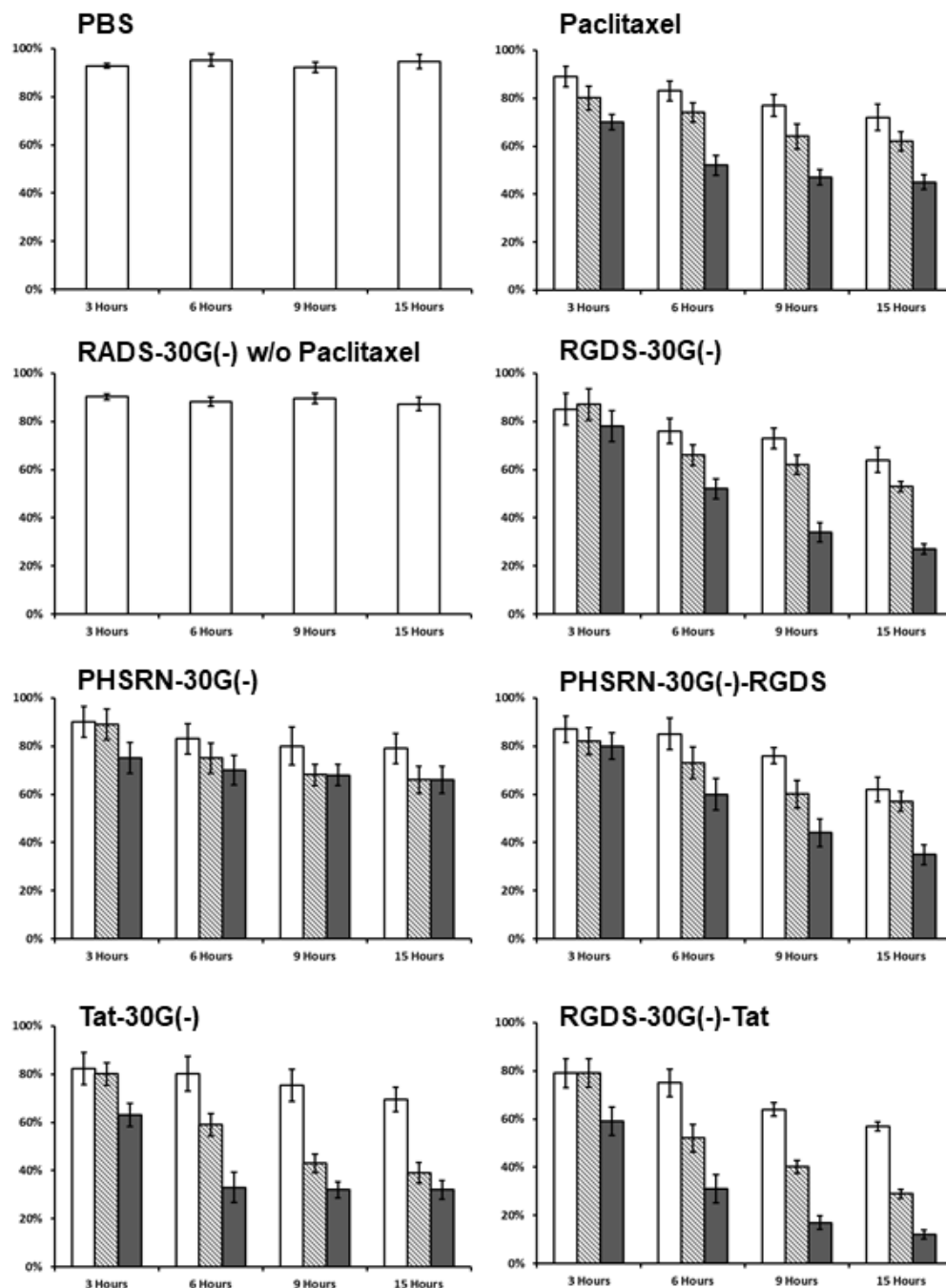
Figure 3.9. Percentage of live cells at the end of cell viability study, quantified by the trypan blue assay. White bar, grey bar, and black bar represent final paclitaxel concentrations at 35 nM, 105 nM and 350 nM, respectively.
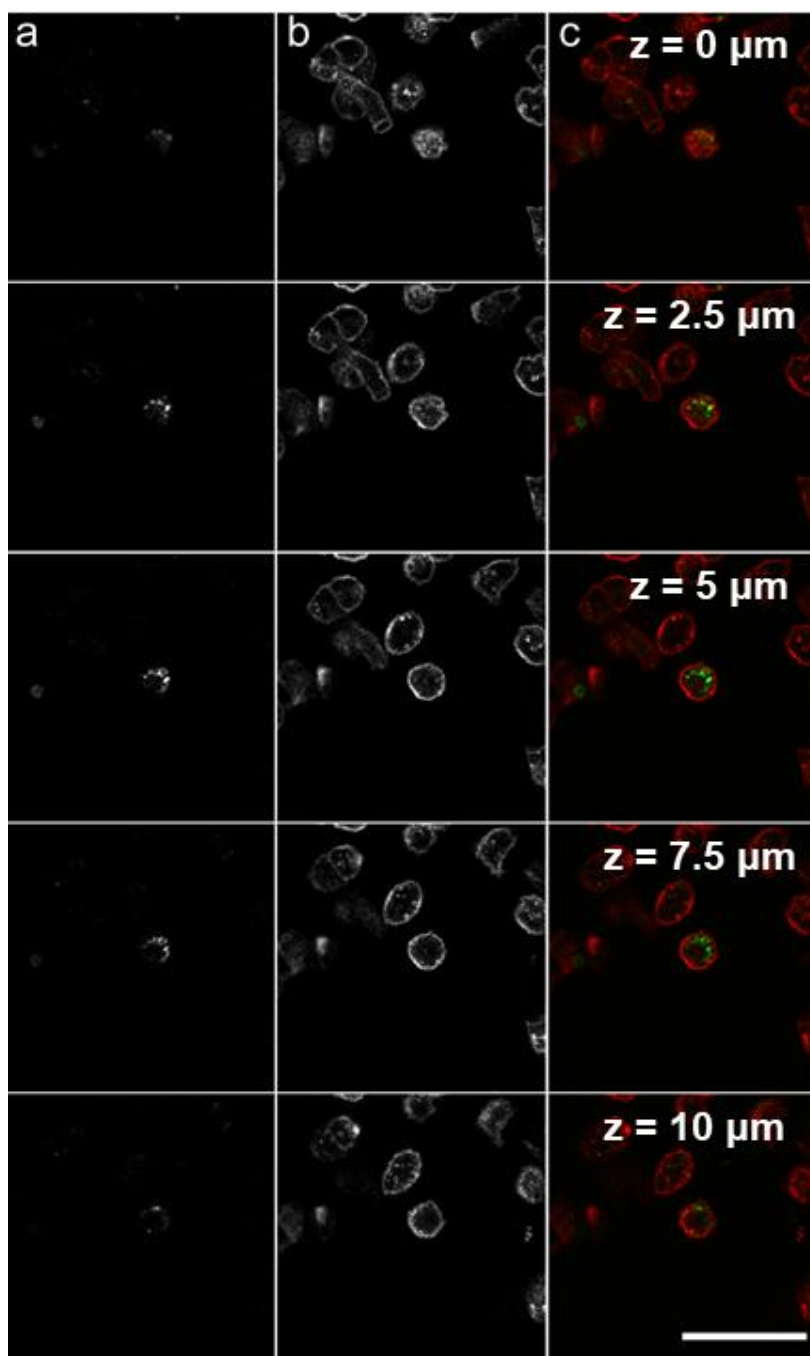
Figure 3.10. In vitro confocal microscopy images of DyLight 488 labeled RGDS-30G(-)-Tat on MDA-MB-231 cells, incubated for 15 h under 37 °C, scale bar represents 50 μm. Each panel is (a) 488 nm channel showing labeled oleosin micelles, (b) 633 nm channel cell membrane labeled with Alexa Fluor 633, and (c) merged channels where labeled oleosin in shown in green and cell membrane is shown in red.

Finally, the cell viability was repeated for blends of 1:1 Tat-30G(-) : RGDS-30G(-) and 1:1 RADS-30G(-) : RGDS-30G(-)-Tat to investigate the effects of Tat on cell penetration, shown in **Figure 3.11**. The two blends of oleosin variants have statistically similar cell killings, and do not improve cell killing than the Tat-30G(-) variant where only Tat is present. In the scope of this study, there is no evidence that suggests that the Tat peptide and RGDS motif interfere with each other. The RGDS-30G(-)-Tat remains as the variant with the highest cell killing potential.
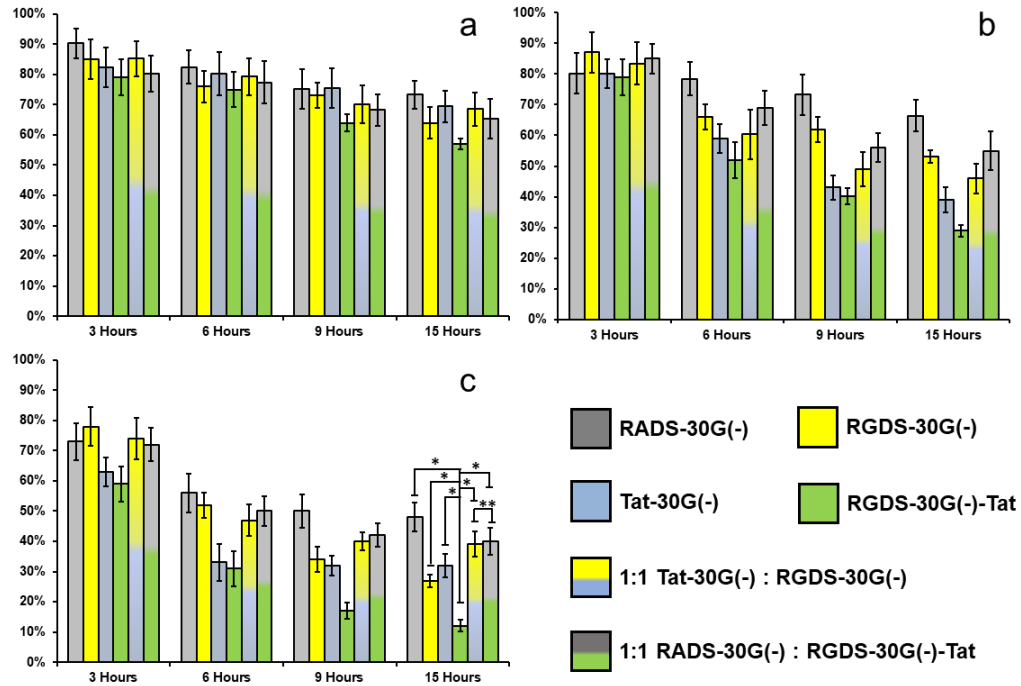
Figure 3.11. Viability of MDA-MB-231 cells treated with (a) 35 nM paclitaxel (b) 105 nM paclitaxel and (c) 350 nM paclitaxel encapsulated with oleosin 30G(-) variants, under 37 °C. * indicates $p < 0.001$, ** indicates $p = 0.57$.

3.4 Conclusions

In this study, we explored the effects of PHSRN and the Tat peptides on cellular uptake, and proved oleosin micelles as a practical tool towards targeted drug delivery. We have shown that PHSRN act synergistically with RGDS when both present on the same oleosin micelle, and this synergy effect can be further tuned by altering PHSRN and RGDS ligand ratios. In addition, we have created a variant of oleosin, RGDS-30G(-)-Tat, that incorporated both integrin bioactivity as well as a cell penetrating peptide, which can significantly improve cellular uptake. We have also proved that the oleosin micelles are capable of carrying a paclitaxel cargo that fits the therapeutic dosing concentration, can be effectively internalized by breast cancer cells, and achieve cell killing. These constructs of oleosin variants broadened our understanding on ligand behavior and interactions, and established oleosin micelle as a stable and versatile drug carrier. There exists a huge body of information about cellular metabolic and signaling pathways yet to be made applicable in practice, and oleosin presents an exciting new solution that can transfer theoretical knowledge to applications.

3.5 Acknowledgements

Chapter 4. Oleosin Drug Carriers Specifically Targeting ErbB Receptors

Abstract

The targeted delivery of chemotherapeutic agents to specific cell lines is becoming an attrative solution to localize drugs on desired disease cells and reduce systematic side effect. Members of the erbB family receptor tyrosine kinases are shown to overexpress in a variety of human cancer cells and are important targets for the design of a smart drug carrier. Previously, AFA and BPT peptide ligands were identified to bind to and inhibit erbB receptors, which raised the possibility of targeting erbB recpetors as a mean of drug delivery. However, the limitations of current synthesized materials make it difficult to generate a carrier that can be functionalized with these identified peptide ligands with a uniform quality. Here we present recombinant oleosin as an alternative drug delivery

material and created an series of recombinant oleosin variants functionalzied with AFA and BPT ligands. The new variants self-assemble into spherical micellar structures, can encapsulate a therapeutic dose of paclitaxel, and achieve 50% cell killing of lung cancer cells *in vitro* in 4 hours, and 90% cell killing in 16 hours. The variants presented here may be developed as a new group of drug carriers.

4.1 Introduction

In this work, we took the previously established knowledge on oleosin functionalization and explore outside the regime of RGDS bioactivity and breast cancer cell lines. Members of the erbB family receptor tyrosine kinases (erbB1, erbB2, erbB3, and erbB4) are overexpressed in a variety of human cancers, and are important targets for the design of drugs and drug carriers.[100–103] Approaches in targeting erbB receptors include monoclonal antibodies, ligand-linked immunotoxins, antisense, and tyrosine kinase inhibitors.[100,101,103,104]

An interesting approach developed by Murali et al. to disable erbB receptor activity was to target protein-protein interaction surfaces.[100,105] Protein-protein interactions plays an important role in mechanisms of cell growth and differentiation, and

emerges as a promising approach towards rational targeted drug delivery design. Murali et al. has demonstrated that two peptide ligand sequences, AFA (YCFPDEEGACY) and BPT (PCPINCTHSCVDLDDKGCPAEQRASPLTSI) exhibit outstanding binding affinity to all three receptors of erbB1, erB2, and erbB3.

We have previously engineered oleosin to self-assemble into spherical micelles, incorporate one or multiple bioactivities, and carry a payload of anti-cancer drug paclitaxel. These oleosin variants can be readily engineered for specific drug delivery applications. Here we present a new series of oleosin variants, incorporated with AFA and BPT peptides, and investigate their potential of being paclitaxel carriers targeted with non-small cell lung cancer cells.

This work is in collaboration with Dr. Ramachandran Murali's lab, who discovered the peptide sequences and established parameters such as integrin binding activities and inhibitory effects.

4.2 Materials and Methods

4.2.1   Protein Design and Expression

Oleosin Gene Construction and Expression: Modified genes were ordered from Integrated DNA Technologies and were inserted into the expression vector pBamUK and later transformed into the BL21 (DE3) strain of *E. coli* for expression. DNA sequencing was performed before protein expression by the *E. coli* strain BL21 DE3 (Stratagene) controlled by the *lac* promotor on the pBamUK. Cultures are grown at 37°C in Luria Broth (LB) with 50 µg/ml kanamycin until OD_{600} reaches 0.6. Isopropyl β-D-thiogalactoside (IPTG) was added to the culture to a final concentration of 1.0 mM to induce the expression of oleosin. Cells were collected by spinning down the culture at 15,000g for 15min and were kept frozen at -20°C until purification. All oleosin variants presented in this study adds a 6-histidine tag to the C-terminus of oleosin molecule which facilitates purification through immobilized metal affinity chromatography (IMAC). All variants of proteins in this study express solubly. Yields for all variants in this study were within the range of 40-100 mg of purified protein per liter of culture. All oleosin variants were stable in buffered solutions (pH~7.4) for 4 weeks in 4°C, and for at least 48 hours in 37°C.

Protein Purification: All oleosin strands in this study have 6-Histidine tag to the C-terminus and were purified with Ni-NTA columns (Pierce). All protein strands in this study are soluble and can be purified with the protocol suggested by Vargo et al.[31] In brief, frozen protein pellet was re-suspended in B-PER Bacterial Protein Extraction Reagent (Fisher). After spinning down at 15,000g for 15min, the supernatant was left to bind with the Ni-NTA resin for at least 1 hour. Then the column was repeatedly washed and protein sample was eluted out.

4.2.2 Protein Characterization

SDS-PAGE: To determine the purity of protein samples, purified oleosin samples were loaded on NuPAGE Novex 4-12% Bis-Tris mini gels (Invitrogen) in 2-(N-morpholino)-ethanesulfonic acid (MES) buffer. SimplyBlue SafeStain (Invitrogen) was used to stain the gel following electrophoresis. The gel was imaged with a Kodak Gel Logic 100 imaging system.

Mass Spectroscopy: To prepare matrix solution, sinapinic acid was added to 50:50 (v/v) ACN: [0.1 vol.% TFA in water] to a final concentration of 10mg/ml. 0.5 μL of matrix solution was added to Bruker AnchorChip, immediately followed by 0.5 μL of oleosin

solution. Solutions were mixed on the AnchorChip using a pipet tip and air-dried.

Samples were analyzed with matrix-assisted laser desorption ionization (MALDI) mass

spectroscopy (Bruker, PennChemistry Mass Spectrometry Facility).

Circular Dichroism (CD): An AVIV 410 spectrometer (AVIV Biomedical, Inc.) was

used to collect UV CD spectra at 25°C in a 1 mm quartz cell. The protein sample

concentration was 10 μM in 50 mM phosphate and 140 mM NaF. The CD data was

analyzed with the CDSSTR algorithm using Dichroweb.

Dynamic Light Scattering (DLS): 700 μL of protein sample was added to a small-

volume cuvette cleaned with compressed air. DLS was performed with a Malvern

Zetasizer Nano ZS (Westborough, MA).

4.2.3   Mammalian Cell Culture

The human lung cancer cell line NCI-H1975 (ATCC CRL-5908) was acquired from

ATCC. NCI-H1975 cells were cultured in RPMI 1640 (Life Technologies 22400)

supplemented with 10% heat-inactivated fetal bovine serum (Sigma Aldrich F2442) and

100 units/ml penicillin and 100 μg/ml streptomycin (Life Technologies 15140) on tissue-

culture treated plastic in a 37°C humidified incubator with 5% CO_2.

4.2.4   Paclitaxel Encapsulation

Paclitaxel (ThermoFisher P3456) was resuspended in 200 proof ethanol and carefully injected into oleosin micellar solution at concentration of 20 μM. The mixture was then briefly sonicated for 20 seconds and let sit for 10 minutes in room temperature. The mixture was then dialyzed against PBS. Protein concentration was measured by Nanodrop and adjusted to 10 μM. Each sample was verified to be in micellar solution form with Dynamic Light Scattering (DLS) before dosed onto cells. The encapsulation efficiency of paclitaxel by oleosin was measured with a labeled version of paclitaxel (ThermoFisher P22310). A calibration of paclitaxel fluorescence signal vs. concentration was established with a Fluoromax-4 spectrophotometer (Horiba Jobin Yvon), and the procedure described here resulted in a 3.21±1.2% encapsulating efficiency of paclitaxel.

4.2.5   Cell Viability Studies

Trypan Blue: Cell culture was trypsinized and resuspended in RPMI 1640 without phenol red (Life Technologies 11835) and mixed with equal volume of 0.4% trypan blue solution (ThermoFisher 15250061) with only stained dead cells. The mixture solution was injected into a hemacytometer (Reichert Bright-Line) and incubated at room

temperature for 90 seconds. The total number of cells and number of stained cells were counted under an optical microscope within 1 minute after incubation. The cell viability was recorded as:

$$Cell\ Viability = \frac{N_{total\ cells} - N_{stained\ cells}}{N_{total\ cells}}$$

MTT: 12 mM MTT stock solution was prepared by adding 1mL of sterile PBS to 5 mg of MTT (ThermoFisher V13154). Solubilization solution was prepared by adding 10 mL of 0.01 M HCL to 1 g of SDS (ThermoFisher V13154) immediately before use.

10 µL of the 12 mM MTT stock solution was added to each well and the cell culture was incubated at 37°C for 4 hours. 100 µL of the solubilization solution was added to each well and mixed by gently pipetting. The cell culture was then incubated at a 37°C humidified incubator for 12 hours. After the solubilization step, the sample was mixed by pipetting and absorbance was recorded at 570 nm. The cell viability in this study was determined by:

$$Cell\ Vability\ (MTT) = \frac{Abs_{sample} - Abs_{blank}}{Abs_{control} - Abs_{blank}}$$

Blank samples were prepared by adding 100 µL of RPMI 1640 without phenol red to each well. Control samples were 60% confluent cells not treated with Drug Solution A.

4.3 Results and Discussions

4.3.1 Oleosin Design, Self-Assembly and Secondary Structure

In this current study, seven further variants were created from oleosin 30G(-) and 30G family to incorporate AFA and BPT and study their effects on enhancing cellular uptake. AFA-30G-63 was engineered to have the AFA ligand at the N-terminus. AFA-30G-43 was mutated to truncate the C-terminus hydrophilic arm to 43 amino acids, such that by theory the AFA will be more exposed when self-assembled into a spherical micelle. AFA-30G(-) was a variant where both of the hydrophilic arms were negatively charged. Three versions incorporating BPT ligand were constructed in the same fashion. CD4-G is a peptide ligand known to not interact with erbB receptors and therefore CD4-G-30G-43 was constructed to have CD4-G at the N-terminus and serve as the negative control in this study. All variant constructs are illustrated in **Figure 4.1.**

To monitor the purity of the recombinant oleosin products and confirm that the mutated oleosin has the exact peptide sequence as designed, SDS-PAGE and MALDI-TOF (Matrix-Assisted Laser Desorption/Ionization – Time of Flight) were performed on each sample after purification. Both tests confirmed that the recombinant oleosin products are highly purified and monodisperse in molecular weight (**Figure 4.2**). Dynamic light scattering (DLS) was used to verify that the protein self-assembles into

micellar structures at 10 µM (**Figure 4.3**), with the detailed characteristics listed in **Table 4.1**. The secondary structures were analyzed by CDSSTR and shown in **Figure 4.4**.

Figure 4.1. Molecular view of CD4-G, AFA and BPT variants.

Table 4.1. Protein Characterization Results

Oleosin-	Expected Molecular Weight [Da]	Measured Molecular Weight [Da]	Hydrodynamic diameter [nm]	PDI
AFA-30G-63	16194	16192	22.46	0.186
AFA-30G-43	14254	14244	20.96	0.168
AFA-30G(-)	16225	16220	21.60	0.173
BPT-30G-63	16715	16708	23.33	0.183
BPT-30G-43	14775	14767	20.98	0.168
BPT-30G(-)	16746	16734	21.22	0.177
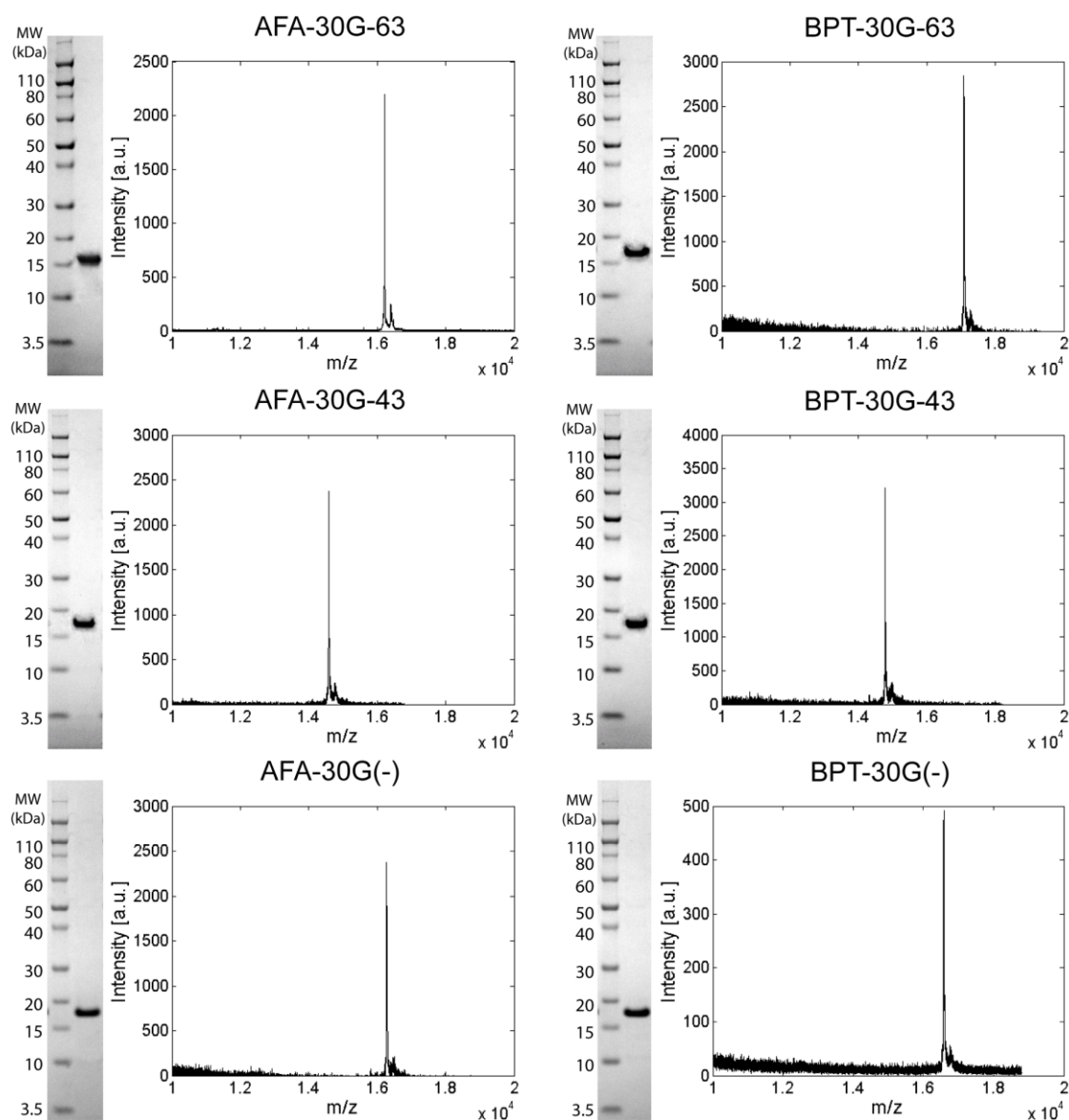
Figure 4.2. Protein characterization and MALDI-TOF spectrum. Protein purity was measured after IMAC purification to be >95% with SDS-PAGE. Protein molecular weight was confirmed by MALDI-TOF and closely match expected weights of protein variants in Table 4.1
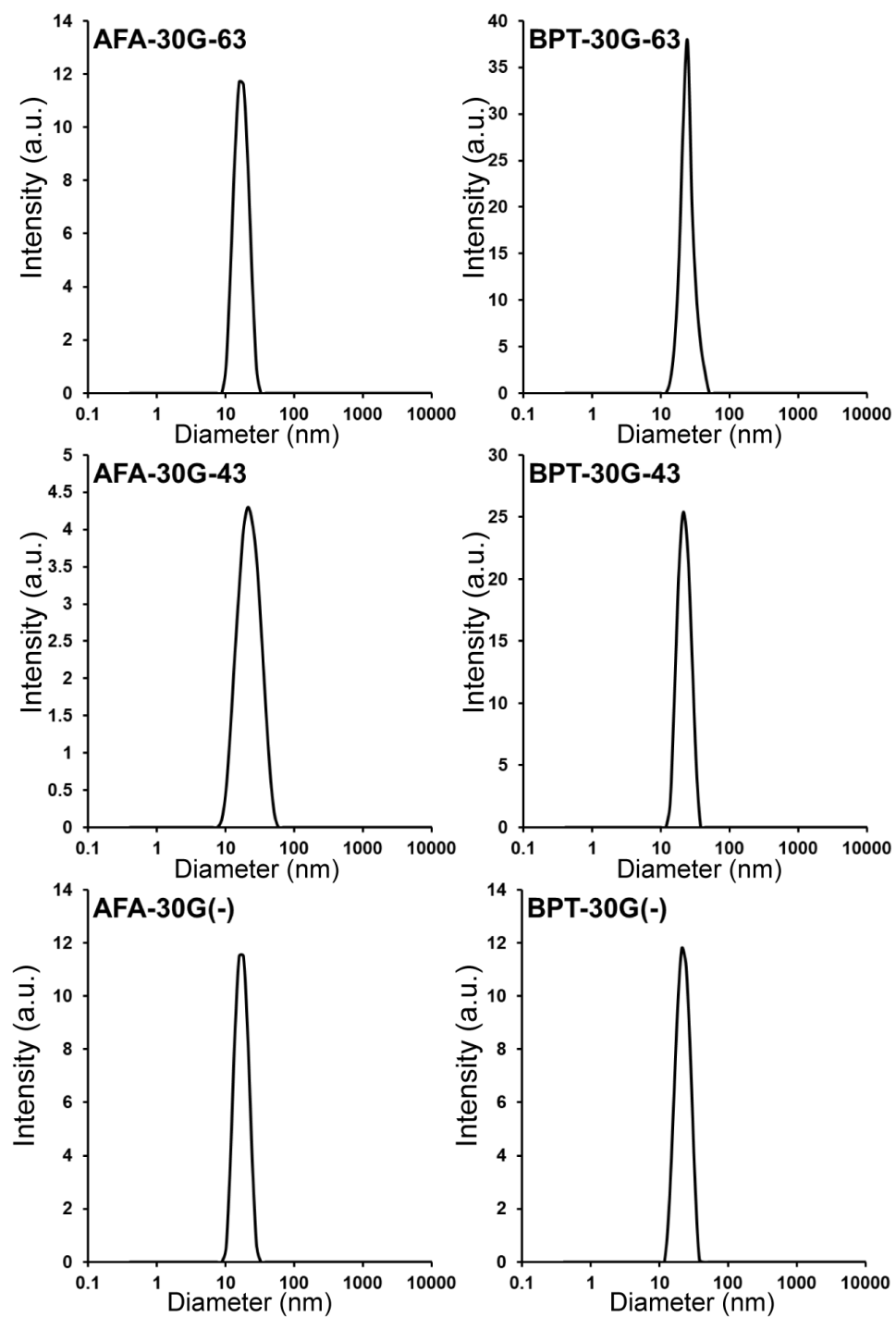
Figure 4.3. Dynamic Light Scattering of all recombinant oleosin variants. Measurement taken at 10 µM and DLS spectrum suggests spherical micellar formation. Hydrodynamic diameters and PDI are listed in Table 4.1.
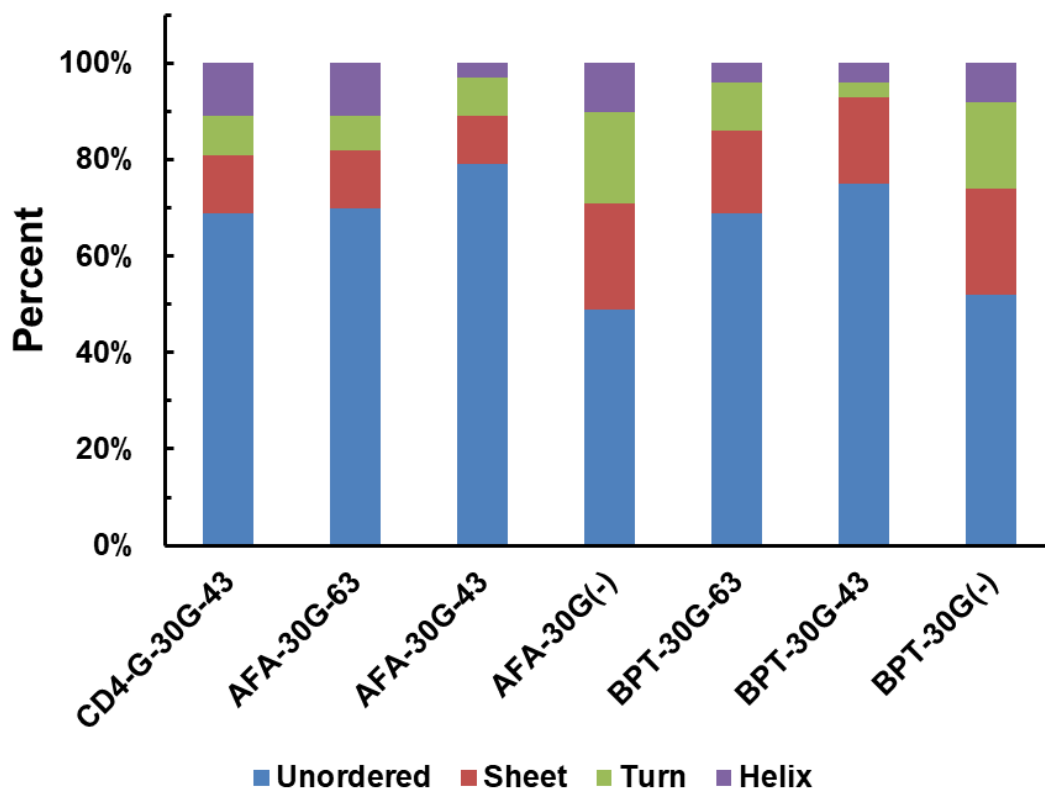
Figure 4.4. Secondary structure of protein variants. CDSSTR analysis shows 60%-80% of the secondary structure for all oleosin variants are unordered, with the exceptions of AFA-30G(-) and BPT-30G(-), where both hydrophlic arms are negatively charged and has a lower unordered secondary structure content at about 50%.

4.3.2 Integrin Mediated Cell Killing

In previous research, the trypan blue assay was used as the quantification method of cell viability. Although easy to implement and reflects true incubation times, the trypan blue method has a limited precision due to the cell resuspension and manual cell counting. A second assessment tool, the MTT assay, was carried out in this work in parallel to the trypan blue assay.

The MTT assay requires a 4-hour incubation time after the time point, and therefore does not provide information for cell viability within 4 hours. A dilemma with the MTT assay is that MTT assay results are indications of average metabolic active level of the cell culture within the incubation time, which tend to overestimate actual cell viability and does not provide information on an exact time point. To best overcome this, cell viabilities in this study were measured at every 4 hours for 16 hours, which gives each data point from the MTT assay two benchmarks from the trypan blue assay. Regardless of the technical issues, the trends of cell viabilities measured from both assays still provide valuable information on the ability of functionalized oleosin to deliver drug into a cell line, mediated by protein-integrin interaction.

First, paclitaxel not encapsulated by oleosin and paclitaxel encapsulated by the non-bioactive variant CD4-G-30G-43 were tested as negative controls, with the cell viability results shown in **Figure 4.5** and **Figure 4.6**. CD4-G-30G-43 does not significantly improve cell killing, and in fact shown to slightly decrease cell killing at high paclitaxel concentrations. This indicates that CD4-G ligand binds poorly to receptors, and the encapsulation of paclitaxel made it less accessible to cross the cell membrane than when paclitaxel is in free molecule form in solution.
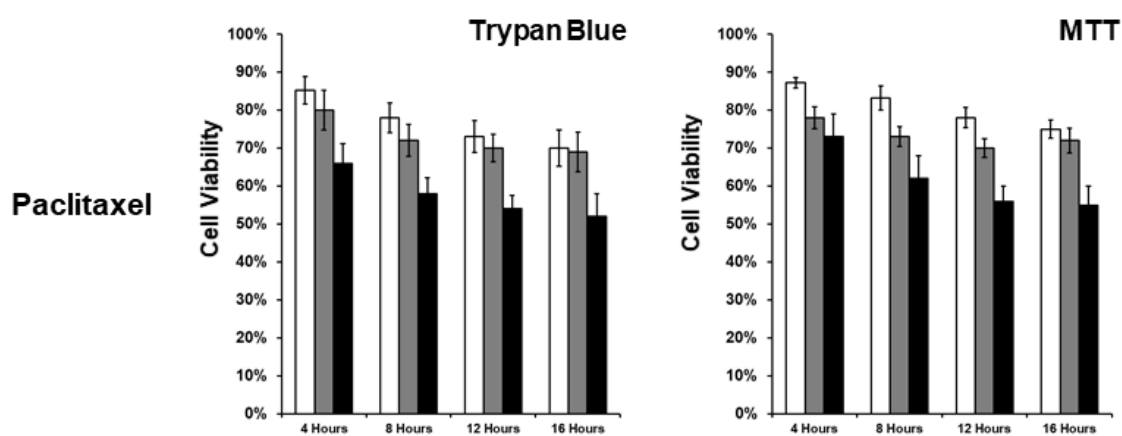
Figure 4.5. Percentage of live cells at the end of cell viability study. White bar, grey bar, and black bar represent final paclitaxel concentrations at 35 nM, 105 nM and 350 nM, respectively.
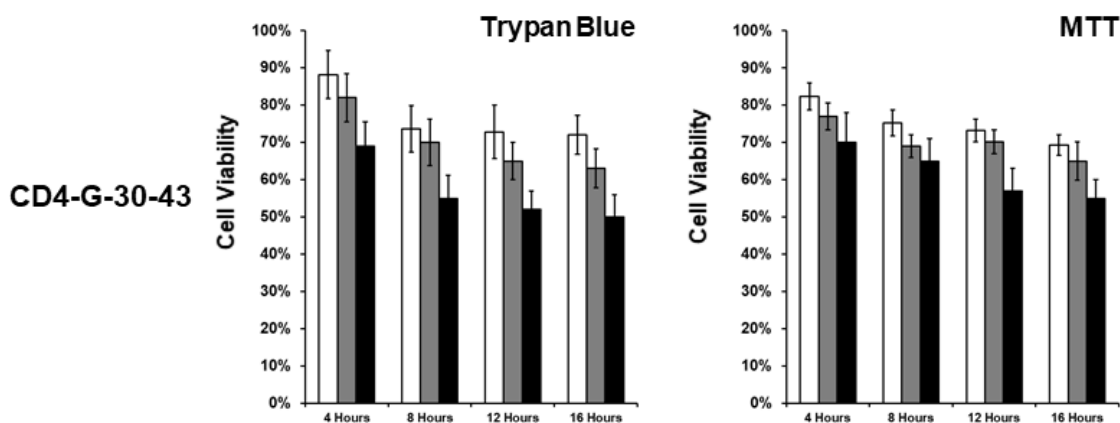
Figure 4.6. Cell viability study results on CD4-G-30-43 as the drug carrier. White bar, grey bar, and black bar represent final paclitaxel concentrations at 35 nM, 105 nM and 350 nM, respectively.

On the other hand, oleosin variants functionalized with AFA and BPT ligands act as effective drug carriers and can increase cell killing significantly in as short as 4 hours. The AFA family of oleosin demonstrates an even higher cell killing in general than the BPT family. In high paclitaxel concentration and 16 hours, The AFA functionalized carriers achieved cell killing rate at over 75%, and the BPT functionalized carriers achieved celling rate at around 70%. Out of all the new variants presented here, AFA-30G-43 is the most effective drug carrier. In 350 nM paclitaxel conditions measured by trypan blue, the AFA-30G-43 led to a 2.3x, 2.0x, 1.9x, and 1.85x increased cellular uptake than paclitaxel in free form in 4, 8, 12, and 16 hours respectively. Both trypan blue and MTT assays indicate that AFA-30G-43 with 350 nM paclitaxel results in cell viability less than 50% in 4 hours, and less than 20% in 12 hours.

89

Within each family of oleosin, the ligand-30G-43 construct (AFA-30G-43 and BPT-30G-43) is the best drug carrier at delivery drug and result in cell killing. This observation may be explained by the truncation of the C-terminus hydrophilic arm. When self-assembled into spherical micelles, the ligand-30G-43 constructs will offer the ligand better exposure since the non-functionalized C-terminus hydrophilic arm has less number of amino acids, therefore in theory shorter than the N-terminus arm carrying the ligand.
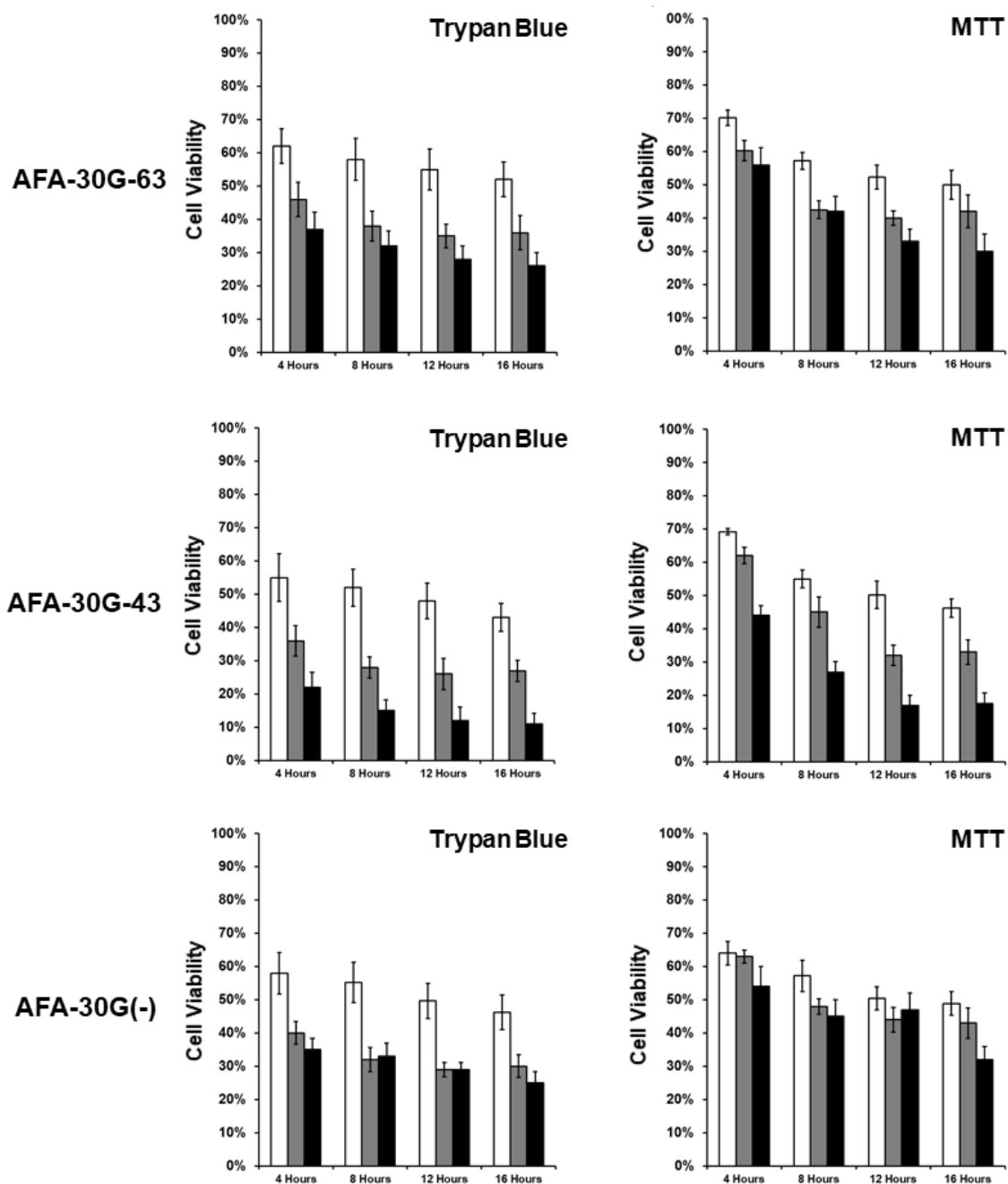
Figure 4.7. Cell viability study results on AFA variants as the drug carrier. White bar, grey bar, and black bar represent final paclitaxel concentrations at 35 nM, 105 nM and 350 nM, respectively.
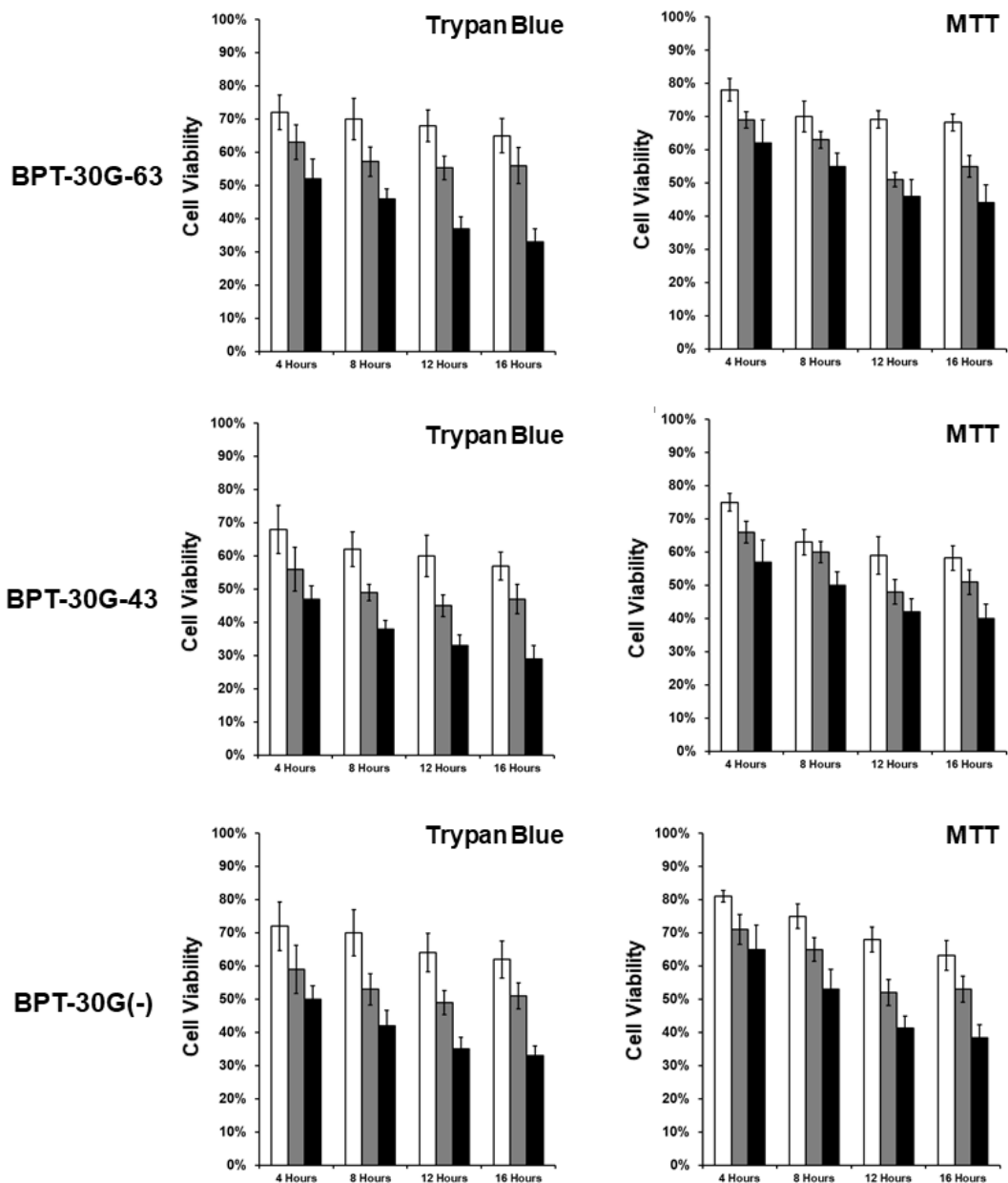
Figure 4.8. Cell viability study results on BPT variants as the drug carrier. White bar, grey bar, and black bar represent final paclitaxel concentrations at 35 nM, 105 nM and 350 nM, respectively.

Finally, we investigated the effect of blending in the previously studies cell-penetrating peptide Tat into the best performing variant AFA-30G-43. 1:1 blend of AFA-30G-43 : Tat-30G(-) was repeated for the cell viability essay with 350 nM paclitaxel, quantified by trypan blue assay. Tat-30G(-) and 1:1 blend of AFA-30G-43 : CD4-G-43 were carried out as a controls. The cell viability results are shown in **Figure 4.9.**

In this case, the blend of AFA and Tat peptide does not indicate any advantage in cell killing. This could be explained by comparing the cell viability where Tat-30G(-) and AFA-30G-43 are used as drug carriers. The cell killing rate from using AFA-30G-43 was 3x – 1.2x higher than Tat-30G(-), from 4 hours to 16 hours. This indicates that AFA-30G-43 has a stronger binding affinity to receptors on NCI-H1975 cells than the Tat-30G(-) variant. The longer arm on the C-terminus of the Tat-30G(-) molecule could also contribute to the lower cell killing.

Drug delivery was visualized by encapsulating paclitaxel with fluorescently labeled oleosin and imaged with confocal microscopy. The z-stack series images of AFA-30G-43 on NCI-H1975 at 15 hours are shown in **Figure 4.10**, indicating effective cell internalization of oleosin micelles, and some degree of localization within the cell. Wide field confocal images of cells treated with paclitaxel loaded CD4-G-30G-43, AFA family

variants, and BPT family variants are shown in **Figure 4.11**, **Figure 4.12**, and **Figure 4.13**, respectively.
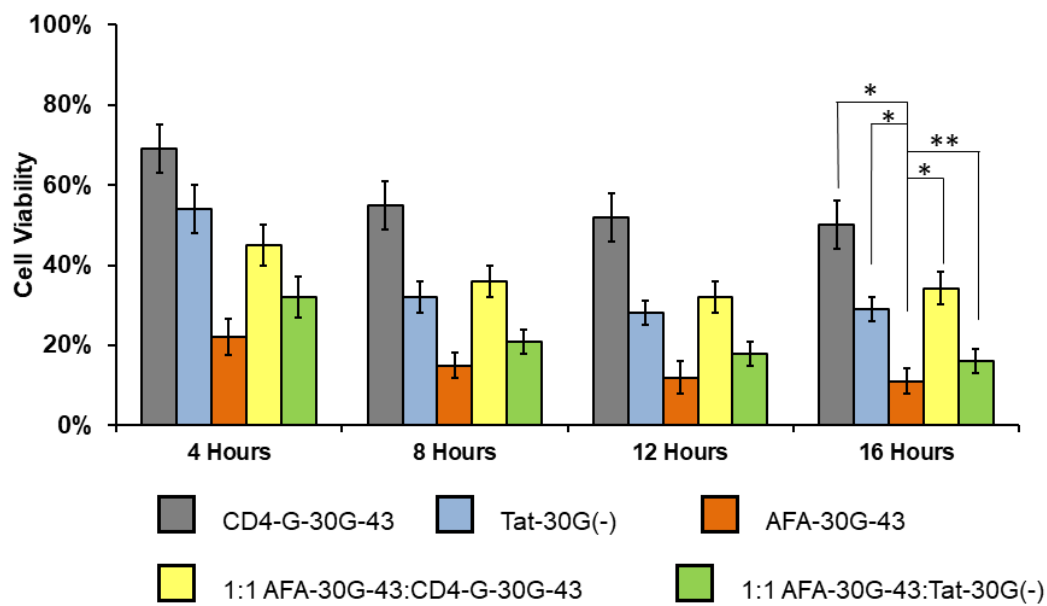
Figure 4.9. Viability of NCI-H1975 cells treated with 350 nM paclitaxel encapsulated with blends of oleosin variants. * indicates $p < 0.001$, ** indicates $p < 0.01$.
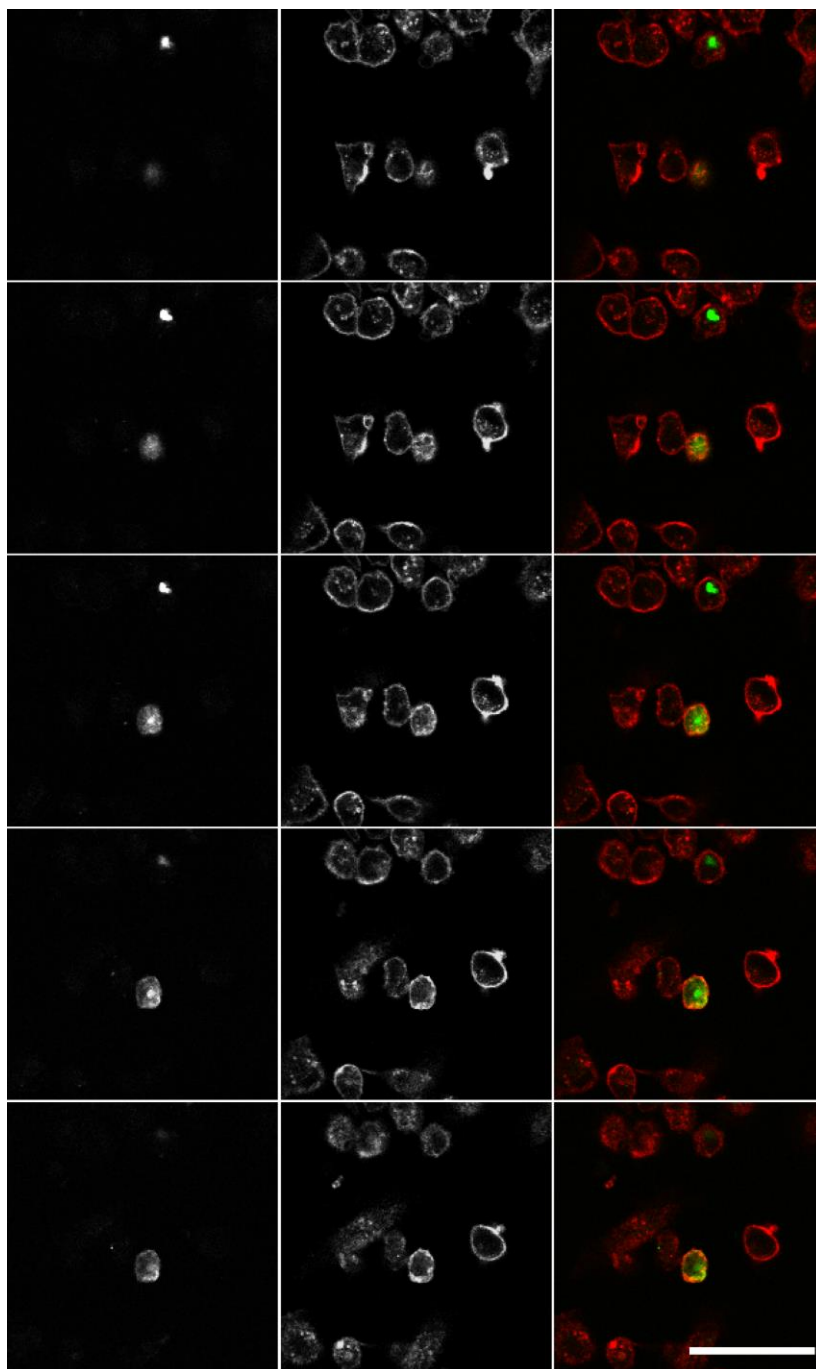
Figure 4.10. In vitro confocal microscopy images of DyLight 488 labeled AFA-30G-43 on NCI-H1975 cells, incubated for 15 h under 37 °C, scale bar represents 50 μm. Each panel is (left) 488 nm channel showing labeled oleosin micelles, (middle) 633 nm channel cell membrane labeled with Alexa Fluor 633, and (right) merged channels where labeled oleosin in shown in green and cell membrane is shown in red. Each panel is 2.5 μm apart in depth.
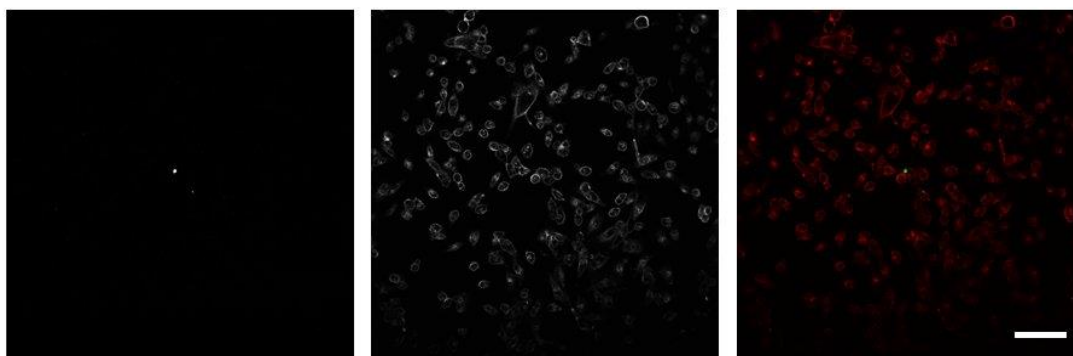
Figure 4.11. In vitro confocal microscopy images of DyLight 488 labeled CD4-G-30G-43 on NCI-H1975 cells, incubated for 15 h under 37 °C, scale bar represents 100 μm. Each panel is (left) 488 nm channel showing labeled oleosin micelles, (middle) 633 nm channel cell membrane labeled with Alexa Fluor 633, and (right) merged channels where labeled oleosin in shown in green and cell membrane is shown in red.
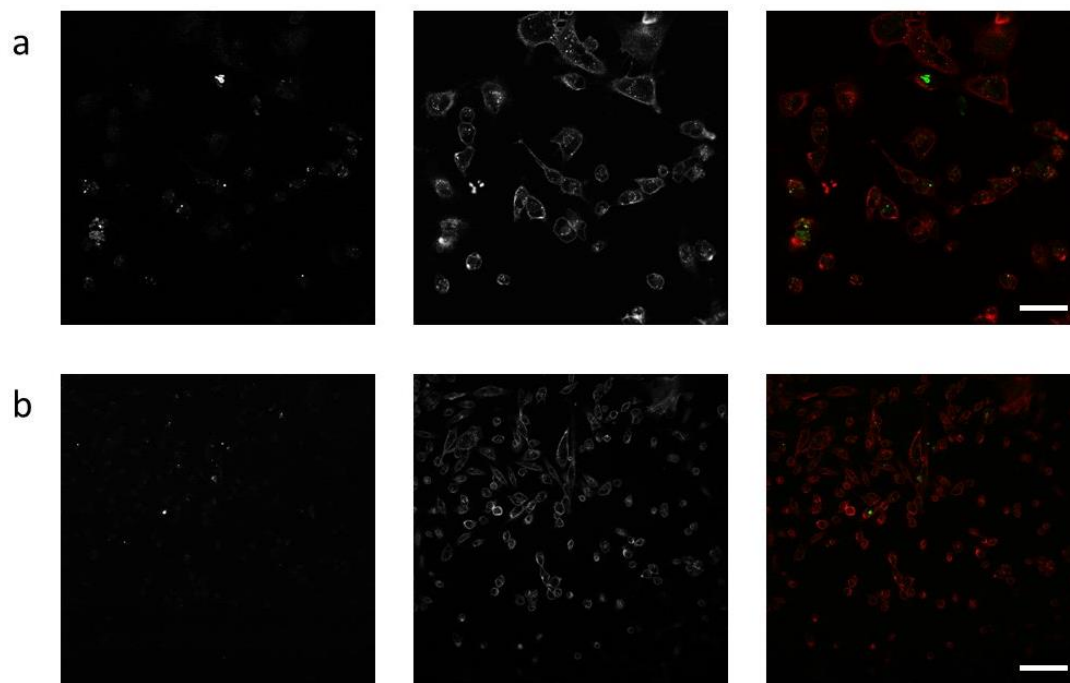
Figure 4.12. In vitro confocal microscopy images of DyLight 488 labeled (a) AFA-30G-63 and (b) AFA-30G(-) on NCI-H1975 cells, incubated for 15 h under 37 °C, scale bar represents 100 μm. Each panel is (left) 488 nm channel showing labeled oleosin micelles, (middle) 633 nm channel cell membrane labeled with Alexa Fluor 633, and (right) merged channels where labeled oleosin in shown in green and cell membrane is shown in red.
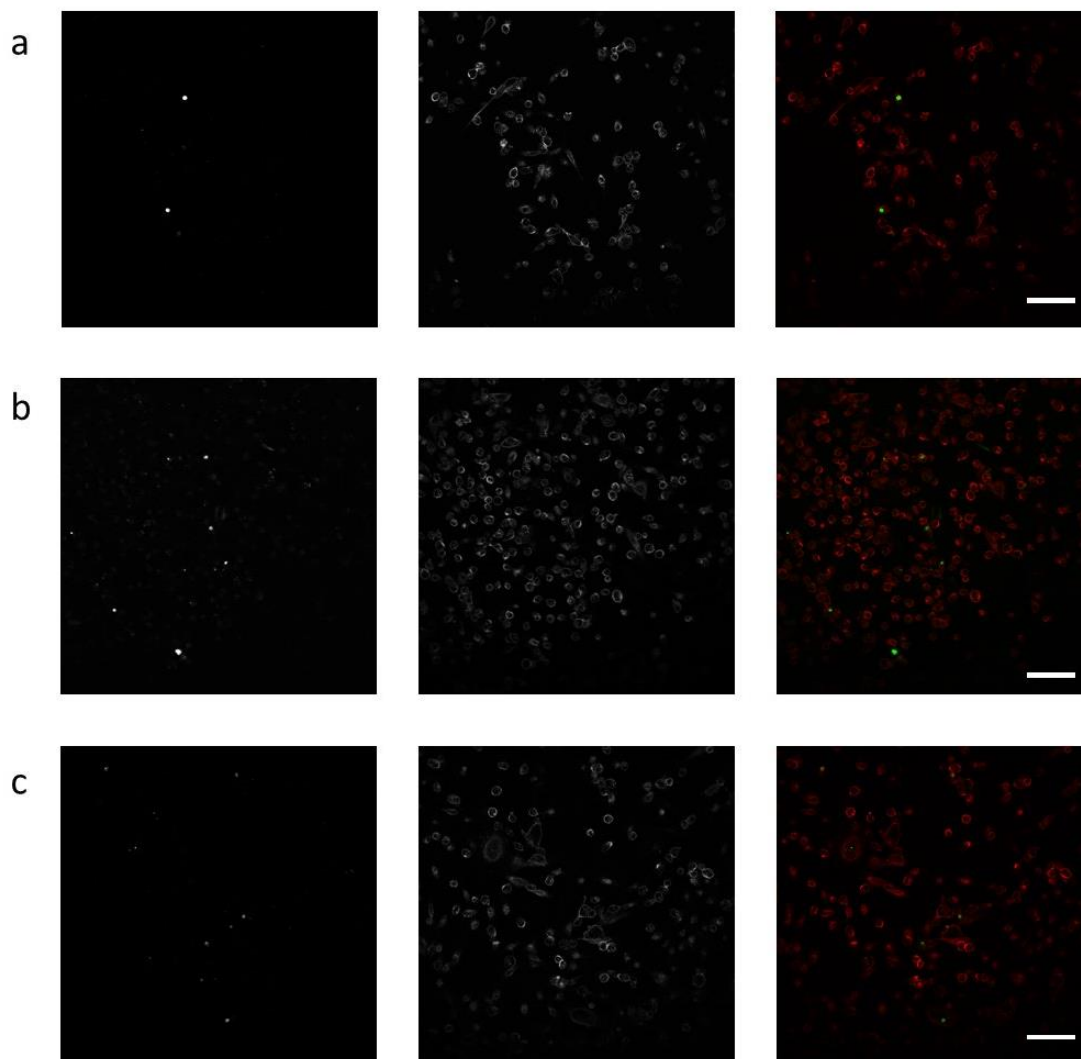
Figure 4.13. In vitro confocal microscopy images of DyLight 488 labeled (a) BPT-30G-43, (b) BPT-30G-63, and (c) BPT-30G(-) on NCI-H1975 cells, incubated for 15 h under 37 °C, scale bar represents 100 μm. Each panel is (left) 488 nm channel showing labeled oleosin micelles, (middle) 633 nm channel cell membrane labeled with Alexa Fluor 633, and (right) merged channels where labeled oleosin in shown in green and cell membrane is shown in red.

4.4 Conclusions

This work demonstrates the engineering of the naturally occurring surfactant protein oleosin towards drug carriers that targets a range of erbB receptors, and results in a significantly increased lung cancer cell killing. We have shown that the oleosin 30G and 30G(-) family can be mutated to carry peptide ligands as large as 30 amino acids on one hydrophilic arm, and retain their spherical micellar self-assembly structure. One particular variant, the AFA-30G-43 achieved the fastest cell killing observed in this thesis. The method of using recombinant oleosin as the platform of building drug carriers demonstrated here is powerful as it can make research in simulation phase readily available for *in vitro* studies. We envision oleosin micelles to be a promising toolbox that can be easily converted for targeted drug delivery, as well as a range of other therapeutic applications.

Chapter 5. Conclusions and Future Directions

5.1 Specific Aims

The research presented within this thesis shows that we are able to successfully create biomaterials from the surfactant protein oleosin, and use it towards targeted drug delivery. The specific aims of this work were as follows:

1. Create a recombinant oleosin that is bioactive and answers to an environmental cue in physiological conditions

2. Encapsulate an anti-cancer drug in self-assembled oleosin nanostructure, and achieve specific cell killing

3. Engineer oleosin drug carriers that target a specific family of receptors

100

5.2 Specific Findings

5.2.1 Create a recombinant oleosin that is bioactive and answers to an environmental cue in physiological conditions

Chapter 2 focuses on creating an oleosin variant that is both integrin-targeted and answers to a environmental cue. To achieve this, a variant Throm-RGDS-30G(-) is created where the bioactive RGDS ligand is shielded by 20 amino acids, and only becomes exposed when in the presence of thrombin. The resulting molecule expresses well, and self-assembles into a spherical micelle shape in aqueous environments. The cellular uptake by a breast cancer cell line (MDA-MB-231) was quantified with confocal imaging, and the results indicates that the bioactive motif RGDS is only fully exposed by the specific protease thrombin. This work completes Aim I of the thesis, and became the steppingstone for the rest of the work presented in this thesis.

5.2.2 Encapsulate an anti-cancer drug in self-assembled oleosin nanostructure, and achieve specific cell killing

Moving on from Aim I, Chapter 3 of this work set out to investigate the potential of engineering oleosin to become a practical drug carrier. Thus, this work explored a range of questions, from enhancing cellular uptake of the existing RGDS motif, to encapsulating an anti-cancer drug in a protein micelle. Three new variants incorporating PHSRN and Tat peptide was initially mutated from the oleosin 30G(-) family, and test for cellular uptake with an improved quantification tool flow cytometry. It was discovered that both PHSRN and Tat peptide enhances the cellular uptake of RGDS-30G(-), and different oleosin variants can be blended at different ratios to further fine-tune the synergy effect. We have also proved that the oleosin micelles are capable of carrying a paclitaxel cargo that fits the therapeutic dosing concentration, can be effectively internalized by breast cancer cells, and achieve cell killing. One particular variant, RGDS-30G(-)-Tat, achieves 88% breast cancer killing in 15 hours when carrying a 350 nM paclitaxel cargo. This work provides practical insight in turning oleosin into a applicable drug carrier, and accomplishes the goal set out in Aim 2.

5.2.3 Expand the oleosin library to target multiple cell lines

In Chapter 4, we collaborated with Dr. Ramachandran Murali and investigated the ability of oleosin as drug carriers that targets non-small cell lung cancer cell lines. Six new variants were constructed to incorporate AFA and BPT ligands, which binds to erbB1, erbB2, and erbB3 receptors. Oleosin variants were shown to be stable micellar forms after adding a peptide ligand as large as 30 amino acids, and encapsulating paclitaxel in a range of 35 nM to 350 nM. The non-functionalized arm was trimmed down such that the added ligand is more exposed. The resulting AFA-30G-43 variants presents a 50% cell killing in as short as 4 hours, and kills 90% of cells in 12 hours with a 350 nM paclitaxel cargo. Chapter 4 shows examples of oleosin variants that can target multiple cell lines, and completes Aim 3.

5.3 Future Directions

The work presented in this thesis arise from the oleosin's unique triblock construct, and ability of be precisely engineered via molecular biology. We have demonstrated many mutations of oleosin that are engineered to be bioactive, and investigate their physical stability and capability of carrying a cargo. However, the potential of generating bioactive mutants from oleosin has very little limit. Numerous mutants can be generated from oleosin to improve on the work presented here, to deepen our understanding of using oleosin as drug carriers, or to explore other applications. Here, I will discuss ideas for expansion and extension of the aims finished in this dissertation.

5.3.1 Immunogenicity Screening

Immunogenicity is the ability of substances (such as antigen and epitope) to trigger an immune response in human or animal bodies. The immunogenic response includes both cellular (T cell) and humoral (antibody) immune responses and is an important but sometimes overlooked aspect of drug discovery. Anti-drug antibodies (ADA) elicited by therapeutics may decrease the therapeutic effect of the drug, and in more serious cases lead to autoimmune thrombocytopenia and pure red cell aplasia.[106,107] Most protein therapeutics induce an unwanted immune response, and the rational next step of the

research presented in this thesis is to screen for the lowest immunogenetic oleosin variant.[107–109]

While the immune response is a complicated cascade, T cell – dependent responses appear to play a critical role in the development of antibody responses.[110] Predictive tools build upon the empirical results from clinical immune response results, and use amino acid pairwise contact potentials to calculate peptide binding to MHC class I and II alleles.[111–114]

A preliminary algorithm by Calis *et al.* predicts immunogenicity of peptides using the NetNHC-3.2 algothrim, the best performing predictor according to a large benchmark study.[115,116] This algorithm is a part of the Immune Epitope Database (IEDB) and can be freely accessed at http://tools.iedb.org/immunogenicity/. The predicted Class I immunogenicity scores of oleosin variants presented in this thesis are listed in **Table 5.1**.

A non-immunogenetic peptide in the algorithm by Calis *et al*. has a score of 0, and a higher score indicated a higher possibility of the peptide eliciting an immune response. According to this predicting algorithm, oleosin with a large hydrophobic core and uncharged hydrophilic arms are less likely to trigger an immune response, which can be a hypothesis for future research. This algorithm, like most available predicting

algorithms, are only validated for short peptides (around 9 amino acids long). Definitive

information on the immunogenicity of oleosin variants can be obtained by doing ELISA

antibody assays.

From an oleosin variants with established functionalities, an array of similar

oleosin variants can be engineered with alternations in the non-functional regions and

screened for the lowest immunogenic variant. The power of generating a library of fully

functional variants for immunogenicity screening is unique to recombinant protein, which

makes recombinant protein a well-rounded material for drug delivery purposes.

Table 5.1. Immunogenicity Score of Oleosin Variants

Oleosin-	Immunogenicity Score*
Wild Type Sunflower	-0.75
30G	-0.43
30G(-)	0.86
RADS-30G(-)	0.59
RGDS-30G(-)	0.59
Throm-RADS-30G(-)	0.20
Throm-RGDS-30G(-)	0.20
PHSRN-30G(-)	0.59
PHSRN-30G(-)-RGDS	0.53
Tat-30G(-)	0.28
RGDS-30G(-)-Tat	0.22
CD4-G-30-43	0.26
AFA-30G-63	-0.27
AFA-30G-43	0.25
AFA-30G(-)	0.96
BPT-30G-63	-0.78
BPT-30G-43	-0.26
BPT-30G(-)	0.45

5.3.2 Physical Properties and Stability

We have established reliable methods that measures basic physical properties of oleosin such as hydrodynamic size, critical micelle concentration, and secondary structures. The limitation of current measurements is the resolution of observing oleosin molecules and micelles finer than the nanoscale. The typical size of oleosin micelles is around 20 nm, which makes it difficult to visualize in cryo-TEM, the most advanced imaging tool we have tried on oleosin so far. AFM has been shown to be a powerful imaging tool that provide information on much smaller length scales, and recent advancements in AFM makes it possible to image a soft ensemble body such as oleosin micelles in solutions. Creating a simulation model of oleosin molecules is also promising in predicting oleosin behavior in the designing phase. Oleosin molecules are typically in the 100-200 amino acid range, which makes them a realistic goal for calculation. These future directions will offer us new information on oleosin, thus helping with understanding and predicting oleosin behaviors.

In the scope of this thesis, we have observed that the self-assembled micelle structure of oleosin is stable for at least one month in 4°C, and for at least 24 hours at 37°C in mammalian cell culture conditions. The assembly structure is also shown to recover itself after a brief perturbation such as sonication up to 30 seconds. These observations made oleosin a practical tool for drug delivery, and a rational next step is to

investigate oleosin stability in a more complex condition that resembles blood circulation. A good in vitro simulation of blood flow can be achieved through microfluidics, where the shape of channels, flow rates, and channel surfaces can all be modified to simulate a range of physiological conditions. Microfluidic devices generated in Dr. Daeyeon Lee's lab and Dr. Scott Diamond's lab have seen promising results in simulating blood flow and offer direct visualization, and can be great collaboration projects in the future.

Cytotoxicity of oleosin has been measured on cancer cell lines, and preliminary results suggest that the negative control of RADS-30G(-) does not exhibit toxicity when compared to PBS. The next steps in this direction is to measure cytotoxicity of a small library of oleosin on healthy cells such as epithelial cells. In Chapter 4, we have demonstrated MTT to be fast and reliable way to measuring cell proliferation. Healthy epithelial cells can be seeded in 96 well plates, dosed with oleosin micellar solutions, and measured for the effect of oleosin on cell proliferation in as short as 4 hours.

5.3.3 Functionalized Oleosin in Other Self-Assembled Structures

Previously, our lab has seen promising results where oleosin variants can assemble into shapes such as worm-like micelles, bilayer sheets, and vesicles.[30] We have observed that insoluble mutants of oleosin are more promising in assembling to more complex structures due to their large hydrophobic core, and that highly asymmetrical variants tend to form into worm-like micelles. These complex constructs have great potential in applications of drug delivery and tissue engineering. Vesicles can carry both hydrophobic and hydrophilic cargos, and worm-like micelles and bilayer sheets have the more surface contact area per molecule with cells than any other nanoscale structures. However, creating those complex structures faced several major limitations. First, those structures were made through emulsion templating instead of self-assembly, which makes the final products unpredictable in sizes. The organic solvents used during emulsion templating also limit the further applications in physiological conditions. Second, the large hydrophobic core (87 amino acids) causes poor expression in bacteria, and the surfactant being insoluble makes it difficult to purify and store.

Future work on making complex structures from oleosin would need to focus on making the oleosin soluble. We have carried out some preliminary work in starting with a insoluble protein in the 87 family and switching out some amino acids that possess high

alpha helix structure, and amino acids that leads to hydrogen bonds, aiming to make the hydrophobic core more flexible and possibly increasing solubility. Even though no mutants have been found to tune the 87 family to complete soluble protein yet, this approach is still the most promising in obtaining a variant that self-assemble into a vesicle. Some additional approaches include changing the hydrophilic arm to charged amino acids. Switching all amino acids on the hydrophilic arm to be negatively or positively charged proteins is most promising in making the structure flexible through repulsion of the arms, but could lead to perturbed self-assembly structure.

Another interesting area to explore is to add multiple protease cleavable domains to the hydrophilic arms of oleosin, and thus creating a molecule that's susceptible to a cascade of enzyme reactions. We have demonstrated that thrombin can be successfully incorporated into the oleosin 30G(-) family, and there's a high possibility for other short cleavable sites to be inserted into the hydrophilic arms. The applications of this direction are sustained release of cargo and change of structure post-assembly.

5.3.4 Expand Established Knowledge to Other Disease Areas and Applications

In this thesis, we have established solid knowledge on using oleosin as drug carriers that targets breast cancer cell lines and lung cancer cell lines, and there remains much need in the drug delivery field that oleosin can readily tackle. To expand upon the work presented here, one can incorporate other drugs, target other cell lines, and transfer to the diagnostic field.

In Chapter 3 and Chapter 4, we have demonstrated that oleosin micelles can encapsulate a hydrophobic drug paclitaxel, which is a common anti-cancer drug. Other hydrophobic drugs include doxorubicin hydrochloride (DOX), and groups of steroids. Most of the hydrophobic drug delivery is still in microencapsulation stage, and requires a volatile organic solvent to dissolve the encapsulation matrix and sometimes the drug as well.[117] Oleosin micelle is a promising approach that will bypass the organic solvent and make the drug more readily accessible.

In Chapter 2 and Chapter 3 of this work, there has been a focus on using RGDS as the bioactive motif. One limitation of using RGDS towards targeted drug delivery is the non-specificity of RGDS. RGDS binds to more than half of the over 20 integrins studied in the human body, and using RGDS as the vector for targeted drug delivery typically requires assistance such as localized injection. In Chapter 4 we have proved that the oleosin 30G and 30G(-) family are capable of incorporating peptide ligands up to the size of 30 amino acids on one hydrophilic arm, which opens up opportunities for the

incorporation of a number of other ligands with higher specificity, as well as sensitivity towards some pathologically relevant enzymes.

This work has demonstrated the potential in engineering oleosin towards targeted drug delivery applications, and the future directions mentioned here contain rational routes to deepen our understanding of oleosin and make it even closer to actual application, as well as ways where our knowledge of oleosin can be used for other applications. The field of bioactive ligand and pathological pathways is continuously evolving at a rate faster than conventional chemically synthesized materials can accommodate, and oleosin emerges as a powerful and versatile platform that transforms theoretical knowledge to actual applications.

References

(1) Siegel, R., Miller, K., and Jemal, A. (2015) Cancer statistics , 2015 . *CA Cancer J Clin 65*, 29.

(2) Steichen, S. D., Caldorera-Moore, M., and Peppas, N. A. (2013) A review of current nanoparticle and targeting moieties for the delivery of cancer therapeutics. *Eur. J. Pharm. Sci. 48*, 416–427.

(3) Caldorera-Moore, M., and Peppas, N. A. (2009) Micro- and nanotechnologies for intelligent and responsive biomaterial-based medical systems. *Adv. Drug Deliv. Rev. 61*, 1391–1401.

(4) Cho, K., Wang, X., Nie, S., Chen, Z., and Shin, D. M. (2008) Therapeutic nanoparticles for drug delivery in cancer. *Clin. Cancer Res. 14*, 1310–1316.

(5) Mastria, E., and Chilkoti, A. (2014) Genetically encoded smart peptide polymers for biomedicine. *MRS Bull. 39*, 35–43.

(6) Gindy, M. E., and Prud'homme, R. K. (2009) Multifunctional nanoparticles for imaging, delivery and targeting in cancer therapy. *Expert Opin. Drug Deliv. 6*, 865–878.

(7) Allen, T. M., and Cullis, P. R. (2004) Drug Delivery Systems: Entering the Mainstream. *Science (80-.). 303*, 1818–1822.

(8) Grimaldi, N., Andrade, F., Segovia, N., Ferrer-Tasies, L., Sala, S., Veciana, J., and

Ventosa, N. (2016) Lipid-based nanovesicles for nanomedicine. *Chem. Soc. Rev. 45*, 6520–6545.

(9) Trent, A., Marullo, R., Lin, B., Black, M., and Tirrell, M. (2011) Structural properties of soluble peptide amphiphile micelles. *Soft Matter 7*, 9572–9582.

(10) Mlinar, L. B., Chung, E. J., Wonder, E. A., and Tirrell, M. (2014) Active targeting of early and mid-stage atherosclerotic plaques using self-assembled peptide amphiphile micelles. *Biomaterials 35*, 8678–8686.

(11) Torchilin, V. P. (2001) Structure and design of polymeric surfactant-based drug delivery systems. *J. Control. Release 73*, 137–172.

(12) Miura, Y., Takenaka, T., Toh, K., Wu, S., Nishihara, H., Kano, M. R., Ino, Y., Nomoto, T., Matsumoto, Y., Koyama, H., Cabral, H., Nishiyama, N., and Kataoka, K. (2013) Cyclic RGD-linked polymeric micelles for targeted delivery of platinum anticancer drugs to glioblastoma through the blood-brain tumor barrier. *ACS Nano 7*, 8583–8592.

(13) Venkataraman, S., Hedrick, J. L., Ong, Z. Y., Yang, C., Ee, P. L. R., Hammond, P. T., and Yang, Y. Y. (2011) The effects of polymeric nanostructure shape on drug delivery. *Adv. Drug Deliv. Rev. 63*, 1228–1246.

(14) Loverde, S. M., Klein, M. L., and Discher, D. E. (2012) Nanoparticle shape improves delivery: Rational coarse grain molecular dynamics (rCG-MD) of taxol in worm-like PEG-PCL micelles. *Adv. Mater. 24*, 3823–3830.

(15) Ahmed, F., Pakunlu, R. I., Brannan, A., Bates, F., Minko, T., and Discher, D. E. (2006) Biodegradable polymersomes loaded with both paclitaxel and doxorubicin permeate and shrink tumors, inducing apoptosis in proportion to accumulated drug. *J. Control. Release 116*, 150–158.

(16) Cai, S., Vijayan, K., Cheng, D., Lima, E. M., and Discher, D. E. (2007) Micelles of different morphologies - Advantages of worm-like filomicelles of PEO-PCL in paclitaxel delivery. *Pharm. Res. 24*, 2099–2109.

(17) Walde, P. (2010) Building artificial cells and protocell models: Experimental approaches with lipid vesicles. *BioEssays 32*, 296–303.

(18) Evans, E., and Needham, D. (1986) Giant vesicle bilayers composed of mixtures of lipids, cholesterol and polypeptides: Thermomechanical and (mutual) adherence properties. *Faraday Discuss. Chem. Soc. 81*, 267–280.

(19) Discher, B. M., Bermudez, H., Hammer, D. A., Discher, D. E., Won, Y. yeon, and Bates, F. S. (2002) Cross-linked polymersome membranes: Vesicles with broadly adjustable properties. *J. Phys. Chem. B 106*, 2848–2854.

(20) Opsteen, J. A., Brinkhuis, R. P., Teeuwen, R. L. M., Löwik, D. W. P. M., and Van Hest, J. C. M. (2007) "Clickable" polymersomes. *Chem. Commun. 49*, 3136–3138.

(21) Fraaije, J. G. E. M., Van Sluis, C. A., Kros, A., Zvelindovsky, A. V., and Sevink, G. J. A. (2005) Design of chimaeric polymersomes. *Faraday Discuss. 128*, 355–361.

(22) Bermudez, H., Brannan, A. K., Hammer, D. A., Bates, F. S., and Discher, D. E.

(2002) Molecular weight dependence of polymersome membrane structure, elasticity, and stability. *Macromolecules 35*, 8203–8208.

(23) Christian, N. A., Milone, M. C., Ranka, S. S., Li, G., Frail, P. R., Davis, K. P., Bates, F. S., Therien, M. J., Ghoroghchian, P. P., June, C. H., and Hammer, D. A. (2007) Tat-functionalized near-infrared emissive polymersomes for dendritic cell labeling. *Bioconjug. Chem. 18*, 31–40.

(24) Sharma, A., and Sharma, U. S. (1997) Liposomes in drug delivery: Progress and limitations. *Int. J. Pharm. 154*, 123–140.

(25) Nel, A., Xia, T., Mädler, L., and Li, N. (2006) Toxic potential of materials at the nanolevel. *Science (80-.). 311*, 622–627.

(26) Dobrovolskaia, M. A., and McNeil, S. E. (2007) Immunological properties of engineered nanomaterials. *Nat. Nanotechnol. 2*, 469–478.

(27) Huang, A. H. C. (1992) Oil Bodies and Oleosins in Seeds. *Annu. Rev. Plant Physiol. Plant Mol. Biol. 43*, 177–200.

(28) Tzen, J. T. C., Lai, K.-Y., Chan, K.-L., and Huang, A. H. C. (1990) Oleosin Isoforms of High and Low Molecular Weights. *Plant Physilogy 94*, 1282–1289.

(29) Frandsen, G. I., Mundy, J., and Tzen, J. T. C. (2001) Oil bodies and their associated proteins, oleosin and caleosin. *Physiol. Plant. 112*, 301–307.

(30) Vargo, K. B., Parthasarathy, R., and Hammer, D. A. (2012) Self-assembly of tunable protein suprastructures from recombinant oleosin. *Proc. Natl. Acad. Sci. 109*, 11657–

11662.

(31) Vargo, K. B., Sood, N., Moeller, T. D., Heiney, P. A., and Hammer, D. A. (2014) Spherical micelles assembled from variants of recombinant oleosin. *Langmuir 30*, 11292–11300.

(32) Vargo, K. B., Zaki, A. Al, Warden-Rothman, R., Tsourkas, A., and Hammer, D. A. (2015) Superparamagnetic iron oxide nanoparticle micelles stabilized by recombinant oleosin for targeted magnetic resonance imaging. *Small 11*, 1409–1413.

(33) Alexander, L. G., Sessions, R. B., Clarke, A. R., Tatham, A. S., Shewry, P. R., and Napier, J. A. (2002) Characterization and modelling of the hydrophobic domain of a sunflower oleosin. *Planta 214*, 546–551.

(34) Perez, E. A. (1998) Paclitaxel in Breast Cancer. *Oncologist 3*, 373–389.

(35) Mastropaolo, D., Camerman, A., Luo, Y., Brayer, G. D., and Camerman, N. (1995) Crystal and molecular structure of paclitaxel (taxol). *Proc. Natl. Acad. Sci. 92*, 6920–6924.

(36) K, P. (2012) Paclitaxel Against Cancer: A Short Review. *Med. Chem. (Los. Angeles). 02*, 139–141.

(37) Ma, P. (2013) Paclitaxel Nano-Delivery Systems: A Comprehensive Review. *J. Nanomed. Nanotechnol. 04*.

(38) Bhattacharyya, J., Bellucci, J. J., Weitzhandler, I., McDaniel, J. R., Spasojevic, I., Li, X., Lin, C. C., Chi, J. T. A., and Chilkoti, A. (2015) A paclitaxel-loaded recombinant

polypeptide nanoparticle outperforms Abraxane in multiple murine cancer models. *Nat. Commun. 6*, 7939.

(39) Gibson, J. D., Khanal, B. P., and Zubarev, E. R. (2007) Paclitaxel-functionalized gold nanoparticles. *J. Am. Chem. Soc. 129*, 11653–11661.

(40) Oh, J., Feldman, M. D., Kim, J., Condit, C., Emelianov, S., and Milner, T. E. (2006) Detection of magnetic nanoparticles in tissue using magneto-motive ultrasound. *Nanotechnology 17*, 4183–4190.

(41) Heo, D. N., Ko, W.-K., Bae, M. S., Lee, J. B., Lee, D.-W., Byun, W., Lee, C. H., Kim, E.-C., Jung, B.-Y., and Kwon, I. K. (2014) Enhanced bone regeneration with a gold nanoparticle–hydrogel complex. *J. Mater. Chem. B 2*, 1584–1593.

(42) Colby, A. H., Liu, R., Schulz, M. D., Padera, R. F., Colson, Y. L., and Grinstaff, M. W. (2016) Two-Step Delivery: Exploiting the Partition Coefficient Concept to Increase Intratumoral Paclitaxel Concentrations in vivo Using Responsive Nanoparticles. *Sci. Rep. 6*.

(43) Maeda, H., Sawa, T., and Konno, T. (2001) Mechanism of tumor-targeted delivery of macromolecular drugs, including the EPR effect in solid tumor and clinical overview of the prototype polymeric drug SMANCS. *J. Control. Release 74*, 47–61.

(44) Hoffman, A. S. (2008) The origins and evolution of "controlled" drug delivery systems. *J. Control. Release 132*, 153–163.

(45) Pankov, R. (2002) Fibronectin at a glance. *J. Cell Sci. 115*, 3861–3863.

(46) Mosher, D. F., and Furcht, L. T. (1981) Fibronectin: Review of its Structure and Possible Functions. *J. Invest. Dermatol. 77*, 175–180.

(47) Ruoslahti, E. (1996) Rgd and Other Recognition Sequences for Integrins. *Annu. Rev. Cell Dev. Biol. 12*, 697–715.

(48) Ruoslahti, E., and Pierschbacher, M. D. (1987) New perspectives in cell adhesion: RGD and integrins. *Science (80-.). 238*, 491–497.

(49) Benoit, D. S. W., and Anseth, K. S. (2005) The effect on osteoblast function of colocalized RGD and PHSRN epitopes on PEG surfaces. *Biomaterials 26*, 5209–5220.

(50) Renigunta, A., Krasteva, G., König, P., Rose, F., Klepetko, W., Grimminger, F., Seeger, W., and Hänze, J. (2006) DNA transfer into human lung cells is improved with Tat-RGD peptide by caveoli-mediated endocytosis. *Bioconjug. Chem. 17*, 327–334.

(51) Zhan, C., Gu, B., Xie, C., Li, J., Liu, Y., and Lu, W. (2010) Cyclic RGD conjugated poly(ethylene glycol)-co-poly(lactic acid) micelle enhances paclitaxel anti-glioblastoma effect. *J. Control. Release 143*, 136–142.

(52) Jin, Z.-H., Furukawa, T., Kumata, K., Xie, L., Yui, J., Wakizaka, H., Fujibayashi, Y., Zhang, M.-R., and Saga, T. (2015) Development of the Fibronectin–Mimetic Peptide KSSPHSRN(SG)$_5$RGDSP as a Novel Radioprobe for Molecular Imaging of the Cancer Biomarker α$_5$β$_1$ Integrin. *Biol. Pharm. Bull. 38*, 1722–1731.

(53) Mardilovich, A., Craig, J. A., McCammon, M. Q., Garg, A., and Kokkoli, E. (2006)

Design of a novel fibronectin-mimetic peptide-amphiphile for functionalized biomaterials. *Langmuir 22*, 3259–3264.

(54) Ebara, M., Yamato, M., Aoyagi, T., Kikuchi, A., Sakai, K., and Okano, T. (2008) A novel approach to observing synergy effects of PHSRN on integrin-RGD binding using intelligent surfaces. *Adv. Mater. 20*, 3034–3038.

(55) Feng, Y., and Mrksich, M. (2004) The synergy peptide PHSRN and the adhesion peptide RGD mediate cell adhesion through a common mechanism. *Biochemistry 43*, 15811–15821.

(56) Ochsenhirt, S. E., Kokkoli, E., McCarthy, J. B., and Tirrell, M. (2006) Effect of RGD secondary structure and the synergy site PHSRN on cell adhesion, spreading and specific integrin engagement. *Biomaterials 27*, 3863–3874.

(57) Cheng, Y. J., Luo, G. F., Zhu, J. Y., Xu, X. D., Zeng, X., Cheng, D. B., Li, Y. M., Wu, Y., Zhang, X. Z., Zhuo, R. X., and He, F. (2015) Enzyme-induced and tumor-targeted drug delivery system based on multifunctional mesoporous silica nanoparticles. *ACS Appl. Mater. Interfaces 7*, 9078–9087.

(58) Bellomo, E. G., Wyrsta, M. D., Pakstis, L., Pochan, D. J., and Deming, T. J. (2004) Stimuli-responsive polypeptide vesicles by conformation-specific assembly. *Nat. Mater. 3*, 244–248.

(59) Oliveira, H., Pérez-Andrés, E., Thevenot, J., Sandre, O., Berra, E., and Lecommandoux, S. (2013) Magnetic field triggered drug release from polymersomes for

cancer therapeutics. *J. Control. Release 169*, 165–170.

(60) Dreher, M. R., Simnick, A. J., Fischer, K., Smith, R. J., Patel, A., Schmidt, M., and Chilkoti, A. (2008) Temperature triggered self-assembly of polypeptides into multivalent spherical micelles. *J. Am. Chem. Soc. 130*, 687–694.

(61) Gonzalez, M. J., Miranda-Massari, J. R., Berdiel, M. J., Duconge, J., Rodríguez-López, J. L., Hunninghake, R., and Cobas-Rosario, V. J. (2014) High dose intraveneous Vitamin C and chikungunya fever: A case report. *J. Orthomol. Med. 29*, 154–156.

(62) Palmer, L. C., and Stupp, S. I. (2008) Molecular self-assembly into one-dimensional nanostructures. *Acc. Chem. Res. 41*, 1674–1684.

(63) Ruoslahti, E. (1996) Rgd and Other Recognition Sequences for Integrins. *Annu. Rev. Cell Dev. Biol. 12*, 697–715.

(64) Humphries, J. D. (2006) Integrin ligands at a glance. *J. Cell Sci. 119*, 3901–3903.

(65) Hynes, R. O. (2002) Integrins: Bidirectional, allosteric signaling machines. *Cell 110*, 673–687.

(66) Danen, E. H. J. (2013) Integrin Signaling as a Cancer Drug Target. *ISRN Cell Biol. 2013*, 1–14.

(67) Hoffman, A. S. (2008) The origins and evolution of "controlled" drug delivery systems. *J. Control. Release 132*, 153–163.

(68) Chen, C.-W., Lu, Yeh, Shiau, and Chiang. (2011) Novel RGD-lipid conjugate-

modified liposomes for enhancing siRNA delivery in human retinal pigment epithelial cells. *Int. J. Nanomedicine* 2567.

(69) Achilefu, S., Bloch, S., Markiewicz, M. A., Zhong, T., Ye, Y., Dorshow, R. B., Chance, B., and Liang, K. (2005) Synergistic effects of light-emitting probes and peptides for targeting and monitoring integrin expression. *Proc. Natl. Acad. Sci. 102*, 7976–7981.

(70) Chung, E. J., and Tirrell, M. (2015) Recent Advances in Targeted, Self-Assembling Nanoparticles to Address Vascular Damage Due to Atherosclerosis. *Adv. Healthc. Mater. 4*, 2408–2422.

(71) Mura, S., Nicolas, J., and Couvreur, P. (2013) Stimuli-responsive nanocarriers for drug delivery. *Nat. Mater. 12*, 991–1003.

(72) de la Rica, R., Aili, D., and Stevens, M. M. (2012) Enzyme-responsive nanoparticles for drug release and diagnostics. *Adv. Drug Deliv. Rev. 64*, 967–978.

(73) Tumors, M. L., Rijt, S. H. Van, Bo, D. A., Eickelberg, O., and Ko, M. (2015) Protease-Mediated Release of Chemotherapeutics from Mesoporous Silica Nanoparticles to ex Vivo Human. *ACS Nano 9*, 2377–2389.

(74) Amiram, M., Luginbuhl, K. M., Li, X., Feinglos, M. N., and Chilkoti, A. (2013) Injectable protease-operated depots of glucagon-like peptide-1 provide extended and tunable glucose control. *Proc. Natl. Acad. Sci. U. S. A. 110*, 2792–7.

(75) Rickles, F. R., Patierno, S., and Fernandez, P. M. (2003) Tissue Factor, Thrombin,

and Cancer. *Chest 124*, 58S–68S.

(76) Radjabi, A. R., Sawada, K., Jagadeeswaran, S., Eichbichler, A., Kenny, H. A., Montag, A., Bruno, K., and Lengyel, E. (2008) Thrombin induces tumor invasion through the induction and association of matrix metalloproteinase-9 and ??1-integrin on the cell surface. *J. Biol. Chem. 283*, 2822–2834.

(77) Henrikson, K. P., Salazar, S. L., Fenton, J. W., and Pentecost, B. T. (1999) Role of thrombin receptor in breast cancer invasiveness. *Br. J. Cancer 79*, 401–6.

(78) Kalyanasundaram, K., and Thomas, J. K. (1977) Solvent-dependent fluorescence of pyrene-3-carboxaldehyde and its applications in the estimation of polarity at micelle-water interfaces. *J. Phys. Chem. 81*, 2176–2180.

(79) Basu Ray, G., Chakraborty, I., and Moulik, S. P. (2006) Pyrene absorption can be a convenient method for probing critical micellar concentration (cmc) and indexing micellar polarity. *J. Colloid Interface Sci. 294*, 248–254.

(80) Dominguez, A., Fernandez, A., Gonzalez, N., Iglesias, E., and Montenegro, L. (1997) Determination of Critical Micelle Concentration of Some Surfactants by Three Techniques. *J. Chem. Educ. 74*, 1227.

(81) Aguiar, J., Carpena, P., Molina-Bolívar, J. A., and Carnero Ruiz, C. (2003) On the determination of the critical micelle concentration by the pyrene 1:3 ratio method. *J. Colloid Interface Sci. 258*, 116–122.

(82) Basu Ray, G., Chakraborty, I., and Moulik, S. P. (2006) Pyrene absorption can be a

convenient method for probing critical micellar concentration (cmc) and indexing micellar polarity. *J. Colloid Interface Sci. 294*, 248–254.

(83) Whitmore, L., and Wallace, B. A. (2004) DICHROWEB, an online server for protein secondary structure analyses from circular dichroism spectroscopic data. *Nucleic Acids Res. 32*, 668–673.

(84) Sreerama, N., Venyaminov, S. Y., and Woody, R. W. (2000) Estimation of protein secondary structure from circular dichroism spectra: Inclusion of denatured proteins with native proteins in the analysis. *Anal. Biochem. 287*, 243–251.

(85) Vellon, L., Menendez, J. A., Liu, H., and Lupu, R. (2007) Up-regulation of αVβ3 integrin expression is a novel molecular response to chemotherapy-induced cell damage in a heregulin-dependent manner. *Differentiation 75*, 819–830.

(86) Zhao, Y., Bachelier, R., Treilleux, I., Pujuguet, P., Peyruchaud, O., Baron, R., Clément-Lacroix, P., and Clézardin, P. (2007) Tumor αvβ3 integrin is a therapeutic target for breast cancer bone metastases. *Cancer Res. 67*, 5821–5830.

(87) Spiess, K., Lammel, A., and Scheibel, T. (2010) Recombinant spider silk proteins for applications in biomaterials. *Macromol. Biosci. 10*, 998–1007.

(88) Tang, K., Zhang, Y., Zhang, H., Xu, P., Liu, J., Ma, J., Lv, M., Li, D., Katirai, F., Shen, G. X., Zhang, G., Feng, Z. H., Ye, D., and Huang, B. (2012) Delivery of chemotherapeutic drugs in tumour cell-derived microparticles. *Nat. Commun. 3*.

(89) Farokhzad, O. C., and Langer, R. (2009) Impact of nanotechnology on drug delivery.

ACS Nano 3, 16–20.

(90) Gao, C., Vargo, K. B., and Hammer, D. A. (2016) Protease-Triggered, Integrin-Targeted Cellular Uptake of Recombinant Protein Micelles. *Macromol. Biosci. 16*, 1398–1406.

(91) Hojo, K., Susuki, Y., Maeda, M., Okazaki, I., Nomizu, M., Kamada, H., Yamamoto, Y., Nakagawa, S., Mayumi, T., and Kawasaki, K. (2001) Amino acids and peptides. Part 39: A bivalent poly(ethylene glycol) hybrid containing an active site (RGD) and its synergistic site (PHSRN) of fibronectin. *Bioorganic Med. Chem. Lett. 11*, 1429–1432.

(92) Kao, W. J., Lee, D., Schense, J. C., and Hubbell, J. A. (2001) Fibronectin modulates macrophage adhesion and FBGC formation: The role of RGD, PHSRN, and PRRARV domains. *J. Biomed. Mater. Res. 55*, 79–88.

(93) Suwandi, J. S., Toes, R. E. M., Nikolic, T., and Roep, B. O. (2015) Inducing tissue specific tolerance in autoimmune disease with tolerogenic dendritic cells. *Clin. Exp. Rheumatol. 33*, 97–103.

(94) Garg, A., Tisdale, A. W., Haidari, E., and Kokkoli, E. (2009) Targeting colon cancer cells using PEGylated liposomes modified with a fibronectin-mimetic peptide. *Int. J. Pharm. 366*, 201–210.

(95) Egleton, R. D., and Davis, T. P. (1997) Bioavailability and transport of peptides and peptide drugs into the brain. *Peptides 18*, 1431–1439.

(96) Ruben, S., Perkins, a, Purcell, R., Joung, K., Sia, R., Burghoff, R., Haseltine, W. a,

and Rosen, C. a. (1989) Structural and functional characterization of human immunodeficiency virus tat protein. *J Virol 63*, 1–8.

(97) Mishra, A., Lai, G. H., Schmidt, N. W., Sun, V. Z., Rodriguez, A. R., Tong, R., Tang, L., Cheng, J., Deming, T. J., Kamei, D. T., and Wong, G. C. L. (2011) Translocation of HIV TAT peptide and analogues induced by multiplexed membrane and cytoskeletal interactions. *Proc. Natl. Acad. Sci. 108*, 16883–16888.

(98) Torchilin, V. P. (2008) Tat peptide-mediated intracellular delivery of pharmaceutical nanocarriers. *Adv. Drug Deliv. Rev. 60*, 548–558.

(99) Brooks, H., Lebleu, B., and Vivès, E. (2005) Tat peptide-mediated cellular delivery: Back to basics. *Adv. Drug Deliv. Rev. 57*, 559–577.

(100) Berezov, A., Chen, J., Liu, Q., Zhang, H. T., Greene, M. I., and Murali, R. (2002) Disabling receptor ensembles with rationally designed interface peptidomimetics. *J. Biol. Chem. 277*, 28330–28339.

(101) Cai, Z., Zhang, H., Liu, J., Berezov, A., Murali, R., Wang, Q., and Greene, M. I. (2010) Targeting erbB receptors. *Semin. Cell Dev. Biol. 21*, 961–966.

(102) Ashkenazi, A., Holland, P., and Eckhardt, S. G. (2008) Ligand-based targeting of apoptosis in cancer: The potential of recombinant human apoptosis ligand 2/tumor necrosis factor-related apoptosis-inducing ligand (rhApo2L/TRAIL). *J. Clin. Oncol. 26*, 3621–3630.

(103) Baselga, J., and Arteaga, C. L. (2005) Critical update and emerging trends in

epidermal growth factor receptor targeting in cancer. *J. Clin. Oncol. 23*, 2445–2459.

(104) Ponde, D. E., Su, Z., Berezov, A., Zhang, H., Alavi, A., Greene, M. I., and Murali, R. (2011) Development of anti-EGF receptor peptidomimetics (AERP) as tumor imaging agent. *Bioorganic Med. Chem. Lett. 21*, 2550–2553.

(105) Schramm, H. J., Boetzel, J., Büttner, J., Fritsche, E., Göhring, W., Jaeger, E., König, S., Thumfart, O., Wenger, T., Nagel, N. E., and Schramm, W. (1996) The inhibition of human immunodeficiency virus proteases by "interface peptides." *Antiviral Res. 30*, 155–170.

(106) Wan, X., Zhang, J., Yu, W., Shen, L., Ji, S., and Hu, T. (2017) Effect of protein immunogenicity and PEG size and branching on the anti-PEG immune response to PEGylated proteins. *Process Biochem. 52*, 183–191.

(107) Wadhwa, M., Knezevic, I., Kang, H. N., and Thorpe, R. (2015) Immunogenicity assessment of biotherapeutic products: An overview of assays and their utility. *Biologicals 43*, 298–306.

(108) Costa, S., Almeida, A., Castro, A., and Domingues, L. (2014) Fusion tags for protein solubility, purification, and immunogenicity in Escherichia coli: The novel Fh8 system. *Front. Microbiol. 5*.

(109) Pisal, D. S., Kosloski, M. P., and Balu-Iyer, S. V. (2010) Delivery of therapeutic proteins. *J. Pharm. Sci. 99*, 2557–2575.

(110) Jawa, V., Cousens, L. P., Awwad, M., Wakshull, E., Kropshofer, H., and De Groot,

A. S. (2013) T-cell dependent immunogenicity of protein therapeutics: Preclinical assessment and mitigation. *Clin. Immunol. 149*, 534–555.

(111) Tung, C. W., and Ho, S. Y. (2007) POPI: Predicting immunogenicity of MHC class I binding peptides by mining informative physicochemical properties. *Bioinformatics 23*, 942–949.

(112) Saethang, T., Hirose, O., Kimkong, I., Tran, V. A., Dang, X. T., Nguyen, L. A. T., Le, T. K. T., Kubo, M., Yamada, Y., and Satou, K. (2013) PAAQD: Predicting immunogenicity of MHC class I binding peptides using amino acid pairwise contact potentials and quantum topological molecular similarity descriptors. *J. Immunol. Methods 387*, 293–302.

(113) Nicolas, J., Mura, S., Brambilla, D., MacKiewicz, N., and Couvreur, P. (2013) Design, functionalization strategies and biomedical applications of targeted biodegradable/biocompatible polymer-based nanocarriers for drug delivery. *Chem. Soc. Rev. 42*, 1147–1235.

(114) Paul, S., Sidney, J., Sette, A., and Peters, B. (2016) TepiTool: A pipeline for computational prediction of T cell epitope candidates. *Curr. Protoc. Immunol. 2016*, 18.19.1-18.19.24.

(115) Larsen, M. V., Lundegaard, C., Lamberth, K., Buus, S., Lund, O., and Nielsen, M. (2007) Large-scale validation of methods for cytotoxic T-lymphocyte epitope prediction. *BMC Bioinformatics 8*, 424.

(116) Calis, J. J. A., Maybeno, M., Greenbaum, J. A., Weiskopf, D., De Silva, A. D., Sette, A., Keşmir, C., and Peters, B. (2013) Properties of MHC Class I Presented Peptides That Enhance Immunogenicity. *PLoS Comput. Biol. 9*, 1003266.

(117) Wischke, C., and Schwendeman, S. P. (2008) Principles of encapsulating hydrophobic drugs in PLA/PLGA microparticles. *Int. J. Pharm. 364*, 298–327.

Appendix: DNA and Protein Sequences

Variant	DNA Sequence	AA Sequence
30G	GGATCCACCACAACCTACGACCGCCACC ATGTCACCACCACCCAACCCCAATACCGC CATGATCAACACACCGGTGACAGACTCA CCCACCCACAGCGCCAGCAACAAGGCCC CTCAACCGGCAAGCTCGCTCTCGGTGCGA CTCCGCTGTTTGGTGTTATAGGTTTCAGC CCTGTTATTGTTCCAGCGATGGGTATAGC GATTGGGCTTGCGGGTGTTACCGGGTTTC AGAGGGATTATGTGAAGGGGAAGTTGCA GGATGTGGGGGAGTATACGGGCCAGAAG ACGAAGGACTTGGGCCAGAAGATACAGC ATACGGCCCATGAAATGGGTGACCAGGG CCAGGGTCAGGGTCAGGGTGGTGGGAAA GAAGGGCGAAAAGAAGGGGGGAAACTC GAGCACCACCACCACCACCAC	GSTTTYDRHH VTTTQPQYRH DQHTGDRLTH PQRQQQGPST GKLALGATPL FGVIGFSPVIV PAMGIAIGLA GVTGFQRDY VKGKLQDVG EYTGQKTKDL GQKIQHTAHE MGDQGQGQG QGGGKEGRK EGGKLEHHH HHH
RADS-30G(-)	GGATCCCGCGCGGATAGCGAAGCCACAA CAACCAACGACCAGCACAAAGTCACCAC CACCCAACCCCAAGATCAGCATGATCAA CACACCGGTGACCAGCTCACCCACCCAC AGGACCAGCAACAAGGCCCCTCAACCGG CGAACTCGCTCTCGGTGCGACTCCGCTGT TTGGTGTTATAGGTTTCAGCCCTGTTATT GTTCCAGCGATGGGTATAGCGATTGGGCT TGCGGGTGTTACCGGGTTTCAGTGGCAGG ATAACGTGAACGGGGAATTGCAGGATGT GGGGGAGCAGACGGGCCAGAACACGAA CGACTTGGGCCAGCAGATACAGCATACG GCCCATGAAATGGGTGACCAGGGCCAGG GTCAGGGTCAGGGTGGTGGGAACGAAGG GCAGAACGAAGGGGGGAACCACCACCAC CACCACCACGATGAC	GSRADSEATT TNDQHKVTTT QPQDQHDQH TGDQLTHPQD QQQGPSTGEL ALGATPLFGV IGFSPVIVPAM GIAIGLAGVT GFQWQDNVN GELQDVGEQT GQNTNDLGQ QIQHTAHEMG DQGQGQGQG GGNEGQNEG GNHHHHHHD D

| RGDS-30G(-) | GGATCCCGCGGCGATAGCGAAGCCACAA CAACCAACGACCAGCACAAAGTCACCAC CACCCAACCCCAAGATCAGCATGATCAA CACACCGGTGACCAGCTCACCCACCCAC AGGACCAGCAACAAGGCCCCTCAACCGG CGAACTCGCTCTCGGTGCGACTCCGCTGT TTGGTGTTATAGGTTTCAGCCCTGTTATT GTTCCAGCGATGGGTATAGCGATTGGGCT TGCGGGTGTTACCGGGTTTCAGTGGCAGG ATAACGTGAACGGGGAATTGCAGGATGT GGGGGAGCAGACGGGCCAGAACACGAA CGACTTGGGCCAGCAGATACAGCATACG GCCCATGAAATGGGTGACCAGGGCCAGG GTCAGGGTCAGGGTGGTGGGAACGAAGG GCAGAACGAAGGGGGGAACCACCACCAC CACCACCACGATGAC | GSRGDSEATT TNDQHKVTTT QPQDQHDQH TGDQLTHPQD QQQGPSTGEL ALGATPLFGV IGFSPVIVPAM GIAIGLAGVT GFQWQDNVN GELQDVGEQT GQNTNDLGQ QIQHTAHEMG DQGQGQGQG GGNEGQNEG GNHHHHHHD D |
| Oleosin-Throm-RADS-30G(-) | GGATCCGAAGCCACCACAACCAACGACC AGCACCATGTCACCACCACCCAACCCCA AGATCAGAAACTGGTGCCGCGTGGTAGC CGCGCCGATAGCGATCAAAAAACCGGTG ACCAGCTCACCCACCCACAGGACCAGCA ACAAGGCCCCTCAACCGGCGAACTCGCT CTCGGTGCGACTCCGCTGTTTGGTGTTAT AGGTTTCAGCCCTGTTATTGTTCCAGCGA TGGGTATAGCGATTGGGCTTGCGGGTGTT ACCGGGTTTCAGTGGCAGGATAACGTGA ACGGGGAATTGCAGGATGTGGGGGAGCA GACGGGCCAGAACACGAACCTGGTTCCG CGCGGCTCTGACTTGGGCCAGCAGATAC AGCATACGGCCCATGAAATGGGTGACCA GGGCCAGGGTCAGGGTCAGGGTGGTGGG AACGAAGGGCAGAACGAAGGGGGGAAC CACCACCACCACCACCACGATGACTGA | GSEATTTNDQ HHVTTTQPQD Q**K**LVPRGSRA DSDQ**K**TGDQ LTHPQDQQQG PSTGELALGA TPLFGVIGFSP VIVPAMGIAIG LAGVTGFQW QDNVNGELQ DVGEQTGQN TNLVPRGSDL GQQIQHTAHE MGDQGQGQG QGGGNEGQN EGGNHHHHH HDD |

Oleosin-Throm-RGDS-30G(-)	GGATCCGAAGCCACCACAACCAACGACC AGCACCATGTCACCACCACCCAACCCCA AGATCAGAAACTGGTGCCGCGTGGTAGC CGCGGCGATAGCGATCAAAAAACCGGTG ACCAGCTCACCCACCCACAGGACCAGCA ACAAGGCCCCTCAACCGGCGAACTCGCT CTCGGTGCGACTCCGCTGTTTGGTGTTAT AGGTTTCAGCCCTGTTATTGTTCCAGCGA TGGGTATAGCGATTGGGCTTGCGGGTGTT ACCGGGTTTCAGTGGCAGGATAACGTGA ACGGGGAATTGCAGGATGTGGGGGGAGCA GACGGGCCAGAACACGAACCTGGTTCCG CGCGGCTCTGACTTGGGCCAGCAGATAC AGCATACGGCCCATGAAATGGGTGACCA GGGCCAGGGTCAGGGTCAGGGTGGTGGG AACGAAGGGCAGAACGAAGGGGGGAAC CACCACCACCACCACCACGATGACTGA	GSEATTTNDQ HHVTTTQPQD Q**K**LVPRGSRG DSDQ**K**TGDQ LTHPQDQQQG PSTGELALGA TPLFGVIGFSP VIVPAMGIAIG LAGVTGFQW QDNVNGELQ DVGEQTGQN TNLVPRGSDL GQQIQHTAHE MGDQGQGQG QGGGNEGQN EGGNHHHHH HDD
RGDS-30G(-)-Tat	GGATCCCGCGGCGATAGCGAAGCCACAA CAACCAACGACCAGCACAAAGTCACCAC CACCCAACCCCAAGATCAGCATGATCAA CACACCGGTGACCAGCTCACCCACCCAC AGGACCAGCAACAAGGCCCCTCAACCGG CGAACTCGCTCTCGGTGCGACTCCGCTGT TTGGTGTTATAGGTTTCAGCCCTGTTATT GTTCCAGCGATGGGTATAGCGATTGGGCT TGCGGGTGTTACCGGGTTTCAGTGGCAGG ATAACGTGAACGGGGAATTGCAGGATGT GGGGGAGCAGACGGGCCAGAACACGAA CGACTTGGGCCAGCAGATACAGCATACG GCCCATGAAATGGGTGACCAGGGCCAGG GTCAGGGTCAGGGTGGTGGGAACGAAGG GCAGAACGAAGGGGGGAACGGCCGCAA AAAACGCCGCCAGCGCCGCCGCCCGCAG TGCCACCATCACCATCACCATGATGAC	GSRGDSEATT TNDQHKVTTT QPQDQHDQH TGDQLTHPQD QQQGPSTGEL ALGATPLFGV IGFSPVIVPAM GIAIGLAGVT GFQWQDNVN GELQDVGEQT GQNTNDLGQ QIQHTAHEMG DQGQGQGQG GGNEGQNEG GNGRKKRRQ RRRPQCHHHH HHDD
PHSRN-30G(-)	GGATCCCCGCATAGCCGCAACGAAGCCA CAACAACCAACGACCAGCACAAAGTCAC CACCACCCAACCCCAAGATCAGCATGAT CAACACACCGGTGACCAGCTCACCCACC CACAGGACCAGCAACAAGGCCCCTCAAC CGGCGAACTCGCTCTCGGTGCGACTCCGC TGTTTGGTGTTATAGGTTTCAGCCCTGTT	GSPHSRNEAT TTNDQHKVTT TQPQDQHDQ HTGDQLTHPQ DQQQGPSTGE LALGATPLFG VIGFSPVIVPA

	ATTGTTCCAGCGATGGGTATAGCGATTGG GCTTGCGGGTGTTACCGGGTTTCAGTGGC AGGATAACGTGAACGGGGAATTGCAGGA TGTGGGGGAGCAGACGGGCCAGAACACG AACGACTTGGGCCAGCAGATACAGCATA CGGCCCATGAAATGGGTGACCAGGGCCA GGGTCAGGGTCAGGGTGGTGGGAACGAA GGGCAGAACGAAGGGGGGAACCACCATC ACCATCACCATGATGAC	MGIAIGLAGV TGFQWQDNV NGELQDVGE QTGQNTNDL GQQIQHTAHE MGDQGQGQG QGGGNEGQN EGGNHHHHH HDD
PHSRN-30G(-)-RGDS	GGATCCCCGCATAGCCGCAACGAAGCCA CAACAACCAACGACCAGCACAAAGTCAC CACCACCCAACCCCAAGATCAGCATGAT CAACACACCGGTGACCAGCTCACCCACC CACAGGACCAGCAACAAGGCCCCTCAAC CGGCGAACTCGCTCTCGGTGCGACTCCGC TGTTTGGTGTTATAGGTTTCAGCCCTGTT ATTGTTCCAGCGATGGGTATAGCGATTGG GCTTGCGGGTGTTACCGGGTTTCAGTGGC AGGATAACGTGAACGGGGAATTGCAGGA TGTGGGGGAGCAGACGGGCCAGAACACG AACGACTTGGGCCAGCAGATACAGCATA CGGCCCATGAAATGGGTGACCAGGGCCA GGGTCAGGGTCAGGGTGGTGGGAACGAA GGGCAGAACGAAGGGGGGAACCGCGGC GATAGCCACCATCACCATCACCATGATG AC	GSPHSRNEAT TTNDQHKVTT TQPQDQHDQ HTGDQLTHPQ DQQQGPSTGE LALGATPLFG VIGFSPVIVPA MGIAIGLAGV TGFQWQDNV NGELQDVGE QTGQNTNDL GQQIQHTAHE MGDQGQGQG QGGGNEGQN EGGNRGDSH HHHHHDD

Tat-30G(-)	GGATCCGGCCGCAAAAAACGCCGCCAGC GCCGCCGCCCGCAGTGCGAAGCCACAAC AACCAACGACCAGCACAAAGTCACCACC ACCCAACCCCAAGATCAGCATGATCAAC ACACCGGTGACCAGCTCACCCACCCACA GGACCAGCAACAAGGCCCCTCAACCGGC GAACTCGCTCTCGGTGCGACTCCGCTGTT TGGTGTTATAGGTTTCAGCCCTGTTATTG TTCCAGCGATGGGTATAGCGATTGGGCTT GCGGGTGTTACCGGGTTTCAGTGGCAGG ATAACGTGAACGGGGAATTGCAGGATGT GGGGGAGCAGACGGGCCAGAACACGAA CGACTTGGGCCAGCAGATACAGCATACG GCCCATGAAATGGGTGACCAGGGCCAGG GTCAGGGTCAGGGTGGTGGGAACGAAGG GCAGAACGAAGGGGGGAACCACCACCAC CACCACCACGATGAC	GSGRKKRRQR RRPQCEATTT NDQHKVTTT QPQDQHDQH TGDQLTHPQD QQQGPSTGEL ALGATPLFGV IGFSPVIVPAM GIAIGLAGVT GFQWQDNVN GELQDVGEQT GQNTNDLGQ QIQHTAHEMG DQGQGQGQG GGNEGQNEG GNHHHHHHD D
AFA-30G-63	GGATCCATGTATTGCTTTCCGGATGAAGA AGGCGCGTGCTATACCACAACCTACGAC CGCCACCATGTCACCACCACCCAACCCCA ATACCGCCATGATCAACACACCGGTGAC AGACTCACCCACCCACAGCGCCAGCAAC AAGGCCCCTCAACCGGCAAGCTCGCTCTC GGTGCGACTCCGCTGTTTGGTGTTATAGG TTTCAGCCCTGTTATTGTTCCAGCGATGG GTATAGCGATTGGGCTTGCGGGTGTTACC GGGTTTCAGAGGGATTATGTGAAGGGGA AGTTGCAGGATGTGGGGGAGTATACGGG CCAGAAGACGAAGGACTTGGGCCAGAAG ATACAGCATACGGCCCATGAAATGGGTG ACCAGGGCCAGGGTCAGGGTCAGGGTGG TGGGAAAGAAGGGCGAAAAGAAGGGGG GAAACATCACCATCACCATCAC	GSMYCFPDEE GACYTTTYDR HHVTTTQPQY RHDQHTGDR LTHPQRQQQG PSTGKLALGA TPLFGVIGFSP VIVPAMGIAIG LAGVTGFQRD YVKGKLQDV GEYTGQKTK DLGQKIQHTA HEMGDQGQG QGQGGGKEG RKEGGKHHH HHH
AFA-30G-43	GGATCCATGTATTGCTTTCCGGATGAAGA AGGCGCGTGCTAT ACCACAACCTACGACCGCCACCATGTCA CCACCACCCAACCCCAATACCGCCATGAT CAACACACCGGTGACAGACTCACCCACC CACAGCGCCAGCAACAAGGCCCCTCAAC CGGCAAGCTCGCTCTCGGTGCGACTCCGC TGTTTGGTGTTATAGGTTTCAGCCCTGTT ATTGTTCCAGCGATGGGTATAGCGATTGG	GSMYCFPDEE GACYTTTYDR HHVTTTQPQY RHDQHTGDR LTHPQRQQQG PSTGKLALGA TPLFGVIGFSP VIVPAMGIAIG LAGVTGFQRD

	GCTTGCGGGTGTTACCGGGTTTCAGAGGG ATTATGTGAAGGGGAAGTTGCAGGATGT GGGGGAGTATACGGGCCAGAAGACGAAG GACTTGGGCCAGAAGATACAGCATACGG CCCATGAAATGGGTCATCACCATCACCAT CAC	YVKGKLQDV GEYTGQKTK DLGQKIQHTA HEMGHHHHH H
BPT-30G-63	GGATCCATGCCGTGCCCGATTAACTGCAC CCATAGCTGCGTGGATCTGGATGATAAA GGCACCACAACCTACGACCGCCACCATG TCACCACCACCCAACCCCAATACCGCCAT GATCAACACACCGGTGACAGACTCACCC ACCCACAGCGCCAGCAACAAGGCCCCTC AACCGGCAAGCTCGCTCTCGGTGCGACTC CGCTGTTTGGTGTTATAGGTTTCAGCCCT GTTATTGTTCCAGCGATGGGTATAGCGAT TGGGCTTGCGGGTGTTACCGGGTTTCAGA GGGATTATGTGAAGGGGAAGTTGCAGGA TGTGGGGGAGTATACGGGCCAGAAGACG AAGGACTTGGGCCAGAAGATACAGCATA CGGCCCATGAAATGGGTGACCAGGGCCA GGGTCAGGGTCAGGGTGGTGGGAAAGAA GGGCGAAAGAAGGGGGGGAAACATCAC CATCACCATCAC	GSMPCPINCT HSCVDLDDK GTTTYDRHHV TTTQPQYRHD QHTGDRLTHP QRQQQGPSTG KLALGATPLF GVIGFSPVIVP AMGIAIGLAG VTGFQRDYV KGKLQDVGE YTGQKTKDL GQKIQHTAHE MGDQGQGQG QGGGKEGRK EGGKHHHHH H
BPT-30G-43	GGATCCATGCCGTGCCCGATTAACTGCAC CCATAGCTGCGTGGATCTGGATGATAAA GGCACCACAACCTACGACCGCCACCATG TCACCACCACCCAACCCCAATACCGCCAT GATCAACACACCGGTGACAGACTCACCC ACCCACAGCGCCAGCAACAAGGCCCCTC AACCGGCAAGCTCGCTCTCGGTGCGACTC CGCTGTTTGGTGTTATAGGTTTCAGCCCT GTTATTGTTCCAGCGATGGGTATAGCGAT TGGGCTTGCGGGTGTTACCGGGTTTCAGA GGGATTATGTGAAGGGGAAGTTGCAGGA TGTGGGGGAGTATACGGGCCAGAAGACG AAGGACTTGGGCCAGAAGATACAGCATA CGGCCCATGAAATGGGTCATCACCATCA CCATCAC	GSMPCPINCT HSCVDLDDK GTTTYDRHHV TTTQPQYRHD QHTGDRLTHP QRQQQGPSTG KLALGATPLF GVIGFSPVIVP AMGIAIGLAG VTGFQRDYV KGKLQDVGE YTGQKTKDL GQKIQHTAHE MGHHHHH

| AFA-30G(-) | GGATCCTATTGCTTTCCGGATGAAGAAGG CGCGTGCTATGAAGCCACAACAACCAAC GACCAGCACAAAGTCACCACCACCCAAC CCCAAGATCAGCATGATCAACACACCGG TGACCAGCTCACCCACCCACAGGACCAG CAACAAGGCCCCTCAACCGGCGAACTCG CTCTCGGTGCGACTCCGCTGTTTGGTGTT ATAGGTTTCAGCCCTGTTATTGTTCCAGC GATGGGTATAGCGATTGGGCTTGCGGGT GTTACCGGGTTTCAGTGGCAGGATAACGT GAACGGGGAATTGCAGGATGTGGGGGGAG CAGACGGGCCAGAACACGAACGACTTGG GCCAGCAGATACAGCATACGGCCCATGA AATGGGTGACCAGGGCCAGGGTCAGGGT CAGGGTGGTGGGAACGAAGGGCAGAACG AAGGGGGGAACCATCACCATCACCATCA CGATGAC | GSYCFPDEEG ACYEATTTND QHKVTTTQPQ DQHDQHTGD QLTHPQDQQQ GPSTGELALG ATPLFGVIGFS PVIVPAMGIAI GLAGVTGFQ WQDNVNGEL QDVGEQTGQ NTNDLGQQIQ HTAHEMGDQ GQGQGQGGG NEGQNEGGN HHHHHHDD |
| BPT-30G(-) | GGATCCCCGTGCCCGATTAACTGCACCCA TAGCTGCGTGGATCTGGATGATAAAGGC GAAGCCACAACAACCAACGACCAGCACA AAGTCACCACCACCCAACCCCAAGATCA GCATGATCAACACACCGGTGACCAGCTC ACCCACCCACAGGACCAGCAACAAGGCC CCTCAACCGGCGAACTCGCTCTCGGTGCG ACTCCGCTGTTTGGTGTTATAGGTTTCAG CCCTGTTATTGTTCCAGCGATGGGTATAG CGATTGGGCTTGCGGGTGTTACCGGGTTT CAGTGGCAGGATAACGTGAACGGGGAAT TGCAGGATGTGGGGGGAGCAGACGGGCCA GAACACGAACGACTTGGGCCAGCAGATA CAGCATACGGCCCATGAAATGGGTGACC AGGGCCAGGGTCAGGGTCAGGGTGGTGG GAACGAAGGGCAGAACGAAGGGGGGAA CCATCACCATCACCATCACGATGAC | GSPCPINCTHS CVDLDDKGE ATTTNDQHK VTTTQPQDQH DQHTGDQLT HPQDQQQGPS TGELALGATP LFGVIGFSPVI VPAMGIAIGL AGVTGFQWQ DNVNGELQD VGEQTGQNT NDLGQQIQHT AHEMGDQGQ GQGQGGGNE GQNEGGNHH HHHDD |

| CD4-G-30G-43 | GGATCCTTTTGCTATATTGGCGAAGTGGAAGATCAGTGCTAT

ACCACAACCTACGACCGCCACCATGTCACCACCACCCAACCCCAATACCGCCATGATCAACACACCGGTGACAGACTCACCCACCCACAGCGCCAGCAACAAGGCCCCTCAACCGGCAAGCTCGCTCTCGGTGCGACTCCGCTGTTTGGTGTTATAGGTTTCAGCCCTGTTATTGTTCCAGCGATGGGTATAGCGATTGGGCTTGCGGGTGTTACCGGGTTTCAGAGGGATTATGTGAAGGGGAAGTTGCAGGATGTGGGGGGAGTATACGGGCCAGAAGACGAAGGACTTGGGCCAGAAGATACAGCATACGGCCCATGAAATGGGTCATCACCATCACCATCAC | GSFCYIGEVEDQCYTTTYDRHHVTTTQPQYRHDQHTGDRLTHPQRQQQGPSTGKLALGATPLFGVIGFSPVIVPAMGIAIGLAGVTGFQRDYVKGKLQDVGEYTGQKTKDLGQKIQHTAHEMGHHHHHH |